Aus der

Medizinischen Klinik und Poliklinik III

Klinikum der Ludwig-Maximilians-Universität München

Metabolic engineering of murine cytotoxic T cells by solute carrier Slc2a1/GLUT1 overexpression to enhance anti-tumor activity

Dissertation

zum Erwerb des Doctor of Philosophy (Ph.D.)

an der Medizinischen Fakultät der

Ludwig-Maximilians-Universität München

vorgelegt von

Martin Edwin Kirmaier

aus

Trostberg

Jahr

2023

Erstes Gutachten:	Prof. Dr. Sebastian Theurich
Zweites Gutachten:	Prof. Dr. Sebastian Kobold
Drittes Gutachten:	Prof. Dr. Irmela Jeremias
Viertes Gutachten:	Prof. Dr. Andreas Humpe

Dekan:	Prof. Dr. med. Thomas Gudermann

Tag der mündlichen Prüfung: 13.11.2023

Table of Contents

1. Abstract

In the last decade, adoptive T-Cell therapy (ACT) has emerged as a successful treatment of hematological malignancies. However, solid tumors pose challenges created by various factors, including poor infiltration, immunosuppressive factors, and the lack of nutrient viability. In combination with the low vascularisation, the nutrient-deprived tumor microenvironment (TME) is mainly created by the elevated aerobic glycolysis in tumor cells. As one of the main precursor metabolites, glucose is used in vast amounts by the tumor, therefore causing a massive concentration drop in the surrounding matrix. The increased surface expression of facilitative glucose transporters from the solute carrier family 2 (GLUT1/*Slc2*) on tumor cells plays an essential role in this process, giving them a selective advantage in the created TME. Infiltrating T cells would face a deserted tumor landscape that heavily interferes with their metabolism and consequently, their metabolic need to be functionally active could not be fulfilled. This new paradigm of immune escape mechanism has long been ignored but was more and more shifted into the spotlight, recently. Herein, we propose a novel strategy for ACT of metabolically engineered cytotoxic CD8+ T cells to adapt immune cells to the prevalent glucose concentrations in the TME. In this study, we could reveal that the ectopic overexpression of the glucose transporter GLUT1 encoded by *Slc2a1* increased the fitness of primary murine CD8+ T cells (CD8+^{Slc2a1}) in hypoglycemic conditions. Additionally, our results showed augmented functional activity and anti-tumor efficacy, *in vitro* and partially *in vivo*. We observed CD8+^{Slc2a1} undergo a changed metabolic reprogramming affecting their transcriptional landscape, oxidative state, and memory formation. These findings set the foundation for future studies on ACT in combination with GLUT1 overexpression in pre-clinical settings.

Im letzten Jahrzehnt hat sich Adoptive T-Zell Therapy (ACT) als erfolgreiche Therapie gegen Blutkrebserkrankungen bewährt. Jedoch bergen solide Krebsarten eine größere Herausforderung, welche durch die schlechte Immunzellinfiltration, immunsuppressive Faktoren und nicht zuletzt dem Mangel an Nährstoffen definiert werden. In Kombination mit der schlechten Vaskularisierung kreieren Tumorzellen ein nährstoffarmes Tumormikromillieu (TME) durch ihre hochregulierte glykolytische Aktivität. Als eine der wichtigsten Grundmetabolite wird Glukose in großen Mengen vom Tumor entzogen, wodurch ein substanzieller Konzentrationsabfall in der umliegenden Matrix folgt. Die Überexpression des Glukosetransporters GLUT1/*SLC2A1* an der Oberfläche der Tumorzellen spielt eine zentrale Rolle in diesem Prozess, indem es diesen einen selektiven Vorteil im entstandenen TME verleiht. Einwandernde T-Zellen sind daher mit einer nährstoffverlassenen Tumorlandschaft

konfrontiert, welche signifikant ihren Stoffwechsel beeinträchtigt und folglich ihre metabolischen Bedürfnisse nicht erfüllen kann. Dieses neue Paradigma der Immunflucht würde lange ignoriert aber findet mehr und mehr Beachtung in diesem Kontext. In dieser Arbeit präsentieren wir eine neue Strategie der ACT indem wir metabolisch modifizierte zytotoxische T-Zellen an die vorherrschenden Glukosekonzentrationen des TME anpassen. Wir konnten zeigen, dass die ektope Überexpression des Glukosetransporters GLUT1 (codiert in *Slc2a1*) die Fitness von primären murinen CD8+ T-Zellen (CD8+[Slc2a1]) in hypoglykämischen Bedingungen erhöht. Unsere *in vitro* und *in vivo* Ergebnisse zeigen zusätzlich eine erhöhte funktionelle Aktivität und Zeichen verbesserter anti-tumor Effektivität. Außerdem konnten wir beobachten, dass CD8+[Slc2a1] Zellen eine metabolische Reprogrammierung durchlaufen, welche zur Veränderung des transkriptionellen und oxidativen Zustandes führt und die Gedächtnisbildung beeinflusst. Diese Ergebnisse sollen als einen Grundstein für künftige präklinische Studien der ACT in Kombination mit GLUT1 Überexpression dienen.
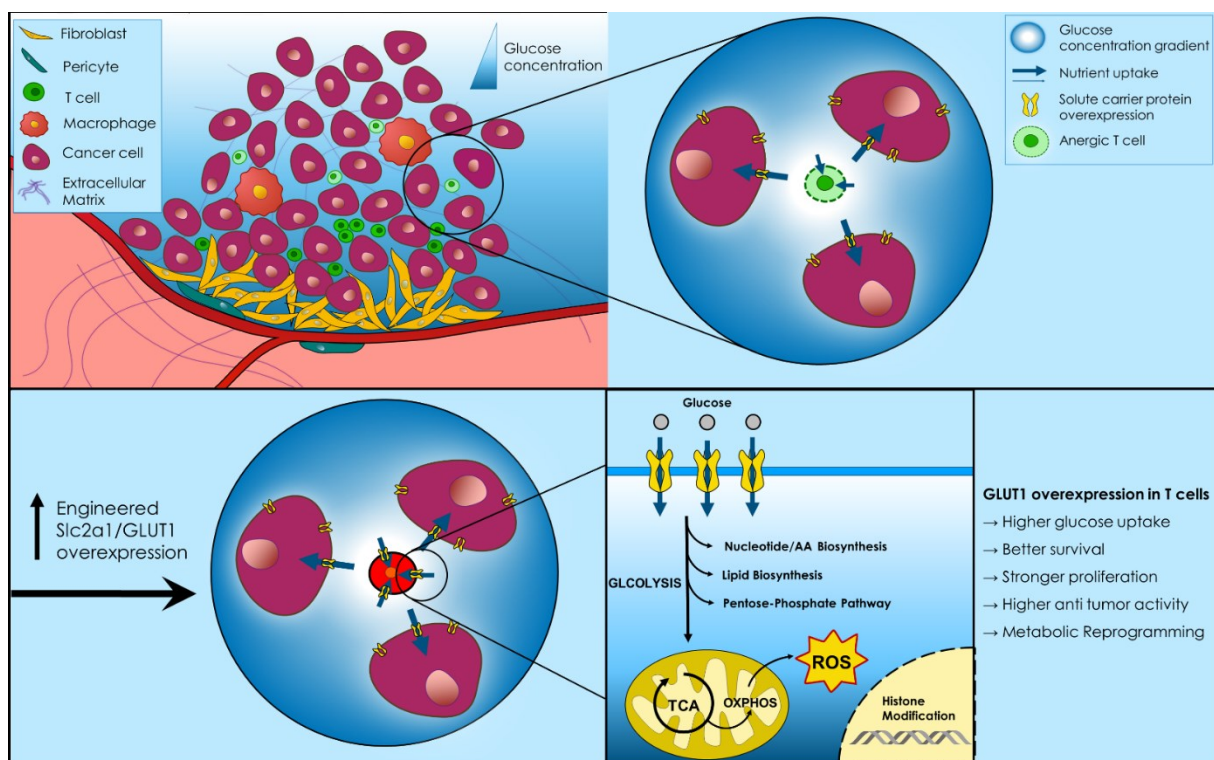
Figure 1 Graphical Abstract depicting the project rationale.
Slc2a1 transduced primary murine CD8+ T cells (CD8+[Slc2a1]) show augmented functionality in hypoglycemic TME conditions and undergo heavy metabolic reprogramming

2. Introduction

2.1 The "bitter-sweet" tumor microenvironment (TME): Tumor cells establish a hostile environment for TILs

2.1.1 Cancer development, progression, and the interplay with the immune system

Cancer is the second leading cause of death worldwide, following cardiovascular diseases. Despite the advance of cancer therapy in recent decades, it still poses a significant challenge due to its complex and heterogenous appearance leading to a total of 10 million deaths worldwide in 2020, according to the world health organization (WHO). Therefore, the investigation of tumor biology is of high interest for understanding the key features that drive cancer formation. These hallmarks of cancer include the loss of differentiation, continuous proliferative signaling, resistance to cell death and growth suppression, and invasion. These hallmarks set the start of the formation of primary cancer that further leads to secondary metastases if the evasion from immune surveillance is guaranteed (Hanahan and Weinberg 2011; Joyce and Pollard 2009). Immune surveillance, the described immune response to degenerated, senescent, or damaged cells, is an important part of the maintenance of tissue integrity and protection against cancer formation. The interplay between the immune system and the tumor formation emerging from malignant cells thereby follows three phases illustrated by Mittal and colleagues in 2014: The first stage describes the elimination of the majority of the degenerated cells by immune cells, followed by an equilibrium in which selected tumor cells undergo mutations and epigenetic changes. These changes grant the tumor cells the selective advantage to escape the immune system which ultimately leads to the third phase. In this last stage, the evasion phase, the immune system is not able to detect the malignant cells which results in cancer development, eventually (Mittal et al. 2014).

2.1.2 Immune evasion strategies of solid cancers

Solid cancers are complex structures shaped by tumor cells and various other cells harnessed for their progression and development. The bi-directional interplay of the tumor cells and the surrounding environment plays a crucial role in the further development of cancer. Together with stromal cells, attracted anti-inflammatory immune cells, and the surrounding extracellular matrix (ECM) the cancer cells form a heterogenous tumor microenvironment (TME). The discovery of anti-inflammatory epitopes on tumor cells and inhibiting factors secreted by those and associated cells exploited by the tumor showed that a dynamic TME is established for cancer progression (Wang et al. 2017). These explain the poor immunogenicity in most solid tumor malignancies. A typical example of a solid

immunologically cold tumor is pancreatic ductal adenocarcinoma (PDAC/PAAD) which is characterized by a highly fibrotic and desmoplastic TME. Additionally, PDAC cells are known to produce and release several factors that interfere with anti-tumor immunity (Ullman et al. 2022). Early studies on solid tumors focused on inhibitory cytokines expressed by cancer-associated fibroblasts (CAF), tumor-associated macrophages (TAMs), and regulatory T cells, for example, TGF-β, IL-10, or PGE. Also, checkpoint molecules expressed on the tumor surfaces arose as a promising target for immunotherapeutic approaches (Jiang et al. 2019; Crane et al. 2012; Raz, Levine, and Khomiak 2000; Terres and Coffman 1998; Pardoll 2012). These immune checkpoints are described to interfere with T-cell activation by inhibiting intracellular mechanisms. Clinically approved immune-checkpoint inhibitors are monoclonal antibodies against PD-1 (Nivolumab) or CTLA-4 (Ipilimumab). These strategies led to better overall survival in melanoma patients and higher infiltration of circulating immune cells (Friedman et al. 2022; Eggermont et al. 2016). Also, ongoing studies of PD-1 blockade in combination with chemotherapy increased 1-year overall survival in PDAC patients (O'Hara et al. 2021). One can say, these novel therapeutic strategies tackling immune-checkpoint interactions have shown promising results in pre-clinical and clinical applications. In a broader spectrum, however, studies on solid cancers have remained widely disappointing (Patnaik et al. 2015; Royal et al. 2010; Wienke et al. 2021; Sahin et al. 2017).

2.1.3 Tumor cell metabolism influences the suppressive microenvironment

A reason infiltrating immune cells fail to elicit their cytolytic function is that they face a hostile matrix within the tumors, which is not only defined by the above-mentioned factors. Another big impact on the TME characteristics is closely related to the tumor cells' metabolism. Not only do cancer-associated cells secrete anti-inflammatory factors but also metabolites that have inhibitory functions on effector cells. It is described that metabolites like kynurenic acid, or lactic acid heavily interfere with T-cell metabolism that these cells do not function as intended. On the other hand, tumor cells consume vast amounts of nutrients from their surroundings to maintain their homeostasis regarding their need for fast proliferation and cell cycle progression (Ho et al. 2015; DePeaux and Delgoffe 2021; Binnewies et al. 2018; Giraldo et al. 2019). The main metabolite that is needed to ensure the synthesis of building blocks for proteins and nucleotides for proliferation is glucose. To meet their metabolic needs tumor cells within solid cancers heavily upregulate their glycolysis similar to activated immune cells (Figure 2). In 1924, the biochemist Otto Warburg first documented the phenomenon that neoplastic cells undergo a metabolic switch, similar to activated T lymphocytes. The so-called "Warburg effect" describes the feature of these cells to change their metabolism from the efficient ATP-producing

tricarboxylic acid cycle (TCA) to the more in-efficient glycolytic pathway even under aerobic conditions (Warburg, Wind, and Negelein 1927). Thereby pyruvate does not enter the TCA in the form of acetyl-CoA but is degraded to lactate to replenish nicotinamide adenine dinucleotide (NAD+) for glycolytic steps. The biological rationale for uncoupling glycolysis from the TCA is now well established. This process enables more glucose molecules to enter the glycolytic pathway, resulting in increased production of building blocks for nucleotide synthesis and amino acids through branching pathways such as the pentose-phosphate pathway (PPP) (Chen, Qian, and Wu 2015). The consequence resulting from the excessive uptake of glucose by the tumor cells is a drastic drop in the glucose concentration within the TME down to below 1 mmol/l (mM) in the tumor intestinal fluid (TIF)(Burgess and Sylven 1962; Sullivan et al. 2019). Due to limited diffusion and vascularisation of the tumors, the low glucose availability cannot be compensated to the entire extent. All of the above-mentioned factors impact the TME dynamics and lead to the formation of a "cold" tumor, which is characterized by decreased immunogenicity and a low abundance of immune cell infiltrates (Kleeff et al. 2016; Bonaventura et al. 2019).

There is a debate on whether glucose deprivation affects T cells since they still constitute the majority of the TME. In 2021 Reinfeld et al showed by [18F]fluorodeoxyglucose *in vivo* uptake – *ex vivo* analysis that glucose is predominantly consumed by T cells over tumor cells in various cancer cell lines (Reinfeld et al. 2021). However, it is not entirely solved if the need of the T cells is fulfilled since the competition for glucose in the TME is well described and glucose is an important player in T-cell functionality (Chang et al. 2015). Also, other tumor-associated cells like myeloid cells heavily impact glucose partitioning in the TME. Thus, the distribution and consumption in the TME is more complex than initially thought and remain to be in the focus of future studies (Reinfeld et al. 2021; Kohl, Kao, and Ho 2021).

2.1.4   Facilitative glucose transporters (GLUTs) in immune and tumor cells

To fulfill their energetic needs, tumor cells, and activated T cells are known to overexpress glucose transporters on the cell surface (Airley and Mobasheri 2007; Macintyre et al. 2014). Two main transporter groups are described for the transport of glucose in humans that are part of the solute carrier family (*SLC*). One group is the sodium–glucose linked transporters (SGLT encoded in *SLC5A*) that can transport glucose against the concentration gradient and rely on Na+ ions for symport. Members of this family are mostly expressed in cells of the luminal surface in the small intestine to take up diet or take over the task of physiologic renal glucose. The most ubiquitously expressed glucose transporter family in the human body and most relevant to immune and cancer cells are facilitative glucose

transporters (GLUT) encoded by the gene family *SLC2A*. Out of the over 400 SLCs, the GLUT family is composed of 14 members that facilitate the transport of hexoses or polyols down its concentration gradient. This passive transport guarantees the uptake of hexoses for basal respiration and can be regulated through expression attenuation or endosomal trafficking mechanisms from and to the plasma membrane depending on the extracellular glucose concentration and demand (Scheepers, Joost, and Schurmann 2004; Mueckler and Thorens 2013; Ancey, Contat, and Meylan 2018; Li et al. 2020). GLUTs are responsible for cellular glucose uptake in the brain (GLUT3/4), adipose tissue, heart, and skeletal muscles (GLUT3). Among the GLUT family, the most relevant facilitative glucose transporters for T cells and cancer cells are GLUT1 and GLUT3 which are encoded by the genes *SLC2A1* and *SLC2A3*, respectively. GLUT1 is most widely studied and known to be upregulated in many cancer types (Mueckler and Thorens 2013). It is a high-affinity glucose transmembrane transporter and consists of 12 alpha-helices. Its function is mediated by a Michaelis-Menten mechanism with a constant (K_M) of ~6.5mM, which means that most of the transporters are saturated in physiologic (~5mM) conditions (Manolescu et al. 2007; Burant and Bell 1992). This is especially crucial for highly glycolytic cancer cells and activated immune cells, which require a continuous supply of glucose to meet their energy demands. However, elevated GLUT1 expression is necessary at hypoglycemic conditions to maintain glucose uptake and meet metabolic needs. Hereby, GLUT1 expression is tightly correlated with cell metabolism, and its regulation and trafficking is strongly objected to the Protein kinase B (AKT)/ 5' AMP-activated protein kinase (AMPK) axis (Zhao et al. 2017). Since its involvement in cell survival, cancer progression, and metastasis is evident, new therapeutic approaches are evolving to interfere with GLUT1 activity (Cai et al. 2022; Yu et al. 2017). Studies revealed an equally high relevance in immune cells, as Geltink and colleagues showed that glucose deprivation *in vitro* conditioned murine CD8+ T effector cells (T_{eff}) for elevated GLUT1 expression and metabolism when reintroduced in physiologic glucose conditions. This approach increased the anti-tumor function *in vitro* and *in vivo*. In CD4+ T cells, GLUT1 is shown to be essential for effector function and it is described that GLUT1 can modulate mammalian target of rapamycin (mTOR) activity independent from glucose concentration and AMPK involvement (Macintyre et al. 2014; Buller, Heilig, and Brosius 2011). Previous data generated by Cretenet and colleagues could already demonstrate augmented functional activity of GLUT1 overexpressing T cells in hyperglycemic *in vitro* conditions (Cretenet et al. 2016).

2.2 Metabolic reprogramming in T cells

2.2.1 The metabolic switch is a key factor in T-cell activation and maturation

T cells as the main effector immune cells in the human body play a crucial role in responding quickly to pathogens and degenerated cells. In particular, CD8+ T lymphocytes (CTL) are essential for eliminating tumors through major histocompatibility complex I (MHC-I)-restricted cytotoxicity. To achieve this, CD8+ T cells must undergo clonal expansion and produce cytotoxic proteins as well as pro-inflammatory cytokines. Upon a primary cognate antigen recognition on an MHC-I molecule in combination with a co-stimulatory input via CD28, the downstream AKT/mTOR - pathway is stimulated via upregulated phosphatidylinositol-3-kinase (PI3K) activity that in turn initiates a broad cascade of gene regulatory pathways. These pro-inflammatory pathways ensure further recruiting of immune cells via cytokine-dependent paracrine mechanisms as well as immune-modulatory and supporting pathways within the cell. Changes in the metabolic state of the effector cells are of very high importance in this process. Unlike resting naive T cells that rely mainly on oxidative phosphorylation (OXPHOS) and display a quite moderate metabolism, activated T_{eff} cells rapidly upregulate their glutaminolysis and glycolysis to elicit their function for cytokine production and proliferation (Figure 2)(Menk et al. 2018; Gudmundsdottir, Wells, and Turka 1999; Rangel Rivera et al. 2021; Bental and Deutsch 1993). However, T_{eff} cells are also described to show plasticity regarding the interplay between glycolysis and OXPHOS, since the latter is important for proliferation and survival (Figure 2)(Chang et al. 2013). Nevertheless, glucose availability is highly needed for proper T-cell function. In the absence of glucose, the glycolysis enzyme Glycerinaldehyd-3-phosphat-Dehydrogenase (GAPDH) is known to inhibit interferon-gamma (INF-γ) transcription by binding to AU-rich elements upstream of the gene (Chang et al. 2013). While cytokine production is reliant on glucose availability, glucose uptake itself is heavily dependent on extrinsic stimuli provided by cytokine engagement. Cytokines like interleukin 7 (IL-7) are signaling via the AKT pathway and act to translocate GLUT1 on the cell surface to take up enough glucose for downstream breakdown and prevention of atrophy (Rathmell et al. 2000; Cham and Gajewski 2005; Edinger and Thompson 2002). In the further course of T-cell activation, the differentiation to memory subsets is vital to prevent the relapse of cancer arising from potentially dormant tumor cells. Therefore, a small proportion undergoes a second metabolic change characterized by a balanced metabolism expressed by intermediate glycolysis, mitochondrial biogenesis and OXPHOS, fatty acid oxidation (FAO), and *de novo* lipogenesis and reside as memory cells in secondary lymphoid tissues. As important as for the activation, mTOR is also known to play a key role in the process of memory T-cell formation. (Araki et al. 2009; Lee et al. 2010; Powell and Delgoffe 2010). These cells have the potential for a rapid reaction if they re-encounter the antigen.

Hereby effector memory T cells (T_{EM}) have the potential to increase their glycolysis and mitochondrial activity way beyond primary stimulated T_{eff} cells (Figure 2)(van der Windt et al. 2013). At this stage, the T cells are dependent on glucose for proper reactivation and inflammatory response (Ecker et al. 2018).
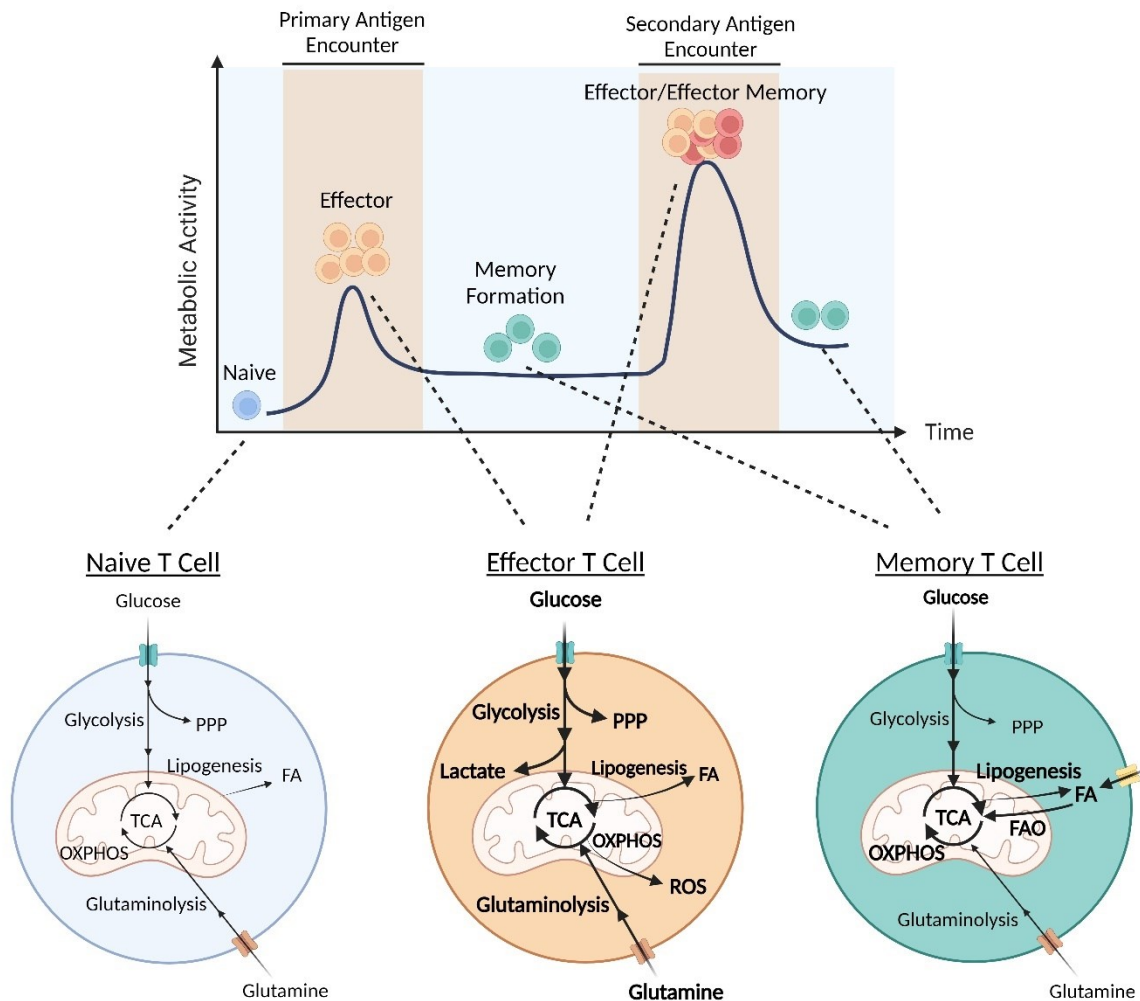
Figure 2 Metabolic profile of naive, effector, and memory T cells
FA = Fatty Acid; FAO = Fatty Acid Oxidation; OXPHOS = Oxidative Phosphorylation; PPP = Pentose Phosphate Pathway; ROS = Reactive Oxygen Species; TCA = Tricarboxylic Acid Cycle; Created with BioRender.com; Adapted from (Zhang and Romero 2018; Rangel Rivera et al. 2021).

2.2.2 "Bottom-Up" signaling in T cells influences inflammation and memory formation

After T-cell stimulation, the canonical metabolic change initiates a well-described characteristic pattern that addresses the cellular needs for activation, memory formation, and long-term persistence. By regulating the metabolic transition in the activation phase after antigen recognition, the cell

produces several metabolites and factors to perpare for further maturation steps. The increased metabolism leads to the enrichment of intermediates that heavily influence key enzymes, trigger post-translational glycosylation, interfere with the activity of RNA-binding proteins, or even impact the epigenetic regulation in the cells (Carey et al. 2015; Chang et al. 2013; Araujo et al. 2017). This is referred to as "Bottom-up" metabolic signaling which describes the potential of environmental factors or metabolites to modulate the signaling network of a cell in contrast to "top-down" signaling represented by canonical TCR-activation impacting metabolic pathways downstream (Shyer, Flavell, and Bailis 2020). An example of a bottom-up signaling metabolite is acetyl-Coenzyme A (Acetyl-CoA) downstream of glycolysis, which has the potential to act in an epigenetic fashion. It is tightly correlated to glucose uptake via glucose transporters as it leads to chromatin modification by acting as an acetyl-donor as Hochrein and colleagues described in 2022. Hereby they showed that the glycolytic transition influences the inflammatory gene expression in T-helper cells through acetyl-CoA production (Hochrein et al. 2022). Also, it is described by Araujo et al. that elevated glycolysis mitigates the branching of fructose-6-phosphate to N-glycosylation in the hexosamine biosynthesis pathway (HBP). The HBP is known to drive regulatory T cells instead of Th17 formation. However, the HBP is a highly dynamic system and is also important for thymocyte differentiation and clonal expansion of peripheral T cells via c-myc stabilization. Further gene regulatory metabolites are the tricarboxylic acid cycle (TCA) intermediates α-ketoglutarate, succinate, and fumarate. α-ketoglutarate activates histone and DNA-demethylases and promotes the oxygen-sensing HIF prolyl hydroxylases (PHDs) as co-substrates that inhibit the function of hypoxia-inducible factor 1 alpha (HIF-1α). Accumulation of succinate and fumarate, in contrast, is shown to counteract α-ketoglutarate. Particularly in the HIF1-α axis, succinate and fumarate inhibit PHD resulting in HIF1-α downstream signaling. HIF1-α is described to improve and prolong T_{eff} activity and helps to overcome T-cell exhaustion. Additionally, CD8+ tumor-infiltrating lymphocytes (TILs) benefit from HIF1-α signaling by differentiation to tissue-resident memory-like (T_{rm}-like) cells which increase anti-tumor efficacy (Doedens et al. 2013; Liikanen et al. 2021).

2.2.3   Reactive Oxygen Species (ROS) and glutathione (GSH) balance is essential for T-cell differentiation and function

TCA upregulation not only increases certain intermediates but also impacts the electron-transport chain (ETC) which is the main source of reactive oxygen species (ROS) production through electron leakiness in complex I and III leading to partial O_2 reduction (Loschen, Azzi, and Flohe 1973; Turrens et al. 1982; Yarosz and Chang 2018; Kaminski et al. 2013). ROS production by the mitochondrial ETC complexes is tightly correlated to glucose concentrations as hyperglycemia causes excessive ROS

accumulation (Nishikawa et al. 2000). ROS for itself is a central second messenger signaling molecule in T-cell function, reprograming, and development. ROS activates key pathways involved in gene expression for survival and cytokine production like interleukin-2 (IL-2), including mTOR and the transcription factors nuclear factor kappa-light-chain-enhancer of activated B-cells (NFκB) and nuclear factor of activated T-cells (NFAT)(Klein Geltink, O'Sullivan, and Pearce 2017; Mak et al. 2017; Wang et al. 2011; Sena et al. 2013). However, ROS has to be seen as a double-edged sword, since excessive ROS production can lead to oxidative damage of cells and tissues. The state of oxidative stress leads to immunosuppression and ultimately to apoptosis by protein oxidation, lipid peroxidation, and DNA damage (Ghosh and Mitchell 1999; Ghosh et al. 2015; Kaminski et al. 2007; Kaminski et al. 2012) Therefore, ROS concentrations in the cells are tightly regulated by anti-oxidant mechanisms. In mitochondria and peroxisomes, ROS in the form of H_2O_2, is enzymatically reduced to H_2O and O_2 by catalase (CAT) (Ganguli, Mukherjee, and Sonawane 2019; Dan Dunn et al. 2015). The main anti-oxidative response in T cells is regulated by the Nuclear Factor Erythroid-derived 2-like 2 (Nrf2) pathway that leads to Glutathione (GSH) production in downstream pathways and also regulates GSH recycling (Harvey et al. 2009). GSH in its interplay with ROS is essential for immune function and maintaining homeostasis within the cell. As GSH is a tripeptide consisting of γ-L-glutamyl-L-cysteinyl-glycine its *de novo* biosynthesis is dependent on the glutamine catabolism upstream which is critical for T-cell differentiation. While GSH production is essential for the linage decision, Lian and colleagues discovered that its recycling process from its oxidized form glutathione disulfide (GSSG) is important to regulate the redox homeostasis by balancing the GSH:GSSG ratio, which is an indicator of cellular oxidative stress (Lian et al. 2018; Hamilos, Zelarney, and Mascali 1989). GSH recycling is enzymatically controlled by glutathione reductase (GR) under consumption of the cofactor nicotinamide adenine dinucleotide phosphate (NADPH) (Harvey et al. 2009; Wang, Ahn, and Asmis 2020). Maintaining a stable NADPH equivalent is crucial for detoxifying ROS, to which cells respond by upregulating the PPP to replenish this pool (Christodoulou et al. 2019; Daneshmandi et al. 2021). In addition to fuelling the oxidative PPP, glucose anaplerosis also supports NADPH production (Moon et al. 2020). This makes glucose a central piece of ROS production and the maintenance of redox balancing, largely through the generation of NADPH and GSH recycling.

2.3   Adoptive T-cell therapy (ACT)

2.3.1   The different principles of adoptive T-cell therapy

The first-line treatment of cancer diseases is chemotherapy, surgical resection, radiotherapy, sequential conduction, or combinations of those. Responsive failure, adverse reactions, or relapse is

frequently occurring in these therapeutic approaches urgently demanding novel strategies for cancer treatment(Ping et al. 2020; Debela et al. 2021). To rebalance the disturbed equilibrium between immunosurveillance and tumor, the approach of harnessing the cytotoxic potential of TILs paved the way for autologous cellular immunotherapy. The procedure of adoptive T-cell therapy (ACT) includes the isolation from tumor biopsies, *ex vivo* expansion, and reinfusion of TILs which has emerged as an effective treatment of solid cancers (Kalos and June 2013; Melief 1992). However, the ACT using TILs is strongly dependent on sufficient numbers of tumor infiltrates and accessibility for biopsy to promise therapeutic success (Rosenberg et al. 1988). Modern approaches focus on genetically engineered peripheral blood circulating lymphocytes. Therefore, T cells harvested from the patients via apheresis and genetically modified by lenti- or retroviral vectors encoding a high-affinity tumor-antigen specific chimeric antigen receptor (CAR) or T-cell receptor (TCR). Whereas TCR therapy relies on the native T-cell receptor structure, CARs are artificial receptors that combine a single-chain variable fragment (scFv) consisting of the V_H and V_L regions of an antigen-specific monoclonal antibody in combination with intracellular signaling domains. Clinical trials using a CD3ζ intracellular signaling domain were not able to show effective outcomes. Adding the co-stimulatory domains CD28 or 4-1BB to these first-generation CARs lead to improved function and achieved significant results in pre-clinical and clincal studies (Wang et al. 2007; Hombach and Abken 2013). Due to their superior anti-tumor capacity, proliferation, and cytokine production, anti-CD19 second-generation CARs were first approved by the FDA for clinical treatment of relapsed and refractory acute lymphoblastic leukemia (ALL) and large B cell lymphoma in 2017 ('Tisagenlecleucel (Kymriah) for ALL' 2017; 'Axicabtagene ciloleucel (Yescarta) for B-cell lymphoma' 2018). In 4th- or next-generation CARs, more combinations of target-antigen scFv, co-stimulatory, and cytokine signaling domains were developed to further increase CAR T-cell efficacy, persistence, and safety (Tokarew et al. 2019; Andrea et al. 2020). Solid tumors, however, present more difficulties regarding the accessibility and persistence of CAR T cells. This is shown in limited response rates in studies in most entities like glioblastoma, gastrointestinal cancer, or pancreatic cancer (O'Rourke et al. 2017; Hou et al. 2019; Yeo et al. 2022). Combinatorial approaches of immune-checkpoint blockade and ACT demonstrate potential, but still, it needs to be seen how it translates to the human system (Hu et al. 2019; Liu et al. 2021; Ping et al. 2020).

## 2.3.2   Metabolic engineering and adoptive T-cell therapy

In several preclinical studies, the metabolic interference or engineering of immune cells for ACT are currently under investigation. Direct metabolite supplementation in the process of CAR generation have shown to shape the cellular phenotype. While amino acids like arginine and asparagine increase

the responsiveness of T cells, 2-deoxyglucose interferes with glycolysis and consequently influences the memory formation (Sukumar et al. 2013; Wu et al. 2021; Geiger et al. 2016). Other studies suggest genetically engineered immune cells for ACT that either affect the direct metabolism, the uptake of metabolites or associated pathways. Fultang and colleagues proposed the first metabolically engineered CAR T cells by direct modification of the enzyme arginosuccinate synthesase (ASS) and ornithine transcarbamylase (OCT). This led to increases proliferation of CAR T cells which simultaneously maintained their cytotoxic efficacy (Fultang et al. 2020). Another aspect is the elevated metabolic activity in CAR T cells that pose a challenge combined with the highly oxidative TME which needs to be considered for ACT as well. As mentioned above, ROS balance is of high importance for immune cells in order to mature and fulfil their cytolytic functions. To protect T cells from oxidative stress, Ligtenberg and colleagues genetically engineered CAR T cells to overexpress the hydrogen peroxide decomposition enzyme CAT. CAT not only maintained the cytolytic activity under oxidative stress but also protected bystander cells from ROS and therefore led to a synergistic effect (Ligtenberg et al. 2016). In general, metabolic engineering gives a wide spectrum for ACT regarding the TME, cellular nutrition, and enzymatic activities which needs to be addressed extensively to enhance cellular therapy against solid malignancies.

2.4   Research hypothesis and objective

ACT demonstrates a promising and strong tool for novel therapeutic strategies against solid cancer. However, the hostile TME and low glucose concentration prevailing in the TIF offer a big challenge for positive outcome of cellular therapy, as displayed above. In order to improve existing cellular therapies, we are presenting a strategy to overcome the adverse glucose concentration in the TME by *Slc2a1*/ GLUT1 overexpression in T cells. The present work should elaborate the impact of constitutive ectopic *Slc2a1*/GLUT1 (Transcript isoform NM_011400.3) overexpression in primary murine CD8+ T cells (CD8+[Slc2a1]) and investigate following points:

- *In vitro* characterisation of GLUT1 overexpression in primary CD8+ T-cell function in physiologic and hypoglycemic conditions
- Characterisation of the influence of GLUT1 overexpression on T-cell metabolism and transcription in physiologic glucose and hypoglycemic conditions
- Understanding the connections and consequences of metabolic and transcriptomic reprogramming in activated CD8+[Slc2a1] T cells
- Examine antigen-specific anti-tumor effects of CD8+[Slc2a1] T cells *in vitro* and *in vivo*

13
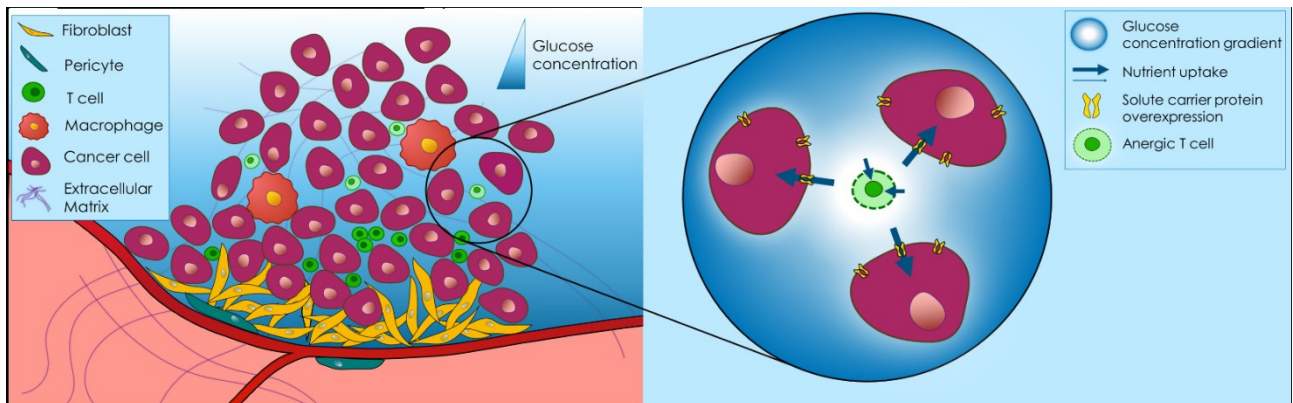
Figure 3 Schematic presentation of the project rationale
TILs facing a hostile TME with hypoglycemic conditions that inhibit proper effector functions. Does ectopic *Slc2a1*/GLUT1 overexpression in CD8+ T cells overcome this hurdle? Do these cells undergo metabolic and transcriptomic reprogramming and what are possible consequences?

3. Material and Methods

3.1 Compounds

Compound	Manufacturer	Catalog ID
2-DG	Sigma Aldrich	D8375
Agarose Standard	Carl Roth	3810.3
Antimycin A	Sigma Aldrich	A8674
Beta-mercaptoethanol	Sigma Aldrich	M6250
Brefeldin A Solution (1,000X)	Biolegend	420601
BSA	Carl Roth	2834.3
CellROX™ Deep Red	Thermo Fisher	C10491
CellTrace Far Red	Thermo Fisher	C34572
CellTrace Violett	Thermo Fisher	C34557
CountBright™ Absolute counting beads	Thermo Fisher	C36950
D-Glucose min 99,5% CELLPURE	Carl Roth	HN06.1
Dimethyl sulfoxide	Sigma Aldrich	D2650
DMEM, high glucose, pyruvate, no glutamine	Thermo Fisher	21969-035
Dynabeads Mouse T-Activator CD3/CD28	Thermo Fisher	11453D
eBioscience™ UltraComp eBeads	Thermo Fisher	1-2222-41
EDTA	AppliChem	A1103
Ethanol Absolute >99,8%	Carl Roth	9065.1
Fast Digest EcoRI	Thermo Fisher	FD0274
Fast Digest NotI	Thermo Fisher	FD0593
FBS, QUALIFIED	Technologies	10270106
FCCP	Sigma Aldrich	C2920
Fixation buffer	Biolegend	420801
Formaldehyde Solution 37%	Carl Roth	7398.1
Glucose-Glo™ Assay	Promega	6022
Hepes Buffer	PAN	P05-01100
Intracellular Staining Permeabilization Wash Buffer (10X)	Biolegend	421002
L-Glutamine min 99% CELLPURE	Carl Roth	HN08.2
Lipofectamine™ 3000	Thermo Fisher	L3000008

Midori Green Xtra	Nippon	MG10
Monensin Solution (1,000X)	Biolegend	420701
Nuclease-Free Water	Thermo Fisher	AM9937
NucleoSnap Plasmid Midi kit for plasmid	Macherey-Nagel	740494.50
Nucleospin plasmid	Macherey-Nagel	740588
Oligomycin	Sigma Aldrich	495455
Opti-MEM™ I Reduced Serum Medium, no phenol red	Gibco	11058021
OVA (257 - 264) SIINFEKL	ANASpec	AS-60193-1
PBS	Pan Biotech	P04-36503
Penicillin/Streptomycin	Pan Biotech	P06-07100
Phusion High-Fidelity DNA Polymerase	Thermo Fisher	F530L
Pierce™ Hoechst 3342	Thermo Fisher	62249
Polybren	Merck Millipore	TR-1003-G
Poly-L-Lysine Solution Bioreagent 0,01%	Sigma Aldrich	P4832
QIAzol Lysis Reagent	Quigen	79306
RBC Lysis Buffer (10X)	Biolegend	420301
Recombinant human Interleukin 2	Immunotools	11340027
recombinant murine IL-15	Immunotools	12340155
Retronectin	Takara	T100B
Rotenone	Sigma Aldrich	R8875
RPMI 1640, w: L-Glutamine, w: 2.0 g/L NaHCO3	PAN Biotech	P04-16500
RPMI1640 W/O GLUCOSE	Biotrend	01-101-1A
Seahorse XFe96 FluxPak	Agilent	102416-100
Sodium pyruvate 100mM	Pan Biotech	P04-43100
T4 DNA Ligase	Thermo Fisher	EL0014
ThiolTracker™ Violet	Thermo Fisher	T10095
True-Nuclear transcription factor buffer	Biolegend	424401
Trypan Blue Stain (0.4%)	Invitrogen	T10282
Trypsin-EDTA (0,05%), phenol red (Gibco)	Thermo Fisher	25300054
XF RPMI Medium pre-pH7.4, 1mM HEPES	Agilent	103576
Zombie NIR Fixable Viability Kit	Biolegend	423105

3.2 Antibodies

Antibody	Clone	Manufacturer	Catalog ID
Alexa Fluor® 594 Donkey anti-Rabbit	Poly4064	Biolegend	406418
Alexa Fluor® 647 Anti-Glucose Transporter GLUT1	EPR3915	Abcam	ab195020
Alexa Fluor® 647 Goat anti-rat	Poly4054	Biolegend	405416
Anti- 5-Methylcytosine (5-mC)	RM231	Thermo Fisher	MA5-24694
Anti-5-hydroxymethylcytosine (5-hmC)		Diagenode	C15220001-50
APC anti-mouse CD95 (Fas)	SA367H8	Biolegend	152604
APC Mouse IgG1, κ Isotype Ctrl (FC)	MOPC-21	Biolegend	400121
Brilliant Violet 421™ anti-mouse CD69	H1.2F3	Biolegend	104545
Brilliant Violet 421™ Armenian Hamster IgG Isotype Ctrl	HTK888	Biolegend	400935
Brilliant Violet 510™ anti-mouse CD279 (PD-1)	29F.1A12	Biolegend	135241
Brilliant Violet 510™ anti-mouse CD8a	53-6.7	Biolegend	100751
Brilliant Violet 510™ Rat IgG2a, κ Isotype Ctrl	RTK2758	Biolegend	400547
Brilliant Violet 650™ anti-mouse CD25	PC61	Biolegend	102038
Brilliant Violet 650™ anti-mouse/human CD44	IM7	Biolegend	103049
Brilliant Violet 785™ anti-mouse CD62L	MEL-14	Biolegend	104440
Brilliant Violet 785™ anti-mouse CD69	H1.2F3	Biolegend	104543
Pacific Blue™ anti-human/mouse Granzyme B	GB11	Biolegend	515408

Pacific Blue™ Mouse IgG1, κ Isotype Ctrl	MOPC-21	Biolegend	400131
PE anti-human/mouse TCF-7/TCF-1	S33-966	Biolegend	564217
PE anti-mouse Perforin	S16009A	Biolegend	154306
PE anti-mouse/human CD44	IM7	Biolegend	103008
PE Rat PE Rat IgG2a, κ Isotype Ctrl	RTK2758	Biolegend	400507
PE/Cy7 anti-mouse CD127 (IL-7Rα)	A7R34	Biolegend	135014
PerCP anti-mouse CD8a	53-6.7	Biolegend	100732
Ultra-LEAF™ Purified anti-mouse CD3ε Antibody145-2C11		Biolegend	100340
Ultra-LEAF™ Purified anti-mouse CD28 Antibody 37.51 functional grade		Biolegend	102116
TruStain FcX™ (anti-mouse CD16/32)		Biolegend	101320
AffiniPure Goat Anti-Armenian Hamster IgG (H+L)		JacksonImmunoResearch	127-005-099
PE anti-mouse CD107a (LAMP-1)		Biolegend	121612

3.3   Technical devices

Device	Manufacturer
CelldropFL Cellcounter	Biozym
Centrifuge 5424 R G	Eppendorf
Centrifuge 5910 R G	Eppendorf
Centrifuge Rotina 420R	Hettich GmbH
CFX connect real-time PCR detection system	Biorad
CO2 – Incubator (BD6220)	Heraeus, ThermoFischerScientific
CytoFlex LX MPL	Beckmann Coulter
CytoFlex S MPL	Beckmann Coulter
DS11FX+ Spektrophotometer	Biozym
GelDoc E-Box-Cx5.TS Edge	Vilber Lourmat
ImageStreamX Mk II Imaging Flow Cytometer	Amnis
MyTemp Mini Digital Incubator	Biozym

MoFlo Astrios Cell Sorter	Beckmann Coulter
Multi-Detection Reader Cytation 1	BioTek/Agilent
Powerpac hc power supply	Biorad
Seahorse XFe96 Analyzer, S7800A	Agilent
T100 thermal cycler	Biorad
Thermomixer C	Eppendorf
Thunder Imager 3D	Leica
BioTek Cytation 1 Cell Imaging Multimode Reader	BioTek/Agilent

3.4   Cell lines

For retrovirus production, we used 293Vec-Galv and 293Vec-Eco which were a kind gift of Dr. Manuel Caruso, Québec, Canada, and Prof. Dr. med. Sebastian Kobold, LMU, Munich. These cell lines have been previously described by Ghani et al. (2009). The murine adenocarcinoma cell line PancO2 (A kind gift from Prof. Dr. med. Sebastian Kobold) served as a model for solid tumors. Using this cell line, the epitope proteins epithelial cell adhesion molecule (EpCAM; UNIPROT ID Q99JW5; PancO2-EpCAM), and chicken-derived ovalbumin antigen (OVA/SIINFEKL; UNIPROT ID P01012; Panc02-OVA), as well as the red fluorescent marker mCherry (Panc02-OVA-mCherry/Panc02-EpCAM-mCherry), were retrovirally introduced to fit the experimental settings (Karches et al. 2019). For this purpose, the retrovirus was produced in 293-Vec-Eco based on the pMP71 retroviral vector (kind gift by Prof. Dr. med. Sebastian Kobold).

3.5   TCGA data analysis

To elaborate the impact of *SLC2A1* expression on survival in pancreatic adenocarcinoma we utilized the tool GEPIA (Tang et al. 2017). We compared cancer cell expression from the TCGA (The Cancer Genome Atlas) and GTEx datasets (Genotype Tissue-expression). The cut-off for overexpression analysis was set at $\log_2(x)=1$, $P < 0.05$ was considered as statistically significant. The expression data was log2(TPM+1) transformed for differential analysis and the fold change (log2(FC)) was defined as median (Tumor TCGA) – median (TCGA normal + GTEx normal) in $\log_2$ scale.

3.6   Isolation of murine splenocytes

Spleens from 8-16 week-old C57BL/6 or C57BL/6-Tg(TcraTcrb)1100Mjb/J mice were harvested and meshed through a 70µm strainer. Erythrocytes were lysed for 2min in erythrocyte lysis buffer (BioLegend), and cells were washed in 1xPBS or mTCM and used for murine transduction.

3.7   Murine transduction and T-cell culture

Splenocytes were activated in murine T Cell Medium (mTCM; RPMI1640, 10%FCS, 1mM Na-Pyruvate, 2mM L-Glutamine, 1-5mM HEPES, 100U/ml P/S, 55µM beta-mercaptoethanol) with CD3ε antibodies (ABs, Biolegend, 1µg/ml), CD28 ABs (Biolegend, 0.1µg/ml) and 10U/ml hrIL2 (Immunotools) at a cell density of $2x10^6$/ml overnight. The next day, 2ml virus supernatant from 293Eco producer cell lines were bound to RetroNectin (16µg/ml; Takara Bio) and goat anti-hamster (50µg/ml; Jackson Immuno Research) coated 24-well plates at 4000g at 4°C for 2h. Prestimulated T cells were resuspended in mTCM containing 0.5µg/ml CD3ε ABs and 0.5µg/ml CD28 ABs (Biolegend), spinoculated at 800g at 30°C for 30min and incubated at 37°C, 5%CO_2 and 95% humidity for 24h. Transduced T cells were further cultivated each 2-3 days in mTCM +50ng/ml mrIL-15 (Immunotools, Biolegend) at an adjusted cell number of 10^6 cells/ml. Functional assays were conducted at least 5 days post-transduction.

3.8   Flow cytometry

Flow cytometric analysis (FACS) was used as a readout for *in vitro* activation, proliferation, and long-term memory formation. Cells were incubated in FACS buffer containing 2.5µg/ml conjugated antibodies and Zombie NIR or Violet according to the manufacturer's instructions for 20 min at 4°C. CellROX^{TM} Deep Red (2µM, Thermo) and ThiolTracker^{TM} Violet (5µM, Thermo) were stained parallel to antibody (AB) staining. After a washing step in FACS buffer, cells were resuspended in 100µl FACS buffer (PBS, 0.1% BSA, 0.5mM EDTA) for direct or FACS Fix (FACS buffer + 3% formaldehyde) for later analysis or subsequent intracellular staining. For *ex vivo* FACS analysis, spleens were processed as described above. Fc receptor block was performed using 10µg/ml TruStain FcX™ PLUS (anti-mouse CD16/32, Biolegend) for 10min at room temperature, followed by extracellular and live/dead staining as described for *in vitro* flow cytometric analysis. FACS data were acquired on CytoFLEX S or CytoFLEX LX (Beckmann Coulter GmbH), and FlowJo 10.8.1 was used for analysis.

3.9   Amnis ® ImageStream analysis

ImageStream analysis was used to determine GLUT1 surface expression on transduced murine T cells. Cell preparation was conducted as described for Flow Cytometry. For Data analysis, IDEAS® and FlowJo 10.8.1 were used.

3.10   Restimulation experiments

Transduced T cells (CD8+$^{MOCK/Slc2a1}$) were washed in 1x PBS and resuspended in mTCM, physiologic Medium (physioRPMI; RPMI1640, 10%FCS, 5mM D-Glucose, 0.5mM L-Glutamine, 5mM HEPES, 100U/ml P/S, 55µM beta-mercaptoethanol), or hypoglycemic medium (hypoRPMI; 10%FCS, 0.5mM D-Glucose, 0.5mM L-Glutamine, 5mM HEPES, 100U/ml P/S, 55µM beta-mercaptoethanol) at a density of 0.5-2x10^6/ml. T cells were stimulated with 0.5µg/ml CD3ε/CD28 Abs (Biolegend) and plated on goat anti-hamster precoated (0.05mg/ml, Jackson Immuno Research) plates.

3.11   Proliferation assays

Proliferation was measured by FACS in a Cell Trace^{TM}-based assay. Overnight pre-stimulated murine splenocytes were stained with Cell Trace violet on the day of transduction according to the manufacturer's protocol (Biolegend). The transduction process was conducted as described above in hypoRPMI, physioRPMI, and mTCM, respectively. T cells were cultured as previously prescribed for T-cell culture in respective media and proliferation was evaluated on days 1, 3, 5, and 7 post-transduction.

3.12   Glucose uptake assay

The glucose uptake capacity of transduced murine T cells was performed using the Glucose Uptake-Glo™ Assay (Promega). Therefore, transduced OT-I T cells were activated in physioRPMI with 100ng/ml SIINFEKL peptide for 4h. For the assay, 10^5 cells were seeded in Poly-L-Lysine precoated half area 96-well bottom plates and it was proceeded according to the manufacturer's protocol using half of the recommended volumes. The colorimetric readout was performed using the Cytation 1 (BioTek/Agilent). For data analysis, the Gen5 software was used.

3.13   Extracellular flux assays

Transduced murine T Cells were activated in mTCM with 100ng/ml soluble SIINFEKL peptide (ANASpec) for 6 hours. Cells were washed in 1x PBS and resuspended in Glycolysis Stress Test Medium (Seahorse XF RPMI medium, pH 7.4, 2mM L-Glutamine, Agilent) or either Mito Stress Test Medium (Seahorse XF RPMI medium, pH 7.4, 5mM Glucose, 2mM L-Glutamine, Agilent), respectively. 2.2×10^5 cells per well were seeded in Poly-L-Lysine precoated (0.05mg/ml) Seahorse assay plates and analyzed in the Seahorse flux analyzer according to the manufacturer's protocol. Analysis was conducted in the Wave software. For the Glycolysis Stress Test the following reagents were injected in sequential order: A) 5mM Glucose (Roth), B) 1.5µM Oligomycin (Sigma Aldrich), and C) 50mM 2-DG (Sigma Aldrich) + 8µM Hoechst3342 (ThermoFisher) and for the Mito Stress Test, A) 1.5µM Oligomycin (Sigma Aldrich) B) 1µM FCCP (Sigma Aldrich, B) and C) 0.5µM Rotenone/Antimycin A (Sigma Aldrich) + 8µM Hoechst3342 (ThermoFisher). For the flux assay 3 baseline measurements were followed by injection A, 3 measurement cycles, Injection B, 3 measurement cycles, Injection C, and 3 measurement cycles. Each measurement cycle consisted of 3 min mixing and 3 min measurement time frames. For normalization cell counts were measured via Hoechst staining in the Cytation1 analyzer (Agilent) with the implemented cell measurement software (Agilent).

3.14   Imaging-based real-time killing assay

Transduced murine OT-I T cells were cultivated for 7-10 days post-transduction and prepared for Fluorescence-Activated Cell Sorting (FACS) by CD8a staining (PE, Biolegend, 1:200) and Zombie NIR™ Fixable Viability (Biolegend, 1:1000) staining in FACS-buffer. Enrichment of transduced CD8+ T cells was performed by CD8+/GFP+ double positive sorting. Subsequently, sorted cells were reactivated with CD3/CD28 Dynabeads^{TM} (Thermo, 2.5cells/bead), 10U/ml hrIL2, 50ng/ml mrIL15 supplemented mTCM for two days and were further cultivated in mTCM +50ng/ml mrIL-15 for 7-8 days. For the imaging-based killing assay, pancO2-OVA-EpCAM-mCherry target cells were Hoechst3342 (ThermoFisher) stained (10µM) at 37°C, for 15 min, washed, and seeded at 3×10^4 cells per well in mTCM. After 3h, the target cells were co-cultivated with sorted CD8+^{Slc2a1} and CD8+^{MOCK} cells in RPMI1640, 10%FCS, 5mM, 2mM, or 0.5mM D-Glucose, 2mM L-Glutamine, 1mM Sodium Pyruvate, 5mM HEPES, 100U/ml P/S and 55µM beta-mercaptoethanol at different effector to target (E:T) ratios. The kinetic was monitored for up to 4 days in 1:30h imaging intervals.

3.15 Degranulation assay

For degranulation OT1 T cells were cultured as described for the killing assay, but without sorting. For the degranulation T cells were restimulated with pancO2-OVA cells at an E:T ratio of 1:1 incubated with 0.2mg/ml anti-CD107a ABs for 1 hour before a golgi stop was performed. The golgi stop was conducted using Brefeldin A (Biolegend) and Monensin (Biolegend) according to manufacturers´ instructions for 4 hours before the cells were stained and analysed as described in the FACS section above.

3.16 Next-generation sequencing – Bulk RNA-Seq and analysis

3 x 10^6 CD8+ ^{Slc2a1} and CD8+^{MOCK} Cells were restimulated with 1µg/ml CD3ε and CD28 Abs in RPMI1640, 10%FCS, 5mM or 0.5mM D-Glucose, 2mM L-Glutamine, 1mM Sodium Pyruvate, 5mM HEPES, 100U/ml P/S, 55µM beta-mercaptoethanol as described above for 18h. Non-stimulated controls were kept in respective medium without stimulating antibodies and were harvested 4h post-seeding. After harvesting the cells were washed with ice-cold PBS and lysed in 700µl QUAzol (QIAGEN). Library preparation and sequencing (Illumina Nextseq1000) was done by LAFUGA (Gencenter Munich). Sequencing was conducted in a depth of 20x10^6 reads. The results were processed and mapped on the Galaxy analysis platform, and processing tools were provided by LAFUGA. After demultiplexing and clipping the 10bp seed sequences, the reads were aligned to the mm10 mouse reference genome sequence. DESeq2 calculations were performed with the HTSeq counts for quantitative differential gene expression analysis.

3.17 Metabolomic analysis

7-8 days post-transduction CD8+^{Slc2a1} and CD8+^{MOCK} cells were reactivated in physioRPMI or hypoRPMI in 6-Well plates at a density of 2x10^6 cells/ml as described before. After 18h incubation, cells were resuspended, centrifuged, and the SN was saved for metabolite analysis. Further, cells were washed twice in ice-cold PBS, 6x10^6 cells were pelleted per sample, and snap frozen in liquid N_2 for quantitative metabolomic analysis. For tracking of metabolite labeling, the supernatant of the culture was replaced by the respective media supplemented with the stable isotypes [U13-C6]glucose or [U13C5]L-glutamine, respectively, after 16h. After 2h of labeling, cells were washed and prepared for mass-spectrometric analysis as described for quantitative analysis. Further sample preparation and LS/MS analysis of water-soluble metabolites were conducted in collaboration with Dr. Werner Schmitz at the campus for biochemistry and molecular biology of the Julius-Maximilians-University Würzburg. The

samples were technically normalized to Lamivudin and data was normalized to total metabolites measured.

3.18 Integrated statistical analysis

Integrated Over Representation Analysis (ORA) of up- and down-regulated Metabolomic and RNA-Seq Data were analyzed using the IMPaLA Web Tool (Kamburov et al. 2011). KEGG Gene Set Enrichment (GSEA) pathway identification and network creation were conducted using the Metaboanalyst Web Tool (Xia and Wishart 2011). The degree centrality measures and betweenness centrality measures are calculated. First mentioned shows the number of links that connect to a node and second mentioned describes the number of shortest paths from all nodes to all the others that pass through a given node.

3.19 Animal experiments

All animal experiments were performed in close collaboration with the research group for Immunopharmacology/Kobold Lab at the Department of Clinical Pharmacology, LMU. C57BL/6 mice were purchased from Charles River (Sulzfeld, Germany) or Janvier (St. Berthevin, France), and C57BL/6-Tg(TcraTcrb)1100Mjb/J (OT-I) mice were kindly gifted by Dr. Reinhard Obst (Institute for Immunology, LMU, Munich). All animals were kept under pathogen-free conditions at the Zentrale Versuchstierhaltung (ZVH) of the LMU Klinikum or at the Core Facility Animal Models (CAM) at the Biomedical Center in Munich. All *in vivo* experimental studies were conducted according to the NIH guide for the care and use of laboratory animals and are approved by the Regierung von Oberbayern (Reference number: 55.2-2532.Vet_02-15-177, 55.2-2532.Vet_02-17-135).

3.20 Software

Software

Gen5 3.10	Agilent
FlowJo™ 10.7.1 – 10.8.1	BD
IDEAS 6.2	Cytek
Wave Desktop	Agilent
R-Studio	Open source
SnapGene 4.2	GSL Biotech

|	
CytExpert 2.3.1.22	Beckman Coulter
GraphPad Prism 9.5	Graphpad Software, Inc

4.   Results

4.1   High expression of SLC2A1 in pancreatic adenocarcinoma (PAAD) is associated with poorer survival rates

As described previously, T cells face a glucose-deprived TME in most solid tumors. To substantiate our rationale, we asked if solid tumor cells overexpress *SLC2A1* and if so, how it impacts clinical outcomes in cancer patients. Analysing TCGA and GTex data, we could observe that pancreatic adenocarcinoma substantially upregulates *SLC2A1* compared to normal tissue (Figure 4 A). Furthermore, *SLC2A1* overexpression is significantly correlated with worse outcomes with a significant hazard ratio (HR) of 1.8. As a therapeutic strategy, we asked if harnessing this upregulation might also help T cells to survive better in the TME and additionally increase the cytolytic effect against carcinoma tumor cells.
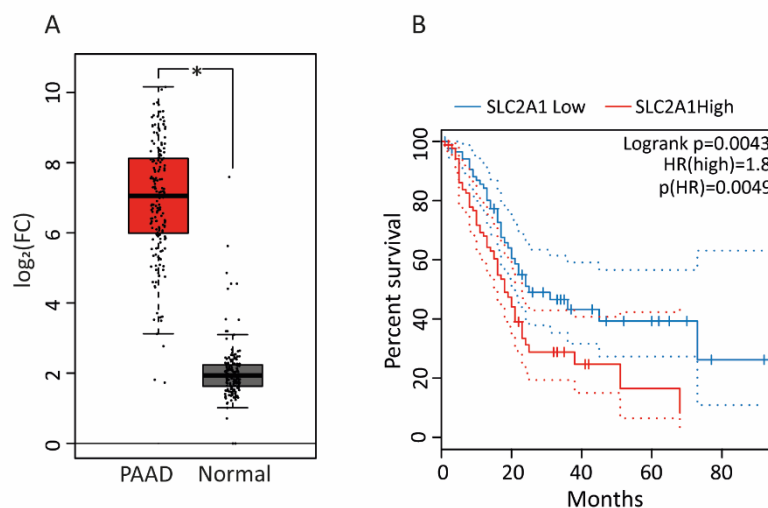

Figure 4 High expression of *SLC2A1* is correlated to worse prognosis in pancreatic adenocarcinoma
A) log2(FC) of combined TCGA and GTEx analysis of differential *SLC2A1* expression in pancreatic adenocarcinoma (PAAD, red, n=179) samples compared to normal tissue samples (grey, n=171). B) Kaplan-Meier plot of median overall survival in *SLC2A1* low (blue, n=89) and *SLC2A1* high (red, n=89) PAAD patients. Data is shown in $\log_2$(FC) of the normalized RNA counts $\log_2$(TPM+1) and statistical analysis is performed using one-way ANOVA, cutoff $\log_2 >1$, $p < 0.05$ was considered statistically significant (A). For overall survival median cutoff of 50% was set for *SLC2A1* high and low, dashed lines indicate 95% percentiles of cox proportional hazard ratio (HR). Statistical analysis was performed with Log-rank (Mantel-Cox) test.

4.2   Ectopic Expression of *Slc2a1*/GLUT1 in primary murine CD8+ T Cells

It is well known, that GLUT1 upregulation in T cells upon activation is a critical step in the import of high amounts of glucose molecules to fill metabolic needs. By *Slc2a1* overexpression in primary T cells, we intended to improve glucose uptake and metabolic utilization in downstream pathways. As a vector of GLUT1 delivery, primary murine T cells were introduced to the retroviral plasmid pMP71 encoding

the murine *Slc2a1* gene and the fluorescent protein eGFP downstream as a marker of transduction. To guarantee the expression of separate GLUT1 and eGFP peptides the F2A peptide cutting sequence was introduced in between the respective genes. The pMP71 vector encoding only eGFP (MOCK) was used as a control. Flow cytometric measurements were used to confirm the successful transduction of the murine T cells minimum 24h post-transduction. For reactivation assays, we used T cells 5-7 days after transduction (Figure 5).
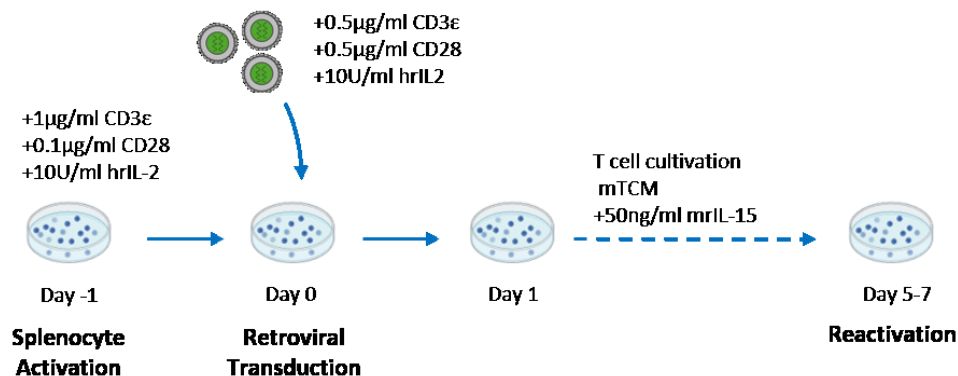
Figure 5 Experimental setup for the retroviral transduction of primary murine splenocyte-derived T cells
General experimental setup for murine transduction, cultivation and the preparation of following experiments. Transduced T cells are kept in culture for 5-7 days before conducting further evaluations in restimulation experiments. Created with BioRender.com

First, we checked the GLUT1 expression by measuring the eGFP reporter signal in pMP71-*Slc2a1*-eGFP transduced (CD8+[Slc2a1]) and pMP71-eGFP transduced (CD8+[MOCK]) CD8+ T cells. We could show that the cells are transduced at a high rate, represented by the eGFP signal (Figure 6 A). Further, the GLUT1 signal correlated significantly to the eGFP reporter signal by a slope of r=0.739 in CD8+[Slc2a1] cells, whereas the GLUT1 signal did not correlate with the eGFP signal in CD8+[MOCK] (Figure 6). Therefore, we concluded, that the eGFP signal could be used as a representative measure for GLUT1 expression in CD8+[Slc2a1] T cells in further studies.
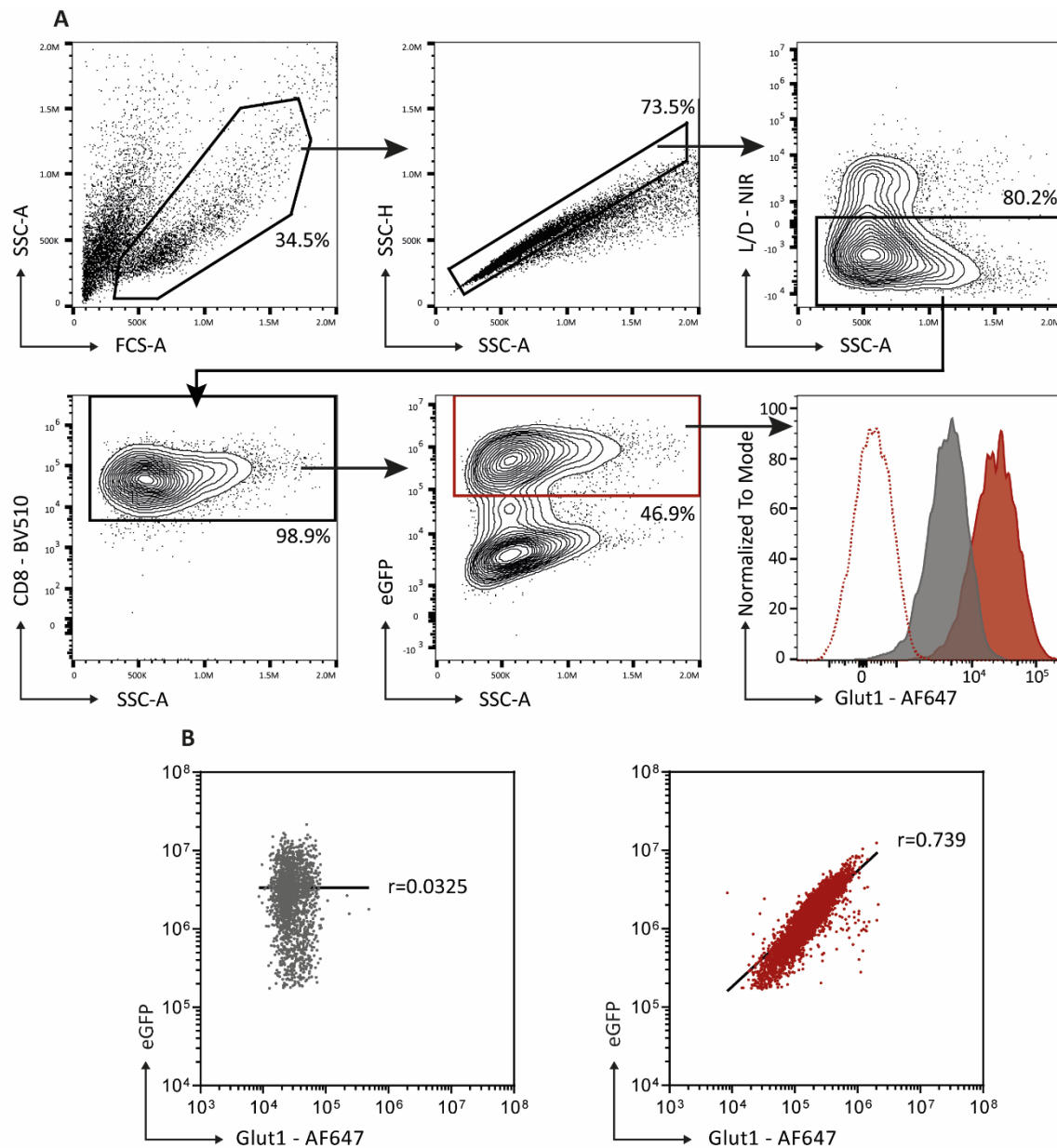
Figure 6 Population gating (A) and correlation of eGFP signal to GLUT1 expression (B) in transduced murine CD8+ T cells.

A) Representative gating strategy of transduced murine CD8+ T cells (from upper left to lower right). Viable CD8+/GFP+ cells are gated from the single-cell lymphocyte population.

B) Representative flow cytometric plots of GLUT1 and eGFP signals of CD8+ T cells for n=3. A linear regression analysis was performed for the correlation of GLUT1 and eGFP signals. CD8+[MOCK] r=0.0325, p=0.4601; CD8+[Slc2a1] r=0.739, p<0.0001.

4.3 Amnis® ImageStream confirms additional surface expression of GLUT1 on CD8+[Slc2a1] cells

Almost all commercially available mouse-reactive anti- GLUT1 antibodies bind the intracellular domain of the transporter. Hence, GLUT1 surface expression was not verifiable on a simple flow cytometric

basis. Since it was previously described that GLUT1 underlies intracellular traffic mechanisms and is only slowly expressed on the cell surface upon stimulation we sought to investigate the GLUT1 expression dynamics in CD8+^{Slc2a1} T cells via ImageStream analysis (Frauwirth et al. 2002; Wieman, Wofford, and Rathmell 2007). We tracked GLUT1 extracellular distribution in OT-1 T cells at 0h, 1h, 6h, 10h, and 24h after stimulation with 100ng/ml SIINFEKL. Here we could observe a strong surface expression of GLUT1 on CD8+^{Slc2a1} T cells before stimulation, which further increased in intensity over time (Figure 7). In contrast, the control CD8+^{MOCK} cells showed low GLUT1 surface expression at 0h and an increasing GLUT1 expression peaking at 24h (Figure 7). Nevertheless, CD8+^{Slc2a1} T cells displayed a substantial additional upregulation of GLUT1, even 24h post-stimulation. We could also observe that *Slc2a1* was the main glucose transporter expressed in CD8+^{Slc2a1} on transcriptomic levels in the RNA-Seq analysis. In contrast, *Slc2a3* is downregulated in CD8+^{Slc2a1} (Figure S 1).
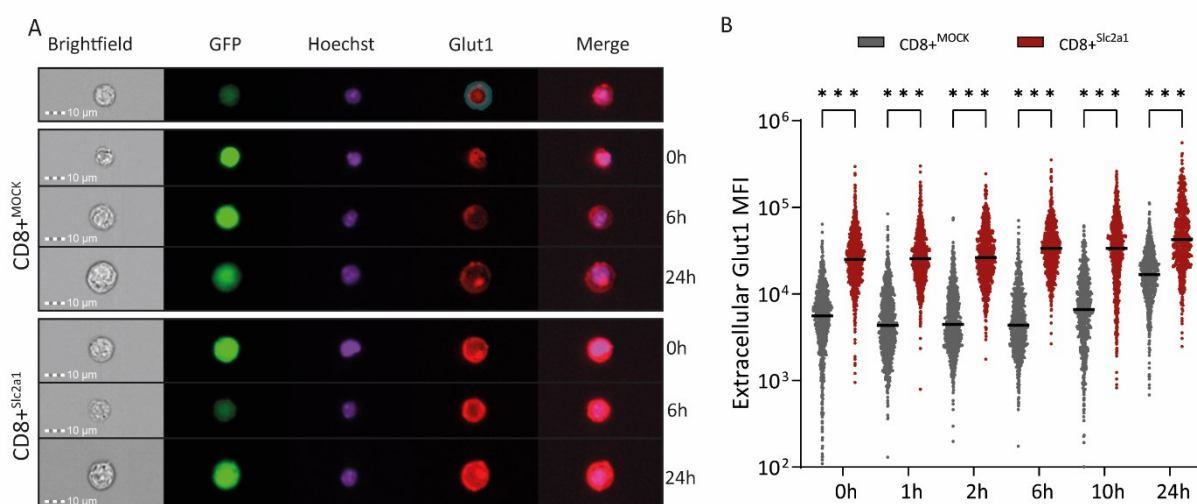

Figure 7 CD8+^{Slc2a1} T cells exhibit strong GLUT1 surface expression before and after SIINFEKL stimulation
Representative events of ImageStream analysis of extracellular GLUT1 expression and exemplary image of the GLUT1 extracellular Mask (A). Cells at 0h, 6h, and 24h timepoints are depicted. The scatter plot in B shows the MFIs for extracellular GLUT1 expression based on the mask depicted in A for CD8+^{Slc2a1} and CD8+^{MOCK} T cells. CD8+^{Slc2a1} 0h: n=1536, 1h: n=937, 2h: n=420, 6h: n=786, 10h: n= 842, 24h: n=287, and CD8+^{MOCK} 0h: n=848, 1h: n=688, 2h: n=689, 6h: n=495, 10h: n= 455, 24h: n=1877 events. p-values are based on one-way ANOVA with correction for multiple testing by the Bonferroni method; p<0.05 was considered statistically significant and is represented as *<0.05, **<0.01, ***<0.001.

4.4 CD8+Slc2a1 cells show higher glucose uptake compared to controls

To validate if the presence of GLUT1 on transduced primary T Cells in fact increases the glucose uptake we performed a Glucose Uptake-Glo^{TM} assay. Therefore, transduced OT-1 T cells were used in a SIINFEKL stimulated and unstimulated status. We could show that CD8+^{Slc2a1} cells already possessed an

elevated glucose uptake rate compared to MOCK in unstimulated conditions by a fold change of 3.048 +/- 0.79 (Figure 8). Furthermore, the lower glucose uptake rate by CD8+^{MOCK} cells could not be compensated by a TCR-directed stimulation by SIINFEKL incubation for 6 hours. This indicates that CD8+^{Slc2a1} cells have an advantageous glucose uptake rate compared to control cells.
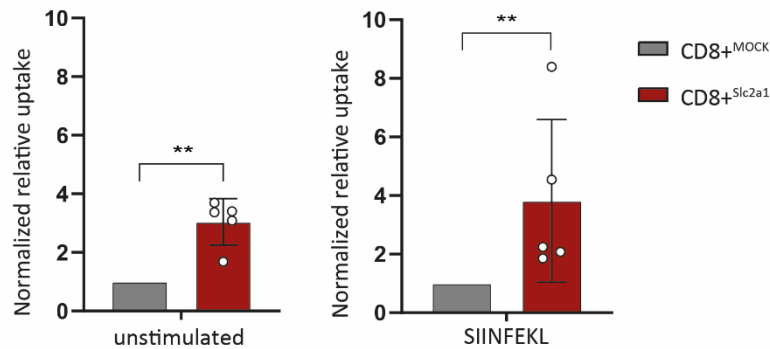

Figure 8 Glucose Uptake-Glo™ Assay of unstimulated and SIINFEKL stimulated (6h) OT-1 T cells
Calorimetric analysis of glucose uptake after 6h of resting or in presence of 100ng/ml SIINFEKL. Experiments are shown in mean fold change +/- STD to control for n=5 biological replicates; p-values are based on an unpaired, non-parametric, two-sided t-Test (Mann-Whitney); $p<0.05$ is considered statistically significant and is represented as *<0.05, **<0.01, ***<0.001

4.5 Extracellular flux analysis reveals a metabolic switch in CD8+^{Slc2a1} T cells

To determine if the GLUT1 overexpression and accompanying elevation of glucose uptake have an impact on the T-cell metabolism we performed a Glycolytic Stress Test (Agilent Seahorse). Hereby, we could draw indirect conclusions about the cells´ glycolysis and mitochondrial performance based on the extracellular acidification rate (ECAR) and oxygen consumption rate (OCR). To test, whether a potential metabolic switch was also observable in TME-like low glucose concentrations we performed the Glycolytic Stress Test in hypoglycemic (0.5mM and 2mM) and physiologic (5mM) concentrations. We observed that *Slc2a1* overexpressing T cells had a higher glycolytic activity in all glucose conditions, yet no significance was achieved (Figure 9, A, B). In particular, a glucose-dependent increase in the glycolytic capacity compared to CD8+^{MOCK} was observable. At the lowest glucose concentration of 0.5mM CD8+^{Slc2a1} cells had a significant, 3-fold increase in glycolytic capacity compared to control cells (Figure 9, C). These findings support our data generated from glucose uprake assays and further suggests an increased glucose metabolism even at hypoglycemic culture conditions. In contrast our data showed that antigen-specific stimulated CD8+^{Slc2a1} T cells also possessed increased basal mitochondrial respiration and with no observable change in the OCR:ECAR ratio (Figure 9, A, D, Figure

S 2). Under complete glucose deprivation CD8+^{Slc2a1} had an even higher elevation of mitochondrial respiration which is observable before glucose injection (Figure 9 A). Seahorse analyses revealed increased fold changes of ECAR and OCR rates in CD8+^{Slc2a1} T cells, suggesting higher overall metabolic activity.
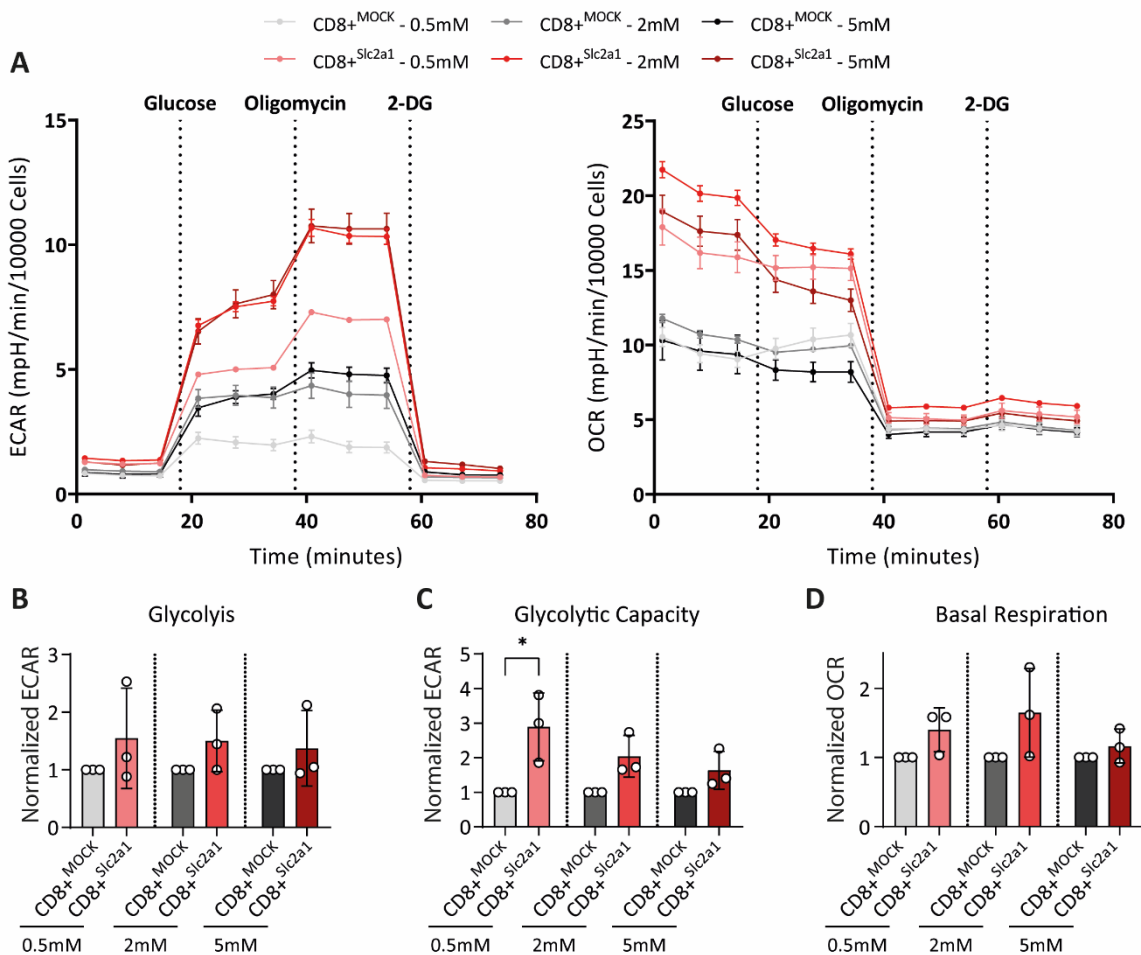

Figure 9 Glycolytic Stress Test of SIINFEKL stimulated (6h) OT-1 T cells indicates increased metabolic activity in CD8+^{Slc2a1} T cells

Extracellular Acidification Rates (ECAR) and Oxygen Consumption Rates (OCR) 6h after SIINFEKL activation (A; representative Figures for n=3). Relative quantification for 0.5mM, 2mM, and 5mM glucose was performed for glycolysis (B), glycolytic capacity (C), and Basal Respiration (D) of CD8+^{Slc2a1} compared CD8+^{MOCK}. Representative curves are shown as mean +/- SEM in A, and quantification Data are depicted as mean fold change +/- STD to control for n=3 in B, C, and D. p-values are based on a Kruskal-Wallis Test with Dunn`s correction; p<0.05 was considered statistically significant and is represented as *<0.05, **<0.01, ***<0.001

4.6 CD8+^{Slc2a1} T cells demonstrate enhanced proliferative capacity in hypoglycemic and physiologic media

The effective amplification of glucose uptake and metabolism in CD8+^{Slc2a1} T cells raised the question of whether the ectopic GLUT1 overexpression in primary T cells potentially also increased their functional ability. Since metabolic rewiring and increased nutrient uptake are hallmark features of expansion in T cells we sought to determine the proliferative ability in CD8+^{Slc2a1} T cells on a flow cytometric basis (Marelli-Berg, Fu, and Mauro 2012; Cao, Rathmell, and Macintyre 2014). To investigate the proliferative capacity after the first antigen engagement we labeled primary murine T cells with CellTrace™ on the day of transduction and tracked the expansion for up to 7 days. We could observe that CD8+^{Slc2a1} cells exhibited a significantly higher rate of proliferation compared to CD8+^{MOCK} at day 7 as indicated in a substantial decrease of CellTrace™ Violet fluorescence over time. This was evident in hypoglycemic conditions and physiologic glucose levels, though to a lower extent.
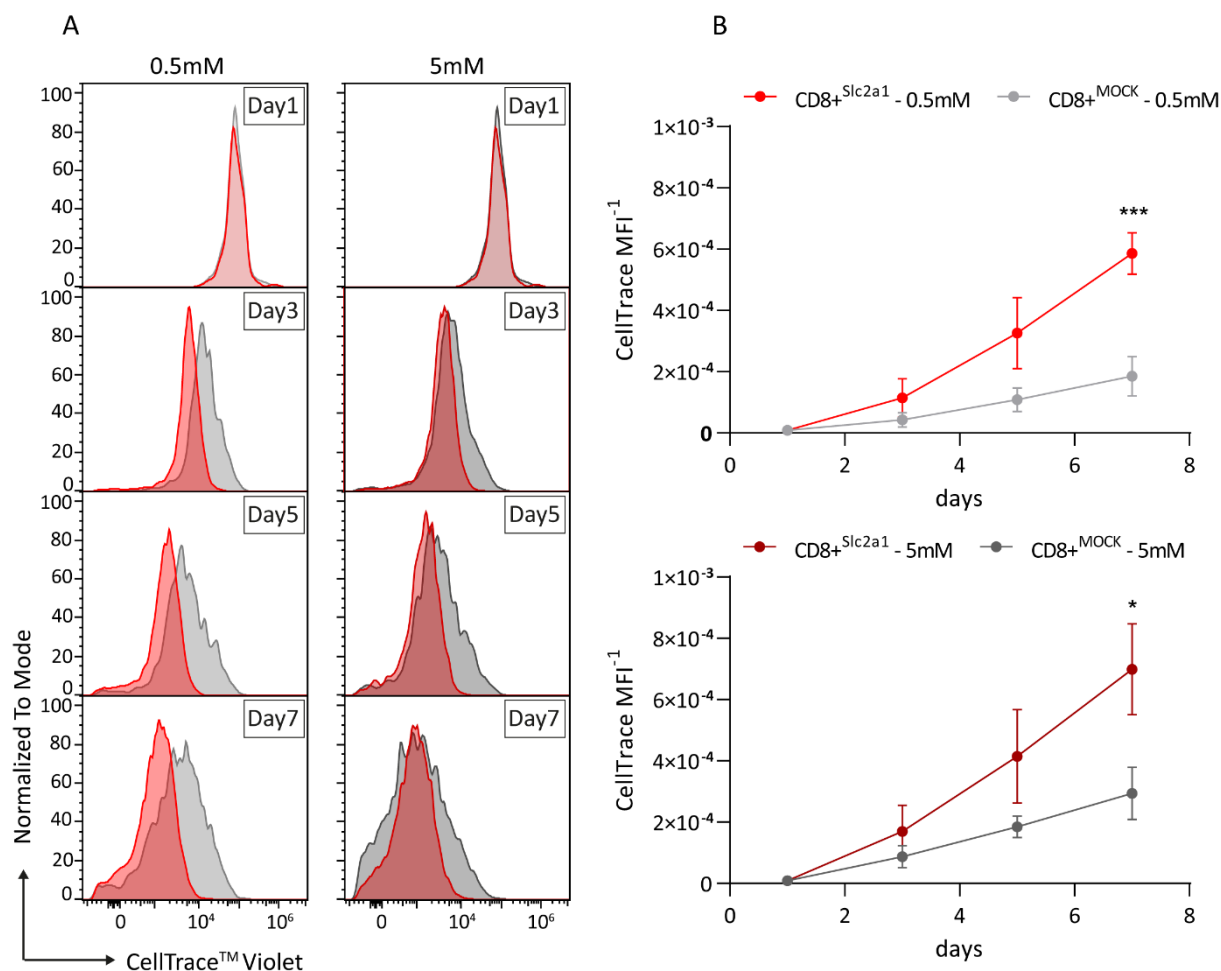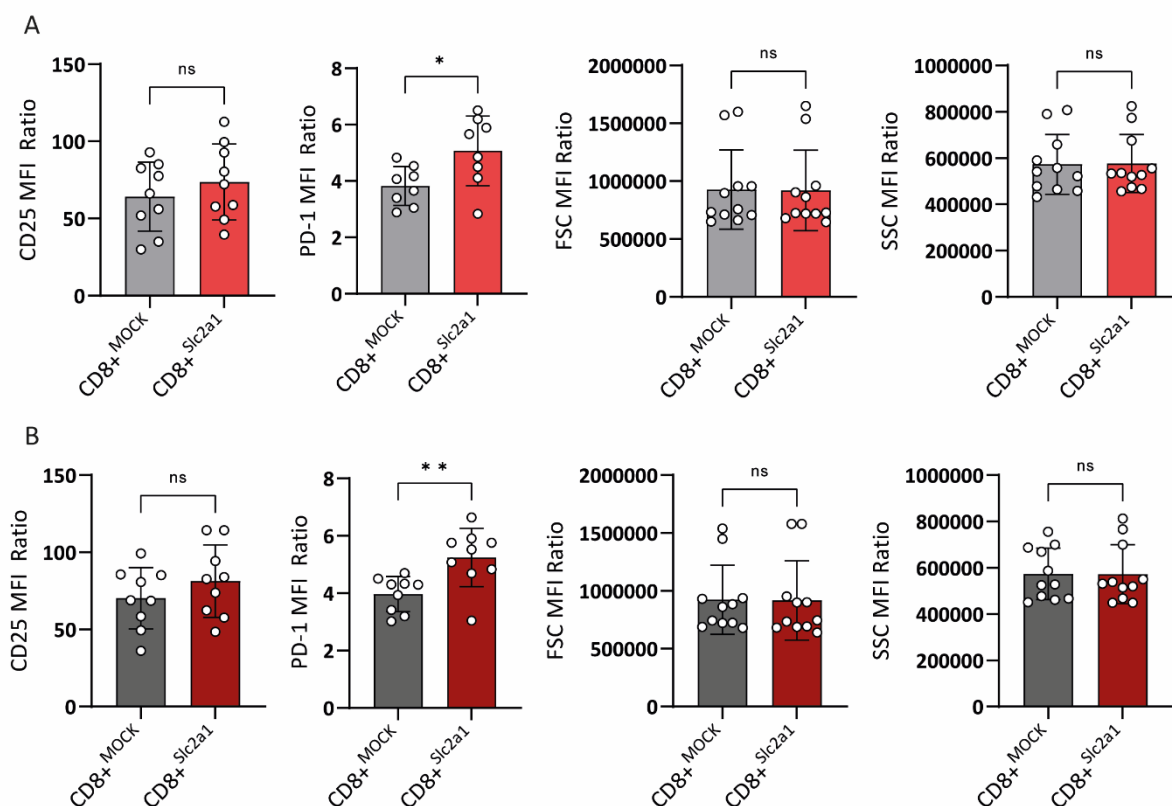

Figure 10 Flow Cytometric Analysis of CellTrace™ proliferation assay reveals high proliferative capacity of CD8+^{Slc2a1} cells *in vitro*

One day post-transduction T cell proliferation was tracked in 0.5mM or 5mM glucose over 7 days. Exemplary histograms for proliferation indicating the proliferative rate represented by a decrease in CellTrace™ fluorescence in CD8+^Slc2a1 (red) and CD8+^MOCK T cells (grey) for timepoints day 1 to day 7 post-transduction (A; representative Figures for n=4). Quantitative analysis of proliferation is depicted as reciprocal of CellTrace™ MFI (B); Data is shown as MFI +/- STD for n=4; p-values are based on two-way ANOVA with correction for multiple testing by the Bonferroni method; $p < 0.05$ was considered statistically significant and is represented as *<0.05, **<0.01, ***<0.001.

4.7   Reactivated CD8+^Slc2a1 T cells exhibit signs of increased activation and exhaustion

Based on the elevated proliferation of GLUT1 overexpressing CD8+ T cells in both, 0.5mM and 5mM glucose, we raised the question of whether CD8+^Slc2a1 cells also show signs of increased immunologic functionality. To investigate this question, we analyzed CD3ε/CD28 (0.5µg/ml) restimulated T cells in hypoglycemic and physiologic media on a flow-cytometric basis after 18h. Overnight stimulation revealed that GLUT1 overexpression in T cells did not significantly alter cell size and granularity. Additionally, no substantial increase in the mid-activation marker CD25 could be detected. However, a significant upregulation in PD-1 expression compared to CD8+^MOCK cells was apparent in both, 0.5mM and 5mM glucose (Figure 11).


Figure 11 Flow Cytometric analysis of restimulated murine T cells shows signs of increased activation and exhaustion but no morphologic alterations of GLUT1 overexpressing T cells

7 Days post-transduction T cells were reactivated with 0.5µg/ml CD3ε/CD28 antibodies in hypoglycemic (A) and physiologic (B) glucose. Samples were analysed via flow cytometry 18h after restimulation. Raw MFI values +/- STD are shown for size and granularity (FSC, SSC) in CD8+^{Slc2a1} (red) and CD8+^{MOCK} control T cells (grey). Data for activation and exhaustion is depicted in MFI ratios +/- STD for n=11 biological replicates; MFI ratios are calculated as the ratio of Sample MFI/Isotype MFI. p-values are based on an unpaired, non-parametric, two-sided t-Test (Mann-Whitney); $p < 0.05$ is considered statistically significant and represented as *<0.05, **<0.01, ***<0.001.

Intracellular staining of cytolytic and pro-inflammatory proteins should further determine the effector phenotype of GLUT1 overexpressing CD8+ T cells.

The data show strong upregulation of the cytokine IFN-γ in both glucose conditions compared to MOCK. Although no change in Perforin 1 (PRF1) was detected, a significant fold change in Granzyme B (GrB) was evident for 0.5mM as well as 5mM glucose conditions (Figure 12 A and B). Of note, it is observable that CD8+^{Slc2a1} T cells exhibit a more pronounced activation phenotype in low glucose levels in comparison to MOCK T cells than in physiologic media conditions (Figure 12 A).
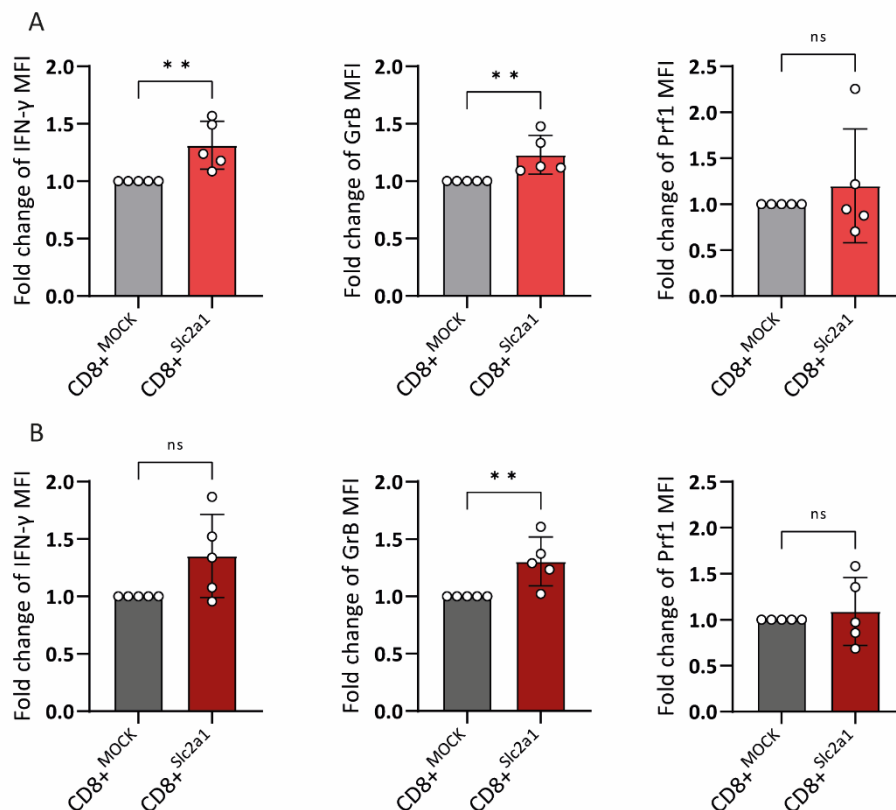
Figure 12 Intracellular labeling of CD8+^{Slc2a1} T cells reveals augmented immune response following reactivation
7 Days post-transduction T cells were reactivated with 0.5µg/ml CD3ε/CD28 antibodies in hypoglycemic (A) and physiologic (B) glucose. Intracellular flow cytometric analysis of IFN-γ, GrB, and PRF1 is depicted. The fold change of MFIs compared to the MOCK ctrl. (grey) was calculated for CD8+^{Slc2a1} (red). Upregulated expression of IFN-γ and GrB in CD8+^{Slc2a1} compared to CD8+^{MOCK} was evident for both 0.5mM and 5mM conditions, yet more prominent in hypoglycemic conditions. No change in expression was observable for PRF1. Data is depicted in MFI +/- STD for n=5 biological replicates; p-values are based on an unpaired, non-parametric, two-sided t-Test (Mann-Whitney); $p < 0.05$ was considered statistically significant and represented as *<0.05, **<0.01, ***<0.001.

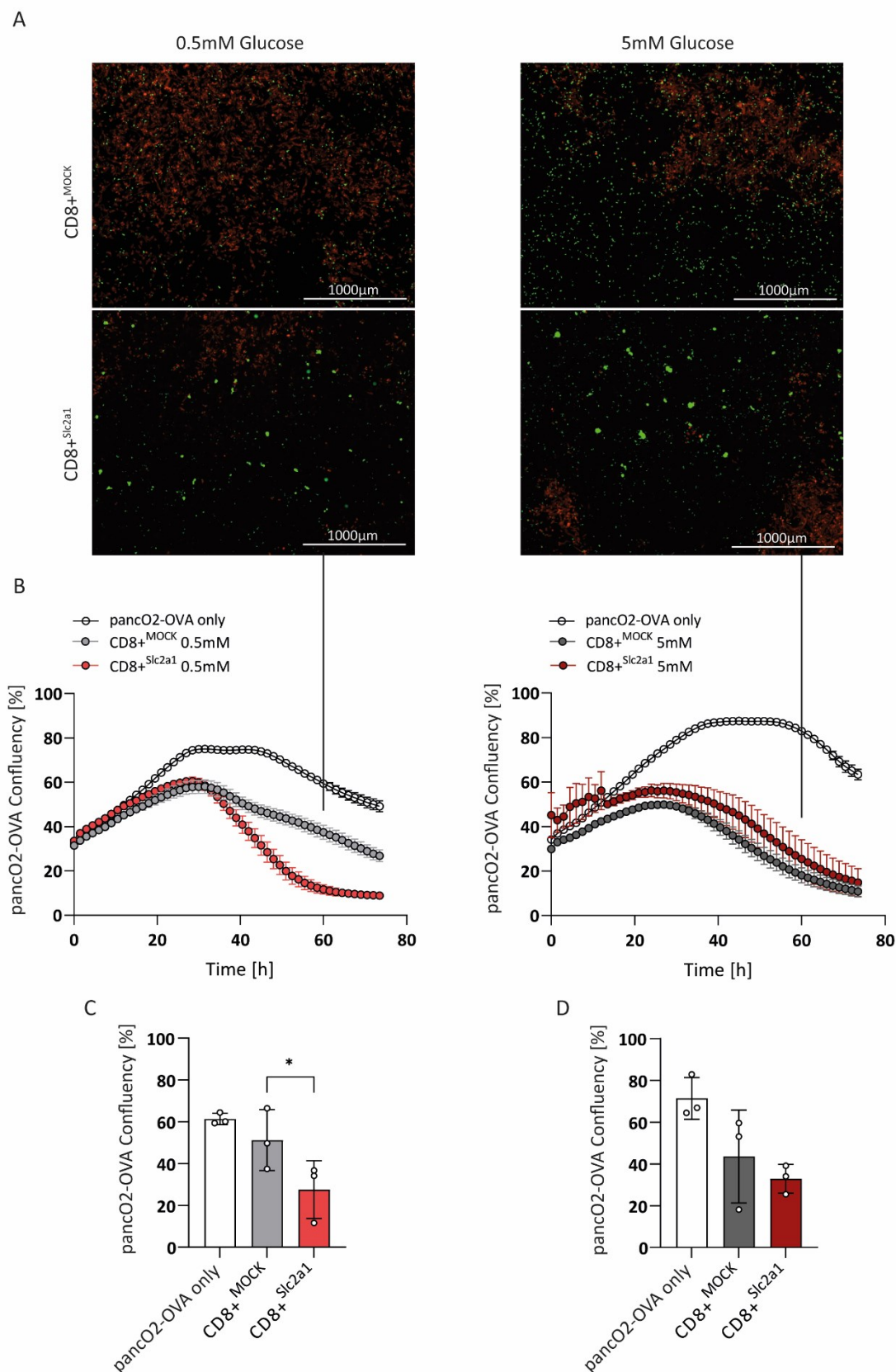## *4.8* Antigen-specific CD8+^Slc2a1 T cells demonstrate improved anti-tumor activity *in vitro*

Given the higher activation status in CD8+^Slc2a1 T cells and the rationale behind the project to increase anti-tumor efficacy, we set up an antigen-specific killing assay. Therefore, transduced OT-1 T cells were co-cultivated with the SIINFEKL-expressing PancO2-OVA-mCherry cell line (Figure 13).
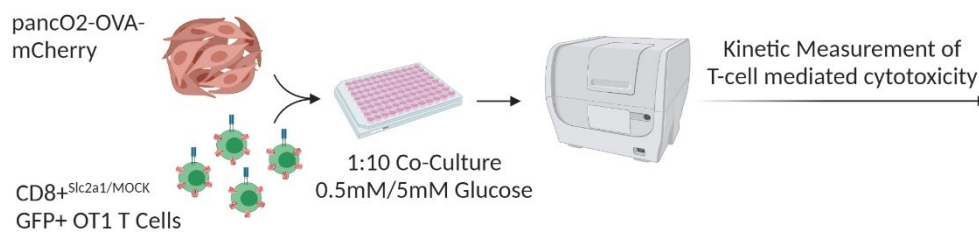
Figure 13 Experimental setup for the kinetic imaging measurement of the antigen-specific killing assay
OT-1 CD8+ T cells were co-cultured with pancO2-OVA-mCherry cells at an E:T ratio of 1:10. The kinetic measurement was imaged in hypoglycemic and physiologic media for up to 4 days in an time interval of 1.5h. Created with BioRender.com

GLUT1 overexpression did not lead to significantly better lysis of target cells in physiologic conditions. Nevertheless, a tendency for increased killing capacity was observable (Figure 14 A and D). Noteworthy, we were able to demonstrate a glucose-dependent increase of specific target-cell lysis. In hypoglycemic conditions, CD8+^Slc2a1 cells demonstrate an augmented killing capacity compared to control cells illustrated at the 60h timepoint (Figure 14 A, B, C). The observed significant cytolytic increase in low glucose conditions supported the previous data, hinting towards T-cell activity reinforcement by GLUT1 overexpression.

Figure 14 Antigen-specific CD8+^Slc2a1 cells exhibit superior killing capacity in hypoglycemic media conditions
Transduced OT-1 T cells were co-cultured with 3×10^4 pancO2-OVA-mCherry cells in 0.5mM (A, B, C) and 5mM (A, B, D) glucose containing media at an E:T ratio of 1:10. Images were taken over a period of 4 days in 1.5h intervals. Exemplary images of both glucose conditions for CD8+^MOCK and CD8+^Slc2a1 at the 60h timepoint are illustrated in

A (Green: OT-1 T cells, red: pancO2-OVA-mCherry). Live-cell kinetic graphs of the target-cell confluency represent the killing capacity in 0.5mM and 5mM glucose (B, Representative for n=3). Quantified data shows pancO2-OVA-mCherry confluencies at the 60h timepoint (A, C, D). Representative curves of B are shown in mean +/- SEM for n=3 technical replicates; Data in C and D is depicted in mean +/- STD for n=3 biological replicates; p-values are based on a student`s t-Test; p<0.05 was considered statistically significant and represented as *<0.05, **<0.01, ***<0.001.

To evaluate if the better killing of the target cells not only relies on a selective advantage of the T cells over the pancO2-OVA-mCherry cells by increased glucose uptake but is also enhanced by an increased cytolytic activity we further assessed degranulation capacity. Here we set up a co-culture (E:T = 1:1) at physiologic conditions to evade the glucose effect in 0.5mM glucose. Here we could demonstrate that a higher proportion of CD8+^{Slc2a1} T cells expressing the degranulation marker CD107a compared to CD8+^{MOCK} (Figure 15).
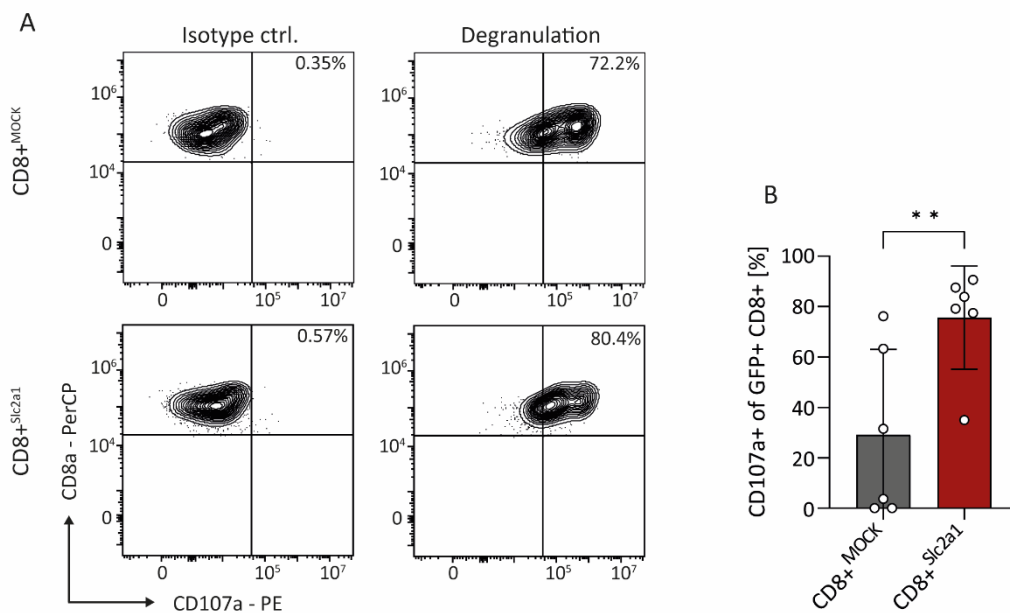

Figure 15 CD8+^{Slc2a1} degranulate at a higher rate in physiologic media condition after restimulation
CD107a FACS staining representing degranulation of CD8+^{MOCK} and CD8+^{Slc2a1} T cells. Cells were restimulated for 1h before golgi stop was performed with Monensin and Brefeldin A followed by further cultivation for 4h. A depicts representative FACS gates for the Isotype control and CD107a staining in GFP+/CD8+ T cells. Quantification of GFP+/CD8a+ T cells for frequency of CD107a+ events in A is shown in B. p-values are based on an unpaired, non-parametric, two-sided t-Test (Mann-Whitney); p<0.05 was considered statistically significant and represented as *<0.05, **<0.01, ***<0.001.

4.9 *In vivo* mouse models show signs of augmented anti-tumor capacities of CD8+[Slc2a1]

T cells

We were able to show that GLUT1 overexpression led to augmented activation and killing capacities *in vitro* experiments. To further explore the anti-tumoral properties of these cells, we performed *in vivo* tumor surveillance assays to assess their ability to suppress tumor growth. In a subcutaneous (s.c.) pancreatic tumor model we implanted $3x10^6$ pancO2-OVA cells and treated the mice with 10^7 T cells when the cancer was palpable (Figure 16 A). For the growth curve, we measured the area of the tumors three times a week until the termination was reached. Both, the MOCK ctrl and GLUT1 transduced OT-1 T cells showed an effective anti-tumor response compared to the vehicle (PBS) control group. However, since the standard error between the individual tumors was quite broad, we could not detect significant differences in mean change compared to the control mice (Figure 16 B). Nevertheless, one can appreciate that CD8+[Slc2a1] treated mice had lower tumor burden compared to the CD8+[MOCK] over the course of the therapy. The therapeutic effect was well observable in the waterfall display for day 44 of Figure 16 C. We chose this time point as the first mouse of the two T-cell groups (CD8+[MOCK] and CD8+[Slc2a1]) reached the point of termination on this day. Here an advantageous anti-tumor potential for CD8+[Slc2a1] OT-1 T cells is indicated since all but one replicate had a lower tumor burden compared to the mean of the control group (CD8+[MOCK] treated, Figure 16 D). Preliminary data showed that tumors that received a delayed T-cell injection, resulting in a bigger tumor, had substantial differences in tumor growth (Figure S 3). Despite the use of only one biological replicate per group, these findings are promising and support the results displayed in Figure 16.
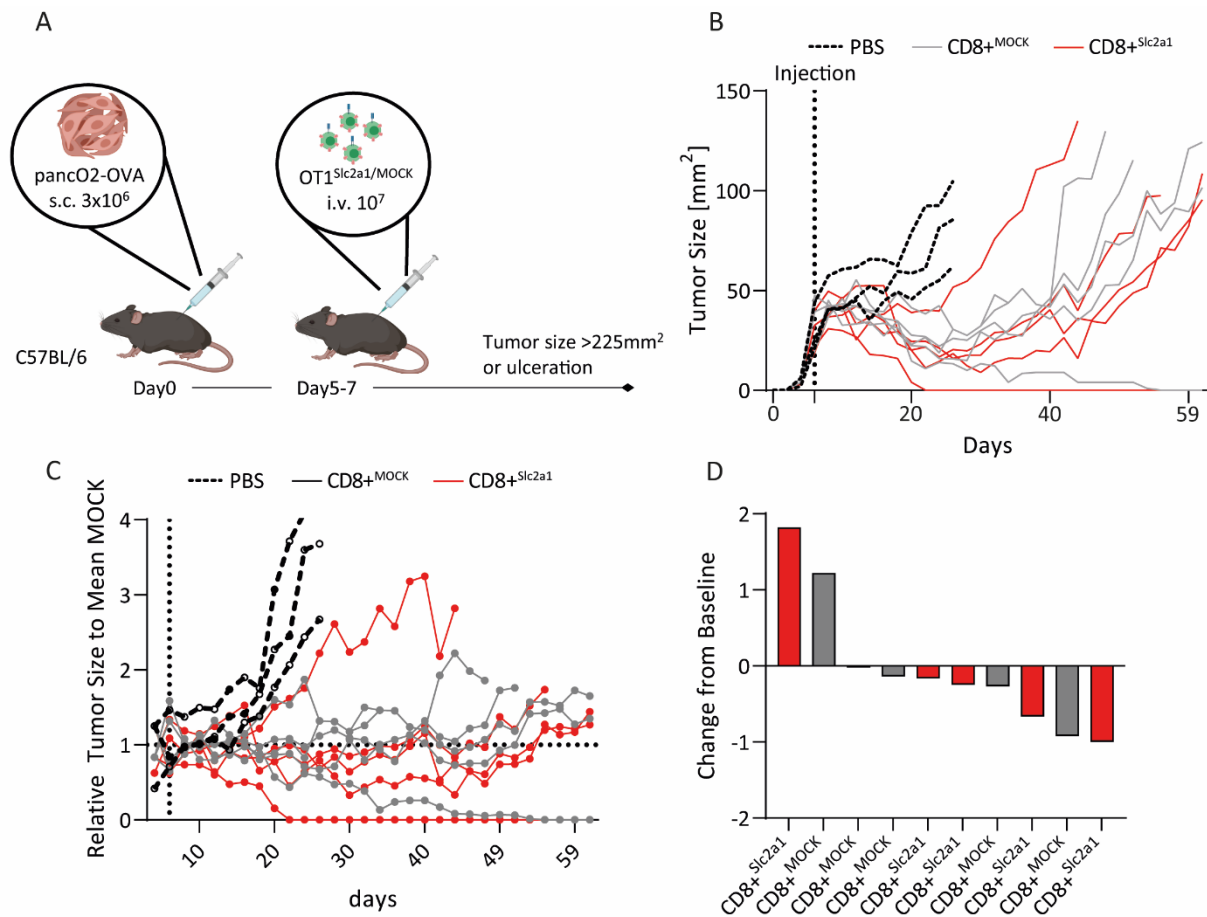
Figure 16 GLUT1 overexpression shows moderate improvement of anti-tumor efficacy in an OT-1-OVA mouse model

Experimental layout for pancO2-OVA – OT-1 tumor challenge in a C57BL/6 mouse model (A). $3x10^6$ pancO2-OVA cells were injected s.c. in flanks and treated with 10^7 OT-1 T cells 5-7 days post-tumor induction. Growth of s.c. pancO2-OVA tumors for individual PBS (black, n=3), CD8+^{MOCK} (grey, n=5), and CD8+^{Slc2a1} (red, n=5) treated mice were tracked (B) and normalized relative to the mean CD8+^{MOCK} tumor areas (C). A waterfall plot analysis is conducted for day 44 (D). No significant differences were detected between the groups. A) created with BioRender

Besides the primary anti-tumor response, memory formation in cellular therapy is an important aspect to counteract possible relapse after treatment. To address this, we checked for allogeneically transferred T cells and the formation of memory subsets in the spleens one week after tumor clearance. Transduced T cells co-expressed the fluorescent protein GFP as described earlier (Figure 6) and served as a marker for later identification purposes. Flow cytometric results showed that CD8+^{Slc2a1} T cells had tendencies towards stronger effector memory formation, while CD8+^{MOCK} T cells were more represented by central memory T cells, yet not significant. Besides memory formation, we also focused on the number of cells homing to the spleens. Here we observed a significant increase in the numbers

of CD8+/GFP+ cells resident in the spleens of CD8+^{Slc2a1} treated mice compared to the control group (Figure 17).
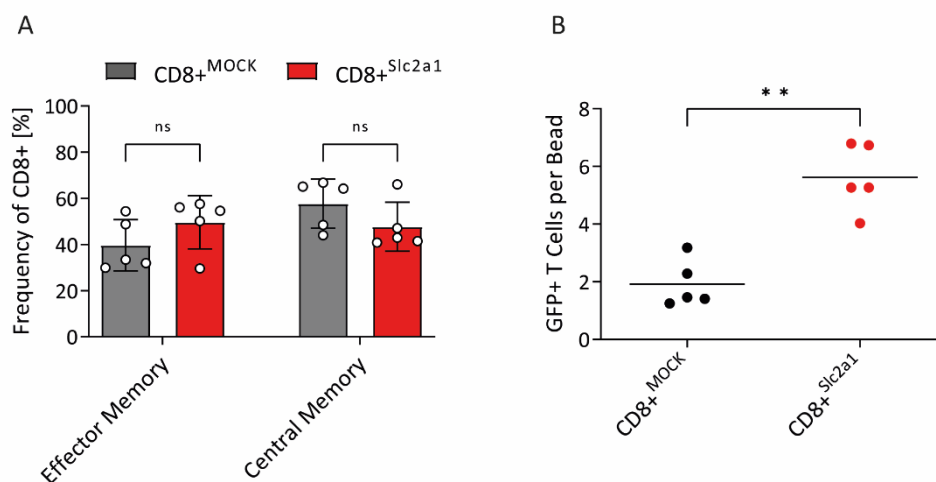

Figure 17 CD8+^{Slc2a1} T cells demonstrate higher effector memory subset representation and greater splenic homing capacity upon successful eradication of tumor cells

Effector and central memory flow cytometric analysis one week after successful tumor elimination CD8+^{Slc2a1} (A). CD107a+/CD62L+ cells were assigned as central memory and CD107a+/CD62L- cells as effector memory T cells. T cell counts in the spleens were calculated by adjusting CD8+/GFP+ events to the initial transduction efficiencies followed by normalization to CountBright™ Absolute Counting Bead events (B). Experiments are shown in mean fold change +/- STD to control for n=5 biological replicates; p-values are based on an unpaired, non-parametric, two-sided t-Test (Mann-Whitney); p<0.05 is considered statistically significant and is represented as *<0.05, **<0.01, ***<0.001

4.10 Bulk RNA sequencing revealed CD8+^{Slc2a1} T cells exhibit distinct expression profiles

Taken together, the collected data suggested an alteration in intracellular mechanisms in GLUT1 overexpressing T cells. To assess this in further detail, we performed bulk RNA sequencing of *Slc2a1* and MOCK transduced murine T cells in hypoglycemic and physiologic glucose concentrations 18h after CD3ε/CD28 Ab-reactivation. The normalized counts' principal component analysis (PCA) displayed distinct clustering of the T-cell constructs and glucose media. The closer proximity of the two CD8+^{Slc2a1} clusters to each other is well observable, whereas the CD8+^{MOCK} clusters settled at a greater distance (Figure 18, A). To detect differentially expressed genes we performed a DESeq2 analysis for CD8+^{Slc2a1} VS CD8+^{MOCK} in 5mM (Figure S 4 A) and 0.5mM (Figure S 4 B) glucose conditions. We could identify 471 significantly upregulated and 328 downregulated genes in the hypoglycemic condition. In the physiologic media condition, 911 up- and 561 downregulated genes were differentially expressed (p_{adj} < 0.05; <75% FC or >125% FC to CD8+^{MOCK}). In addition to the volcano plot depiction, unsupervised clustering of the top 100 differentially expressed genes in both 0.5mM and 5mM glucose was performed.

Based on the expression patterns in the heat-map clustering, a higher degree of similarity of the CD8+^{Slc2a1} T cell samples was discovered, which was consistent with the results of the PCA. These findings suggest a stronger impact of GLUT1 overexpression on T cells compared to glucose media concentration in this setting. It was observable that stimulation-associated genes (IFN-γ, IL-2, PRF1, IL3, IL1r, Irf7) representing the response to external stimuli in the ORA for biological processes were downregulated in CD8+^{Slc2a1} T cells in both glucose conditions. Conversely, differentially upregulated gene clusters associated with leukocyte differentiation (Inpp4b, Itgb3, CCR2, Ceacam1), cell migration (CCR2, Itgb3, Trp53inp1, S1pr1), and most notably, cellular oxidative stress (Gsto1, Mt3, Nqo1, Cox6a, Ulk1) were represented for CD8+^{Slc2a1} T cells.
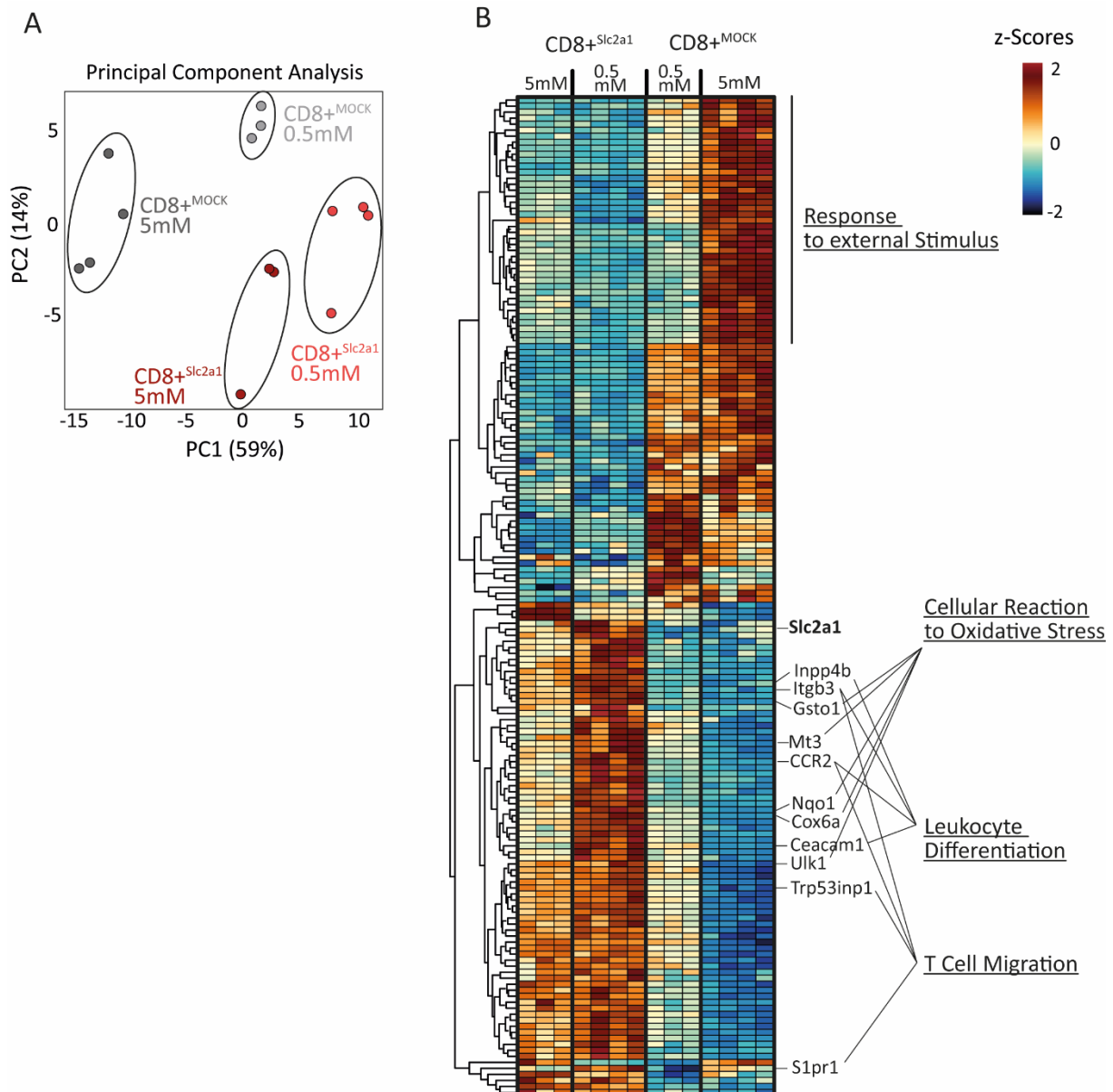
Figure 18 Bulk RNA-Seq reveals transcriptomic changes in CD8+Slc2a1 T-cell differential expression analysis
Bulk RNA sequencing data is represented in Principal Component Analysis (A) and unsupervised hierachial clustering of primary murine CD8+Slc2a1 VS CD8+MOCK T cells in hypoglycemic and physiologic conditions. Heatmap clustering of z-Scores was performed for the TOP 100 differentially expressed genes (B).

The collected RNA sequencing data indicated that ectopic *Slc2a1*/GLUT1 overexpression alone could lead to a strong response by the transcriptional regulation in CD8+ T cells independent from the glucose concentration. Hence, we next tried to pinpoint these specific *Slc2a1*-dependent genes as well as synergistic *Slc2a1*-glucose-dependent genes. To do so, we created a Venn-giagram of up- and down-regulated genes for different criteria. Differential gene expression of CD8+Slc2a1 VS. CD8+MOCK in both, hypoglycemic and physiologic glucose, as well as differentially expressed genes in 5mM VS. 0.5mM conditions in CD8+MOCK and CD8+Slc2a1 cells, were elaborated and analysed for overlapping genes. Out

of the named gene clusters, we extracted corresponding genes from a Venn-diagram and further subjected these sets to a Gene Set Enrichment Analysis (GSEA). Here we could identify that *Slc2a1* induces genes related to autophagy, T-cell activation, and most prominent chromatin modification, suggesting reprogramming taking place in CD8+[Slc2a1]. Enriched *Slc2a1* and glucose-dependent gene sets were connected to the cytoskeleton (actin filament organization) and inhibitory mechanisms on T cells (negative regulation of cell activation). Additionally, the inclusion of mitochondrial changes was detected, represented by downregulation in organelle fission. As described previously, a decreased response to cytokine stimulus was connected to *Slc2a1* and glucose-dependent genes. Interestingly, both clusters showed gene sets for response to oxygen levels or oxidative stress, with evidence of increased mitochondrial and cellular metabolic pathways.
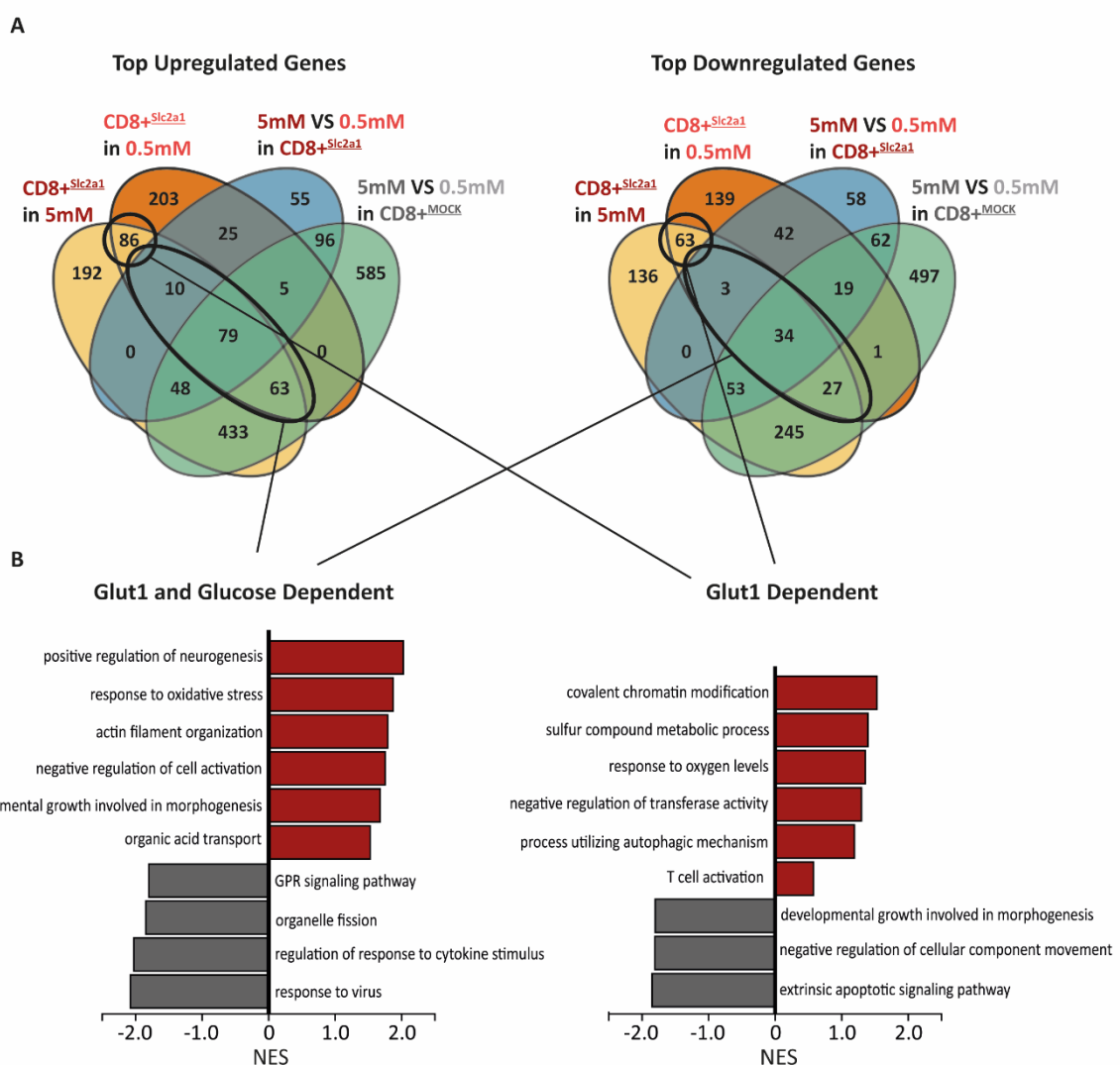

Figure 19 Venn-analysis unveils distinct *Slc2a1* and glucose-dependent genes sets in CD8+[Slc2a1]
Venn-diagrams of the significant up- and down-regulated genes from the DeSeq analyses. Marked clusters represent GLUT1 only dependent (86 up- and 63 downregulated genes) or synergistic GLUT1 and Glucose-dependent (152 up- and 64 downregulated genes) genes (A). Mentioned clusters are individually analysed for GSEA Biological Processes depicted (B).

4.11 Metabolomic analysis suggests adapted metabolic reprogramming in CD8+^{Slc2a1} for the optimization of cellular processes

The elevated cellular metabolism observed in the Seahorse analysis coupled with the higher activation status and the signs of reprogramming in *Slc2a1* transduced CD8+ T cells raised the question of how CD8+^{Slc2a1} cells utilize primary metabolites. To approach this, we conducted quantitative metabolomic analysis and metabolic flux ^{13}C-labeled isotope tracing to reveal the dynamics of glucose and glutamine downstream metabolism pathways. First, we conducted a quantitative analysis to identify metabolite enrichment patterns in CD8+^{Slc2a1} T cells. The PCA for 20% deregulated metabolites in 0.5mM and 5mM glucose did not reveal distinct clustering of groups in the 2-dimensional depiction (Figure S 5). However, the 3D plot showed that the CD8+^{Slc2a1} T-cell samples for hypoglycemic and physiologic conditions clustered more closely together than the control samples (Figure 20 A). This suggests that there may be metabolic differences between the groups that are not apparent in the 2D plot. To further investigate this, we quantified the mean fold changes in CD8+^{Slc2a1} T cells compared to CD8+^{MOCK} in both, 0.5mM and 5mM glucose. Here we found a considerable increase of metabolites involved in downstream pathways of the glycolysis, most notably the TCA cycle and branching pathways, represented by citrate, fumarate, malate, aconitate, and arginosuccinate. Additionally, the enrichment of metabolites representing nucleotide synthesis (GMP, IMP, UMP, CMP) and metabolites involved in the sulfur pathways could be appreciated (GSH, cystein, taurine, methionine sulfoxide, and SAH) (Figure 20 B). These data underlined the findings of the isotope tracing experiments indicating enhanced glycolysis, TCA cycle, PPP, and downstream nucleotide synthesis. We also observed enrichment of carnitine and acylcarnitines (AC2:0, AC4:0, AC5:1).
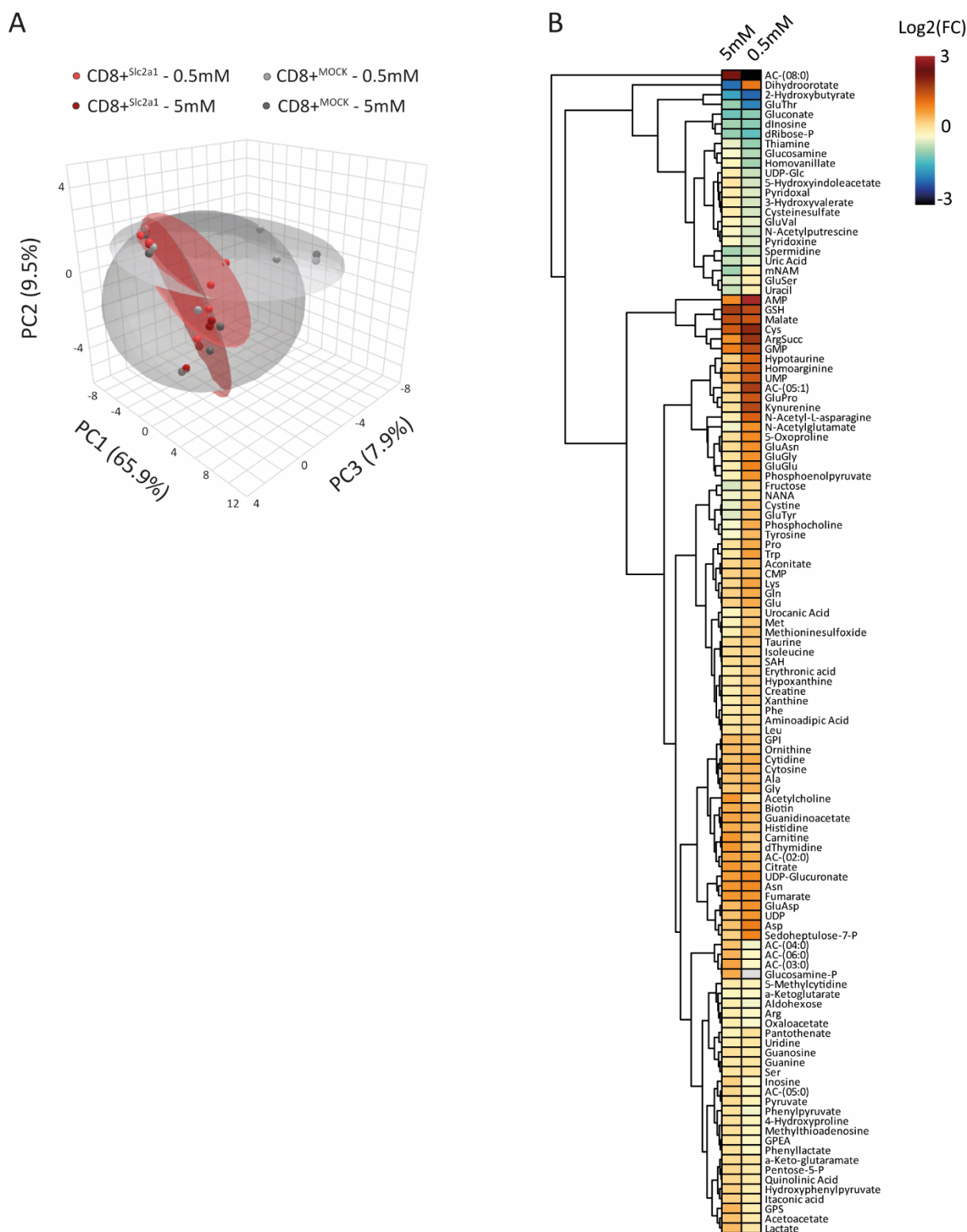
Figure 20 Principal Component Analysis of metabolomic data and foldchange for 20% deregulated metabolites in CD8+[Slc2a1] T cells

Three-dimensional Principal Component Analysis (PCA) for quantified metabolomic data (A). Unsupervised hierarchical clustering was performed for the log2(FC) in CD8+[Slc2a1] compared to CD8+[MOCK]. Metabolites with Log2(FC) < -0.32 or Log2(FC) > 0.26 were plotted (B).

To investigate how CD8+^{Slc2a1} cells metabolize glucose in detail, we performed isotype labelling. 14h pre-stimulated T cells were cultivated in either ^{13}C-Glucose or ^{13}C-L-Glutamine for 4h before preparing cell pellets for mass spectrometric analysis (Figure 21 A, Figure 23 A). Glucose isotype labeling revealed significant enrichment of ^{13}C in Citrate, indicated by two labeled carbon atoms (M2). However, downstream metabolites in the TCA, e.g. α-Ketoglutarate, did not show increased enrichment in CD8+^{Slc2a1} T cells. Although significant isotope labeling in Pentose-Phosphate-Pathway (PPP) metabolites was not detectable, downstream metabolites of the branching nucleotide synthesis, particularly the purine synthesis, exhibited substantial isotope enrichment (IMP, AMP, and GMP) (Figure 21).
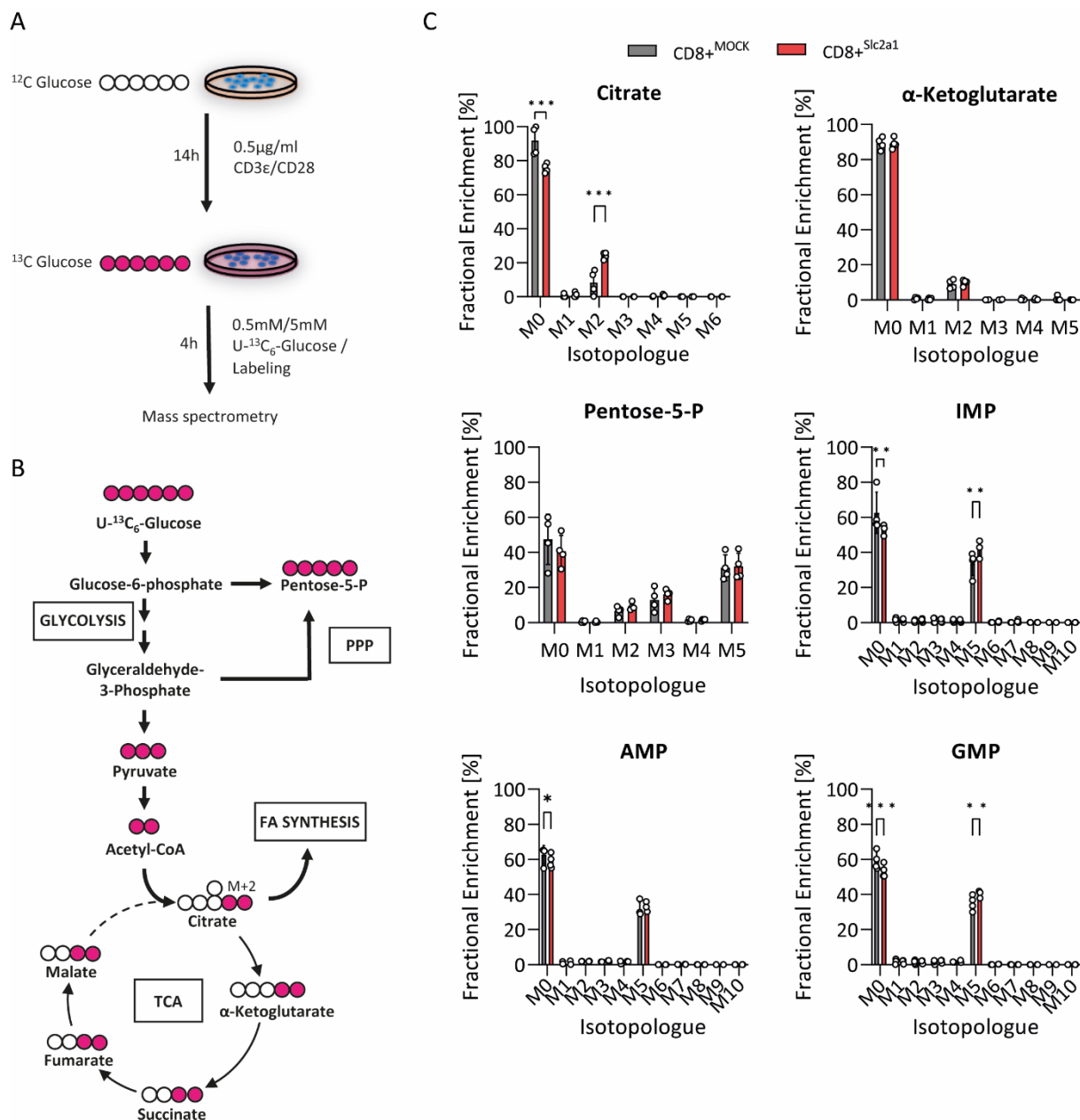
Figure 21 ^{13}C-Glucose Isotope Flux Analysis reveals increased enrichment of downstream metabolites in CD8+^{Slc2a1} T cells

Experimental setting of ^{13}C-Glucose labeling (A) should reveal downstream metabolism and isotope enrichment in CD8+^{Slc2a1} (red) and CD8+^{MOCK} (B). Selected key metabolites of the TCA downstream of the glycolysis, the Pentose-Phosphate-Pathway, and nucleotide synthesis were analysed. Data is shown as MFI +/- STD for n=4; p-values are based on two-way ANOVA with correction for multiple testing by the Bonferroni method; $p<0.05$ was considered statistically significant and is represented as *<0.05, **<0.01, ***<0.001.

In hypoglycemic conditions, we could observe significantly lower unlabelled GSH as well as α-ketoglutarate levels after the labeling. This indicates better utilization of the low glucose availability of CD8+^{Slc2a1} and confirms the glucose uptake and extracellular flux assays (Figure 8, Figure 9).
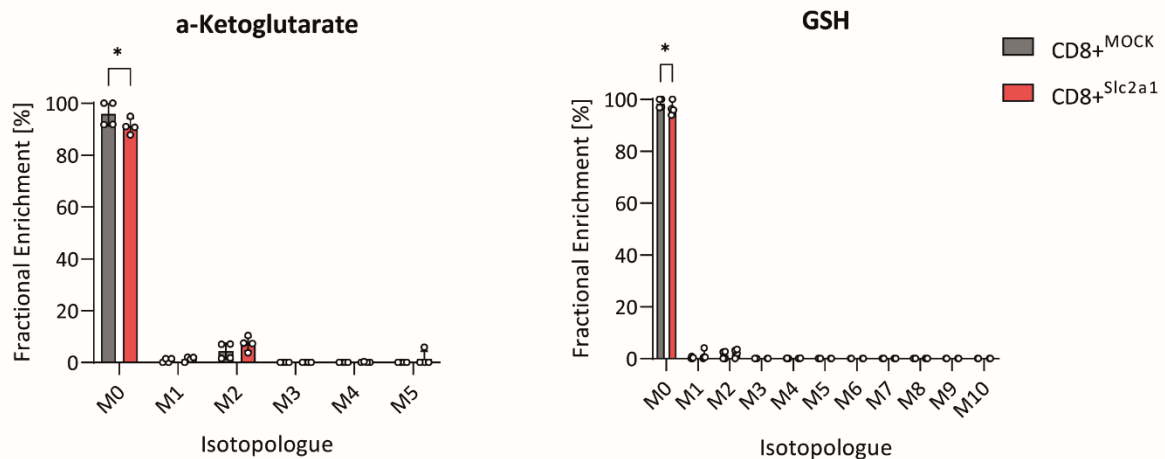
Figure 22 ^{13}C-Glucose Isotope Flux Analysis shows increased enrichment of glutathione and α-ketoglutarate in CD8+^{Slc2a1} T cells in hypoglycemic conditions.
Fractional enrichment of heavy isotope labeled (red) and unlabeled (grey) carbon atoms in alpha-Ketoglutarate and GSH deriving from ^{13}C$_5$-Glucose. Data is shown as MFI +/- STD for n=4; p-values are based on two-way ANOVA with correction for multiple testing by the Bonferroni method; p<0.05 was considered statistically significant and is represented as *<0.05, **<0.01, ***<0.001.

Since the extracellular flux assay and quantitative metabolomics suggested involvement of the TCA and glucose did not appear to fuel the TCA cycle significantly different, indicated by low M2 enrichment of α-Ketoglutarate (Figure 21), it raised the question if there was a change in glutamine utilization in CD8+^{Slc2a1} T cells. Here we could show that the metabolism of L-glutamine to α-Ketoglutarate was significantly enhanced in CD8+^{Slc2a1} T cells (Figure 23 C). Also, the circulation in the TCA via malate to citrate was elevated in CD8+^{Slc2a1}. This is indicated by the increased M4 enrichment in citrate incorporating all four carbon atoms from the U-^{13}C$_5$-L-Glutamine (Figure 23 B and C). Additionally, we observed an increase in the activity of the TCA cycle branching pathways, as evidenced by a significant decrease in the fractional abundance of unlabeled carbon atoms (M0) and a substantial increase in M5 of 2-Hydroxyglutarate.
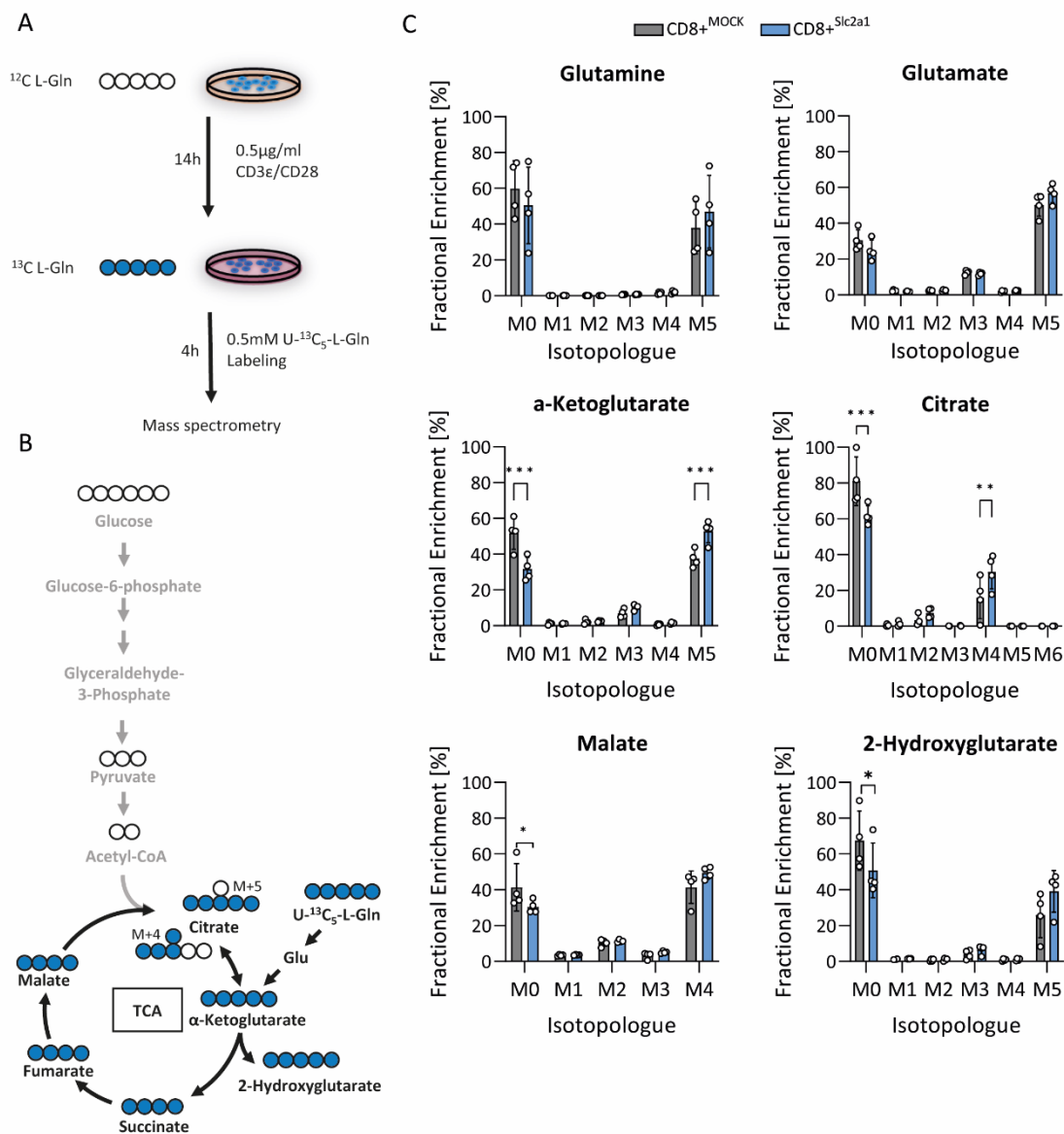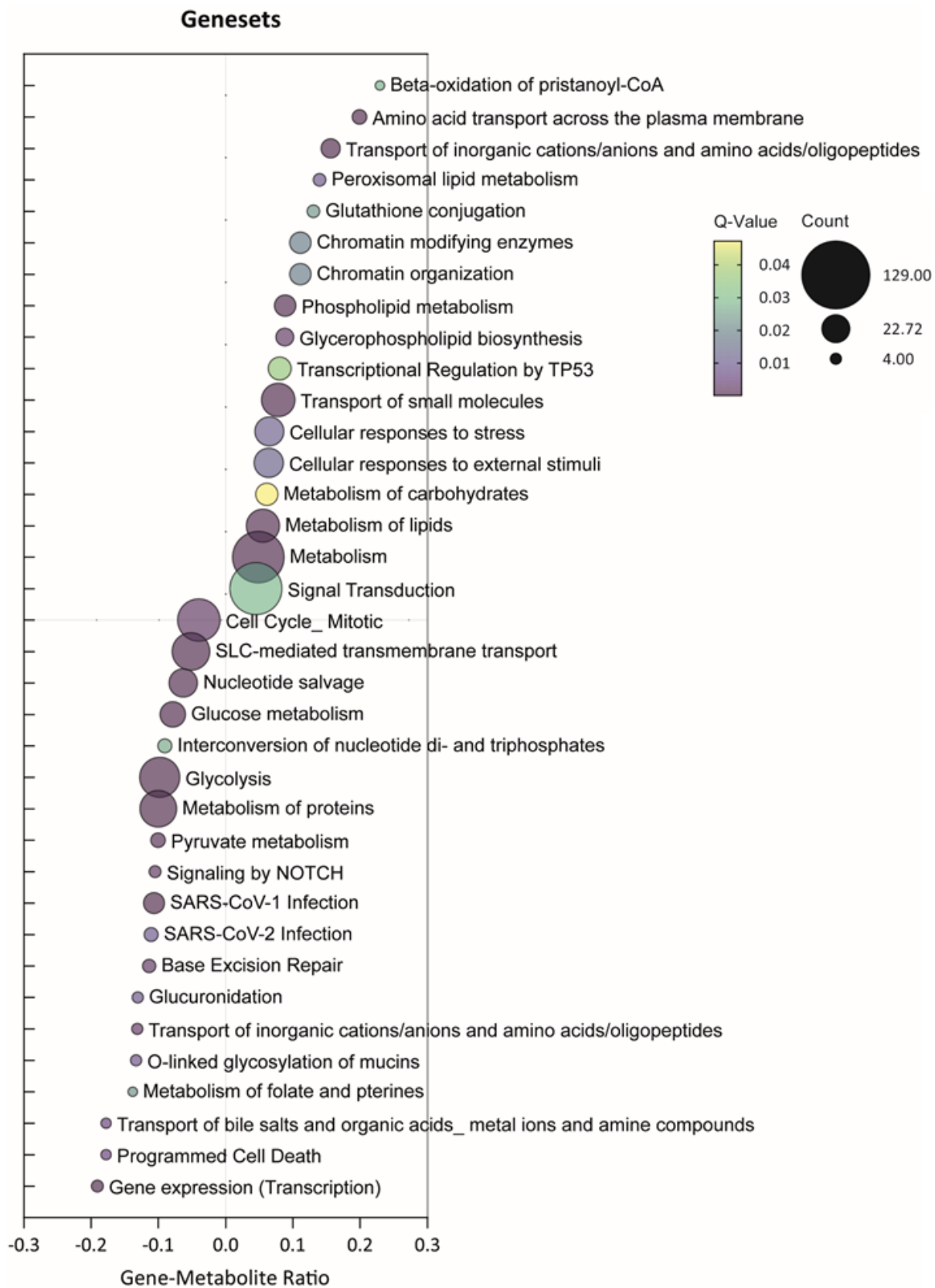
Figure 23 ¹³C-L-Glutamine Isotope Flux Analysis reveals increased enrichment of downstream metabolites in CD8+^{Slc2a1} T cells

Experimental setting of ¹³C-L-Glutamine (A) Key metabolites were analysed for their enrichment in CD8+^{Slc2a1} (blue) and CD8+^{MOCK} (grey) T cells(C) according to the metabolic pathway downstream of glutaminolysis and TCA Cycle (B). Data is shown as MFI +/- STD for n=4; p-values are based on two-way ANOVA with correction for multiple testing by the Bonferroni method; p<0.05 was considered statistically significant and is represented as *<0.05, **<0.01, ***<0.001.

4.12   Integrated analysis reveals increased oxidative stress in CD8+^{Slc2a1}

Due to high batch effects within the metabolomic samples, we could not detect significant findings in fold changes. Therefore, we adapted an unbiased, targeted approach by performing an integrated

analysis. Specifically, we combined the earlier elaborated bulk-RNA and metabolomic data to discern increased metabolic networks in CD8+[Slc2a1] T cells. Therefore, we analysed the significant (p < 0.05) >25% dysregulated genes and >20% enriched or reduced metabolites in CD8+[Slc2a1] T cells cultivated in 5 mM glucose. The integrated ORA revealed significant enrichment in oxidative pathways (Beta-oxidation of pristanoyl-CoA, peroxisomal lipid metabolism) and correlated response mechanisms (glutathione conjugation, cellular stress response). Of note, the overrepresentation of metabolites and genes involved in chromatin modification was also detected (Figure 24). On the other hand, pathways that are connected to programmed cell death were reduced. Further, we could observe reduced metabolic pathways that include glycolysis, pyruvate metabolism, and nucleotide salvage in the reactome ORA sets.

Genesets

Figure 24 Integrated over-representation analysis (ORA) of up- and downregulated pathways in CD8+[Slc2a1] T cells reactivated in 5mM glucose
Reactome pathways detected in CD8+[Slc2a1] T cells are presented with their corresponding counts (size) and q-values (colour), sorted in descending order based on the gene-metabolite ratios for both down- and upregulated pathways. Gene-metabolite ratios represent the sum of combined metabolite and gene hits/total combined representatives in the respective pathways. Pathways with a minimum of 2 overlapping metabolites and genes were considered in the analysis.

Additionally, we conducted a network analysis based on the *Slc2a1* and glucose-dependent up- and downregulated genes (Figure 19) and the specific metabolites overrepresented in CD8+[Slc2a1] cultivated in physiologic and hypoglycemic conditions. The analysis was based on KEGG gene set enrichment. We observed that pathways specifically connected to the TCA, nucleotide synthesis, amino acid, and GSH synthesis are significantly enriched (Figure S 6). Further, we could identify that L-glutamic acid and the gene "*Cat*" show the highest betweenness factors of 1214.45 and 1161.23 in the network analysis (S Table **1**). These happened to be assigned to the GSH pathway in the integrative gene set analysis (Figure 25). Overall, we could detect pathways that indicate increased oxidative stress and responses in CD8+[Slc2a1] T cells.

Figure 25 GSEA Network analysis reveals upregulation of the GSH synthesis pathway
Up- and downregulated pathways of CD8+[Slc2a1] T cells restimulated in physiologic media conditions. Highlighted nodes are the correlated genes (circular) and metabolites (squared) of the upregulated GSH pathway (red) and all genes and metabolites in downregulated pathways detected (blue).

4.13 CD8+^{Slc2a1} T cells have elevated ROS production upon stimulation in hypoglycemic and physiologic media conditions

To confirm the results from the integrated analysis we further investigated the observed increased oxidative stress. Specifically, we analyzed ROS and GSH production in activated primary CD8+ T cells by flow cytometric analysis. No difference in GSH production was observable between MOCK and Slc2a1 transduced CD8+ T cells. However, we could identify significantly elevated ROS production in restimulated CD8+^{Slc2a1} T cells in both glucose concentrations, 0.5mM (A) and 5mM (B, Figure 26). These findings verified our RNA-Seq and metabolomic data, as well as the integrated multi-omics pathway analysis (Figure 18 -Figure 25).
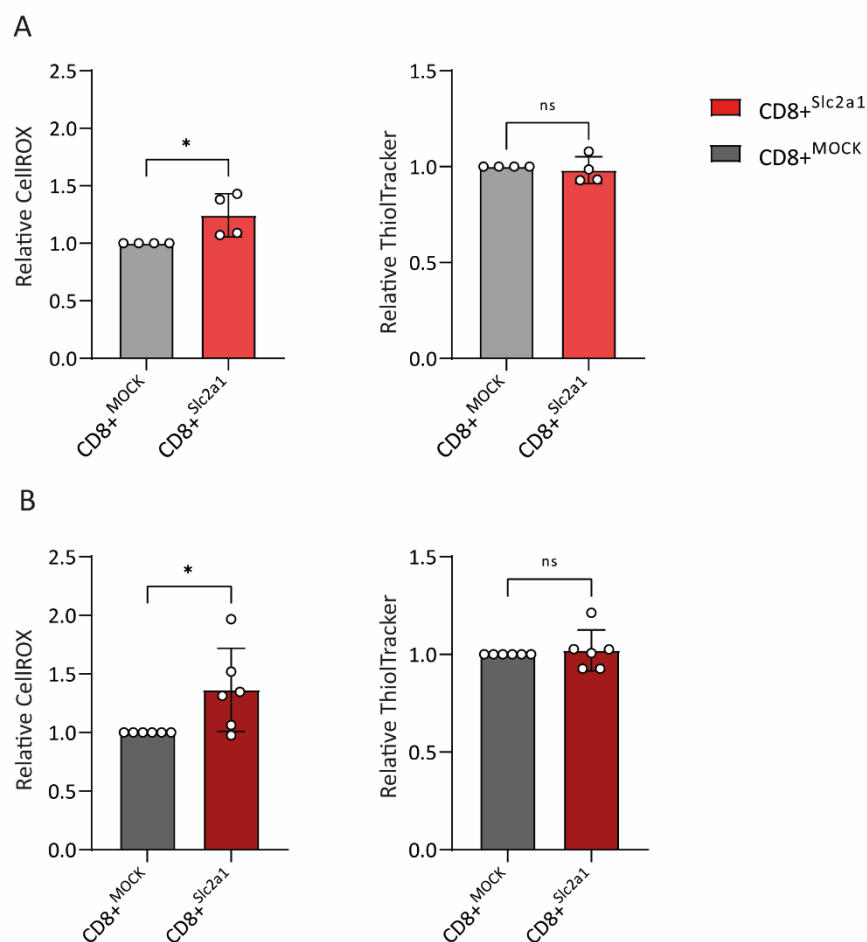
Figure 26 Flow cytometric analysis of restimulated primary murine T cells unveils increased ROS production but no elevated GSH generation in CD8+^{Slc2a1}

Flow cytometric analysis of CellROX ™ Deep Red and ThiolTracker ™ Violet stained murine CD8+ T cells. T cells were restimulated in hypoRPMI (A) or physioRPMI (B) media for 18h before staining. Experiments are shown in mean fold change +/- STD to control for n=7 (A) and n=4 (B) biological replicates; p-values are based on an

unpaired, non-parametric, two-sided t-Test (Mann-Whitney); p<0.05 is considered statistically significant and is represented as *<0.05, **<0.01, ***<0.001

5. Discussion

5.1 Summary of the results

The herein presented data in primary antigen-specific murine T cells showed that the ACT with *Slc2a1*/GLUT1 overexpression is an effective tool to overcome glucose deprivation in the TME. The "metabolic engineering" of CD8+ T cells with ectopic *Slc2a1* displayed sufficient surface expression of functional active GLUT1 transporters which was evident in the glucose uptake and extracellular flux assays. Additionally, increased proliferation and activity in physiologic glucose and hypoglycemic conditions could be detected. In a pancO2 tumor model, we could demonstrate that the increased functional activity was also represented by an augmented anti-tumor efficacy in hypoglycemic conditions. Due to clear changes in activation and exhaustion marker expression and glycolytic and mitochondrial activity, we investigated the transcriptomic and metabolic landscape of the genetically modified T cells. Here we could show ectopic *Slc2a1* expression induces changes in metabolic pathways. Of note, we detected increased activity in ROS-dependent pathways and enrichment in metabolites downstream of the PPP, which includes nucleotide synthesis and GSH recycling. These findings supported the observed increase in proliferation but also suggested increased cellular oxidative stress. In a syngeneic s.c. pancreatic tumor model, we were able to partially translate the anti-tumorigenic activity *in vivo* as we could demonstrate signs of better tumor surveillance in CD8+^{Slc2a1} transfused mice. The impact of *Slc2a1* on metabolic reprogramming was evident in a modified memory subset and substantially better splenic homing *in vivo.* Overall, we were able to show *Slc2a1* overexpression in CD8+ T cells is a promising approach for cellular immunotherapy of solid cancer entities but need further investigation in regard of long-term behaviour and side effects. Additionally, metabolic reprogramming in general poses a powerful approach to modifying immune cells for better functionality and persistence in ACT.

5.2 Functional data and omics hint towards a faster cell cycle progression in CD8+^{Slc2a1}

Since IFN-γ, GrB, and PRF1 are not exclusively downregulated due to GLUT1 overexpression as our data from the Venn analysis suggests, the reason for lower levels of these stimulation-associated genes might be due to two factors. First, glucose depletion in the medium by strong uptake by CD8+^{Slc2a1} could lead to acute cell stress resulting in adverse autophagic effects. On the other hand, the RNA-Seq analysis as with any other experiment in this project reflects the features of the cells at a certain time point post-restimulation. For instance, the kinetics of IFN-γ mRNA and protein expression is well described in literature, as it peaks approximately 24h or even earlier post-stimulation in mRNA levels

(Verfaillie et al. 2001; Curtsinger et al. 2012). Considering, that CD8+^{Slc2a1} progress faster in their cell cycle and division as described in the proliferation assay and display higher intracellular protein levels in the restimulation experiment suggests that the mRNA levels for IFN-γ, GrB, and PRF1 are beyond their peak levels in the transgenic CD8+^{Slc2a1} T cells already. Supporting this assumption, the Venn-diagram revealed that Interferon-gamma (*Ifngr1*) and granzyme B (*Gzmb*) RNAs are enriched in CD8+^{Slc2a1} T cells cultivated in the hypoglycemic condition compared to the physiologic media, pinpointing towards an even faster cell cycle progression and activation at 5mM in those cells.

5.3   Metabolic reprogramming in CD8+^{Slc2a1} T cells supports T-cell function

These findings are in line with the results of the metabolomic analysis, which shows an increased intake and metabolism of glucose and glutamine combined with the elevated metabolism detected in the extracellular flux assay. The observed metabolic switch in T cells is often described to correlate with a decreased anaplerotic importance downstream of glycolysis which could go along with decreased mitochondrial activity (Michalek et al. 2011; Peng et al. 2016). However, the extracellular flux analysis reveals, that CD8+^{Slc2a1} cells not only upregulate their glycolysis but also exhibit a strong mitochondrial respiration. The presence of higher levels of TCA metabolites connected to T-cell activation like malate underline these findings and suggest a stronger cellular activity. Additionally, the increased anti-oxidative pathways observed in the integrative analysis support stronger functionality through anti-oxidative protection (Hiemer et al. 2019; Pilipow et al. 2018).

The enrichment of carnitine and acyl-carnitines observed in the metabolic analysis represent important intermediates for FAO in the mirochondria. Apart from cellular energy delivery, carnitine and its acylated derevatives are known to induce and support T$_{Eff}$-function. Additionally, DNA-protective features linked to its anti-oxidative properties could even further promote T cell activity in CD8+^{Slc2a1} T cells (Thangasamy et al. 2009; Nicholas et al. 2019; Byersdorfer 2014).

The reduced nucleotide salvage observed in the integrated ORA could be connected to the upregulated *de novo* nucleotide synthesis via the PPP discovered in the metabolic tracing (Figure 21, Figure 24). The increased glucose availability in CD8+^{Slc2a1} T cells showed to have a beneficial effect on the accompanying elevation of cell cycle progression observed in the proliferation assay by increased purine levels. IMP as the main precursor and AMP and GMP downstream are central building blocks of the *de novo* nucleotide synthesis for RNA and DNA production which supports the proliferative capacity of the CD8+^{Slc2a1} T cells. Overall, the metabolic analysis revealed that CD8+^{Slc2a1} produces several metabolic intermediates, that support the effector function on several levels in respect to proliferation, cytokine secretion, and cell-protective pathways.

5.4   OT-1 CD8+^{Slc2a1} cells show a superior anti-tumor effect in TME-like glucose conditions

In vitro, we observed significantly better tumor-cell killing by CD8+^{Slc2a1} T cells in the antigen-specific OT-1-OVA model. This effect was strictly restricted to the glucose concentration applied. While no increase but also no negative effect on CD8+^{Slc2a1} in physiologic 5mM glucose was observable we could conclude that GLUT1 overexpression exclusively grants a fitness advantage in hypoglycemic conditions. However, we could observe substantial higher cluster formation in both physiologic and hypoglycemic conditions visible in the representative images (Figure 13) which is in line with the augmented activity and proliferative capacity in CD8+^{Slc2a1}, hinting towards a higher functionality compared to the control also in 5mM. The degranulation at physiologic conditions could underline this assumption. The significant difference could also be due to a better viability observed in CD8+^{Slc2a1} T cells after 14 days of culture including one restimulation cycle at day 7 before the assays (data not shown). This already shows a better long-term functionality of CD8+^{Slc2a1} T cells as we will focus on the memory formation in a later section.

The observations made *in vitro* could also be translated to a syngeneic mouse model as we were able to demonstrate lower tumor diameters in the CD8+^{Slc2a1} treated mice in respect to the mean control. However, it should be mentioned, that no significant change could be achieved in this system which could be due to several reasons. For one it needs to be emphasized that we provoke a strong immune response in the OT-1-OVA model, since all T cells infused heavily react via the artificial, high affinity, antigen-specific TCR (Chua and Salomon 2021; Zhou et al. 2018). This might lead to a premature rejection of the tumors or could interfere with early stages of the tumor development, making it impossible to establish an immunosuppressive TME. The progression to late-stage cancer is an essential step for this purpose (Kleeff et al. 2016; Yang et al. 2022). This leads to the second reason that impacts the only marginal differences in tumor burden between CD8+^{Slc2a1} and CD8+^{MOCK} treated mice which is the initial tumor size at the point of treatment. As mentioned, the TME formation is important for the tumor to interfere with the T-cell metabolism and specifically, reduce glucose availability. Since no significant advantage could be shown *in vitro* this could translate to the mouse model, that small tumors *in vivo* could still offer physiologic glucose levels, that lead to translatable results. To underline this assumption, we showed later T-cell injection is accompanied with substantial differences in tumor burden in the collected preliminary data (Figure S 3). This implies that the tumor size and associated TME establishment is a significant factor for the ACT with GLUT1 overexpressing T cells. The results lead to the conclusion that cellular therapy of cold tumors could benefit from GLUT1

overexpression due to augmented immune cell function in hypoglycemic conditions and better immunosurveillance at later tumor stages. Nevertheless, to further validate this hypothesis, pre-clinical models in a CAR T-cell system and extended *in vivo* studies on larger tumors need to be conducted.

Geltink and colleagues suggested that metabolic conditioning by glucose deprivation increased anti-tumor efficacy of murine CD8+ T cells. They were also able to observe similar metabolic patterns as they were expressed for CD8+^{Slc2a1} cells in our study. In a combinatorial approach with anti-PD-L1 checkpoint blockade, they could show a synergistic anti-tumoral effect *in vivo* (Klein Geltink et al. 2020). Considering this as an indirect way of addressing same pathways and substantially increase GLUT1 expression, a combination treatment of CD8+^{Slc2a1} and checkpoint blockade could have beneficial effects. The increased PD-1 expression observed in CD8+^{Slc2a1} (Figure 11) is a promising indicator for a positive outcome of the combi-treatment approach which might also amplify the efficacy of the ACT with CD8+^{Slc2a1} T cells.

5.5   CD8+^{Slc2a1} reprogramming suggests different behavior in memory formation

As elaborated earlier in the introduction, glucose and downstream metabolites of glycolysis heavily impact T-cell fate via bottom-up signaling. In the multi-omic data analysis we revealed the enrichment of pathways that impact chromatin modifications in CD8+^{Slc2a1}. The change of the epigenetic landscape during transition phase of T cells is tightly connected to their functionality, migration, and memory formation (Chen et al. 2018). Hence, besides the augmentation of proliferation and anti-tumor functionality, we also focused our interest on the impact of ectopic GLUT1 expression on memory transition and subset distribution post-tumor therapy. While short-lived effector cells (SLEC) only contribute to eradication of the primary infection or tumor and remain at the site of inflammation, it is of high importance in ACT to generate a robust memory formation for long-term persistence in tissues and secondary lymphoid organs to prevent tumor recurrence (Joshi et al. 2007; Obar and Lefrancois 2010). As shortly mentioned before, 14-day cultured CD8+^{Slc2a1} could fulfil their functional properties at a bigger extent compared to the MOCK control which was evident in the degranulation experiments. This already suggested a better long-term functionality and viability induced by the *Slc2a1* overexpression.

As the procedure of memory formation is complex and depends on the interplay of epigenetic regulation, transcription factor activity and extracellular cytokine signals, we tried to demonstrate that *Slc2a1* overexpression manipulates the T-cell fate *in vivo.* The two main subsets defining T-cell memory

are central memory (T$_{CM}$) and effector memory (T$_{EM}$) T cells. The major difference between these two subsets is the localization and phenotype and that can be differentiated by the leukocyte (L)-selectin (CD62L) and the IL-7 receptor alpha (CD127) memory-marker expression. T$_{CM}$ (CD62L$^+$/CD127$^+$) reside mainly in lymphoid organs, while T$_{EM}$ (CD62L$^-$/CD127$^+$) express receptors that enable a rapid response and migration to the site of infection or inflammation. As our data suggests, GLUT1 overexpression might prime T cells towards an effector memory type which is in line with the increased aerobic glycolytic discovered in those cells, since constitutive glycolysis supports the formation of this phenotype (O'Sullivan 2019; Phan et al. 2016). However, T$_{CM}$ seem to have superior long-term functionality in regards to cytokine secretion and proliferative capacity (Liu, Sun, and Chen 2020; Klebanoff et al. 2005). The observed difference in memory formation and accumulation of more T$_{EM}$ could therefore significantly impact CD8+^{Slc2a1} cells in their long-term behaviour as lower T$_{CM}$ numbers might impair persistence. Nevertheless, in general the homing to secondary lymphoid organs is considerably important for long-term anti-tumor efficacy which could be represented in our data by the splenic T-cell abundance. Overall, the high relative number of memory T cells that resided in the spleen is a promising indicator of increased long-term persistence of CD8+^{Slc2a1} T cells.

5.6 GLUT1 overexpression is coupled to ROS production and induces anti-oxidative mechanisms

As mentioned above we could observe a strong involvement of the mitochondrial respiration in CD8+^{Slc2a1} T-cell metabolism. This was evident in the OCR of the extracellular flux assay, as well as the strong enrichment of citrate, malate, fumarate, and argininosuccinate in the quantitative metabolomics analysis. The tracing experiments support these results by suggesting anaplerosis not only via glycolysis, but also via the glutaminolysis pathway. The TCA is coupled to the ETC which is the main source of ROS generation in the cell (Zhao et al. 2019; Tirichen et al. 2021). Considering the integrated RNA and metabolomic analysis which was supported by the ROS FACS analysis, we could conclude that CD8+^{Slc2a1} cells undergo a switch to a strong ROS overproduction upon restimulation. Additionally the overrepresentation of compensatory mechanisms to oxidative stress further support this assumption. Specifically, we observed gene enrichment of the Nrf2 gene and downstream pathways like elevated Gclm and GSH production (Zou et al. 2012).

ROS production and response are significant features of activated CD8+^{Slc2a1} T cells. Especially, it is known to be an important second messenger for activation by modulation in metabolic reprogramming as described before (Previte et al. 2017).

In both, 0.5mM and 5mM glucose conditions we encountered a substantial overproduction of ROS in CD8+[Slc2a1] T cells in the FACS analysis data. In the metabolomic and integrated network analysis we showed that the response to oxidative stress is the central network, indicated by the high representation of the GSH synthesis pathway and the high boundness factor for the anti-oxidative enzyme catalase.

ROS production in T cells is one of the key indicators of strong activation which could have several positive and also negative effects on the cells' fate (Havens et al. 2006; Chen et al. 2016; Hildeman et al. 1999). Studies on diabetes mellitus and hyperglycemia revealed that high glucose levels heavily impact the behavior of T cells and that glucose and GLUT1 are tightly connected to the ROS pathway (Rochette et al. 2014; Nishikawa, Edelstein, and Brownlee 2000). On a cellular level, our data suggest that the increased metabolism is tightly connected to the overproduction of ROS. More specifically, the elevated mitochondrial respiration observed in the extracellular flux assays possibly is the key mechanism of ROS production in CD8+[Slc2a1] (Yu, Robotham, and Yoon 2006). An even higher response to ROS in CD8+[Slc2a1] compared to CD8+[MOCK] cells in hypoglycemia could be revealed, which was depicted by increased incorporation of heavy carbon isotopes in GSH in the tracing as well as more genes being differentially expressed in the named compensatory pathway (Hmox1, Gclm, Nrf2). This indicates that GLUT1 overexpression and accompanying glucose uptake support T-cell function. Of note, we could detect a glucose-independent impact of *Slc2a1* overexpression on oxidative stress in the Venn analysis. GLUT1 is known to impact mTOR activity which indicates that the overexpression in T cells alone can already modulate the metabolomic and transcriptomic landscape via intracellular signaling mechanisms (Macintyre et al. 2014).

As mentioned before, an excessive amount of ROS could lead to oxidative stress and even apoptosis. ROS overproduction negatively impacts the functional activity of T cells, which manifests ultimately in malfunction and exhaustion. Imbalanced ROS levels induce mitochondrial depolarisation, dysfunction, and cytochrome C release from the mitochondrial membrane. This, in turn, triggers the downstream arrangement of apoptosomes and the caspase cascade, eventually resulting in cell death (Hildeman et al. 1999). Since our data suggested a strong correlation between *Slc2a1* overexpression and ROS enrichment, there might be concerns regarding the beforementioned apoptotic induction. However, we were able to demonstrate that the T cells overproducing ROS can keep stable concentrations of reduced GSH which is represented by the unchanged Thioltracker[TM] MFIs. This shows that the recycling of GSH from GSSG can maintain the antioxidative equivalent of glutathione probably supported by the elevated PPP metabolism revealed by the metabolomics analysis. By GLUT1 overexpression the T cells are equipped with the ability to shuttle and consume more glucose without directly interfering with the metabolism per se. This ensures, that intrinsic metabolic pathways are still intact and very well

regulated with simultaneous reprogramming for elevated activation and functionality. Additionally, the extracellular flux assay does not indicate any mitochondrial dysfunctionality, displayed in high respiration. Dispite the elevated PD-1 expression, we could not detect direct signs of exhaustion in all glucose conditions since we were able to demostrate augmented tumor-cell lysis. This further supports the assumption that the metabolic reprogramming positiveley impacts CD8+[Slc2a1] functionality. However, the long term impact of GLUT1 induced ROS production on T cells needs to be further investigated to exclude possible toxicities that could not be revealed by the methods conducted in this project.

Excessive ROS is described to have beneficial effects in cancer therapy. Therefore, therapeutic approaches seek to interfere with the anti-oxidant pathways of tumor cells or directly induce ROS production (Nakamura and Takada 2021). The increased ROS production in CD8+[Slc2a1] T cells might be a stress inductor in the TME for the tumor cells leading to apoptotic signaling and reestablishing an equilibrium. The influence of ROS on T-cell activity and the interplay with tumor cells is an interesting topic and needs to be further evaluated in future projects.

6.   Conclusion and Outlook

Adoptive T-Cell therapy have found great success in hematological malignancies but still faces a lot of challenges in solid tumor entities. In recent years, many approaches for the improvement of targeted cellular therapies have been developed in regard to migration, functionality and persistence of chemeric antigen receptor (CAR) T cells (Tian et al. 2020). Although they show promising results in pre-clinical studies, these approaches focus on the interaction of T cells and tumor cells in disregard of the metabolic needs that are essential for proper T-cell function within the TME. Our study focuses on the metabolic reprograming by the ectopic overexpression of *Slc2a1*/GLUT1 to give T cells a selective advantage in the hypoglycemic TME. We were able to demonstrate ameliorated proliferation, metabolic function and anti-tumor efficacy of CD8+^{Slc2a1} T cells and further could show supportive effects on T$_{Eff}$-function and T$_{EM}$-formation.

Slc2a1 overexpression also suggested an impact on the transcriptomic and metabolic landscape of the T cells. The enrichment of several metabolites, naming fumarate or 2-hydroxyglutarate, that influence T-cell function on downstream signalling levels might be essential in this context. Substantial upregulation of the anti-oxidative metabolites, enzymes, and connected pathways like the PPP are indicative for a strong upregulation of ROS and dysregulation of the oxidative state in those cells, independent of glucose levels. Ectopic *Slc2a1* expression and the connection to ROS as a central second messenger in T-cell activation and differentiation needs to be in focus for future studies. Particularly important is the impact on long-term persistence and memory formation in this context. Also, epigenetic changes influenced by the metabolic reprogramming are highly possible and need to be further evaluated. The findings of *Slc2a1*/GLUT1 induced ROS enrichment demands further investigation as it greatly impacts anti-tumor efficacy, too. Whether ROS enrichment is beneficial or detrimental in this context needs to be examined. Since we observed a broad change in the cellular metabolic and transcriptomic landscape, the formation of possible malignancies or autoimmune side effects need to be considered.

In general, the elevated metabolic rate of CD8+^{Slc2a1} caused by facilitated glucose uptake augments the functional activity in ACT against solid tumors *in vitro*. To further solidify the *in vivo* data, we will investigate the combination of GLUT1 and CARs for improved cellular therapy. The exploration of different intracellular co-stimulatory domains CD28 and 4-1BB should be in focus since these greatly impact T-cell metabolism in different ways. CD28 signalling is described to elevate the glycolytic pathway. Consequently, the synergistic effect of GLUT1 overexpression and induced glycolysis could possibly lead to stronger activity in the T cells, but could also drive effector cell differentiation and

impair memory formation. Contrary, 4-1BB signalling drives memory formation by inducing mitochondrial biogenesis (Kawalekar et al. 2016). Glucose uptake by greater extent could supply important metabolites leading to an additive effect. Therefore, the combination of CARs and metabolic reprogramming could further shape the landscape of the T cells which helps to finetune the desired phenotypes for better ACT.

Overall, the data demonstrate that the ectopic expression of *Slc2a1* in T cells might represent a tool to overcome TME-mediated adverse effects on T-cell functionality.

7. Supplementary

7.1 Supplementary Figures
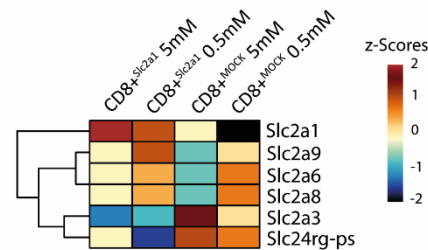
Figure S 1 z-Scores of normalized RNA-Seq data for *Slc2a* transporter show different expression patterns for CD8+^{Slc2a1}

All glucose transporters of the Slc2a family above a DESeq2 normalized count of 50 are depicted for CD8+^{Slc2a1} and CD8+^{MOCK} cells in 0.5mM and 5mM glucose concentration. Cells were restimulated with CD3/28 ABs for 18h before RNA-Seq preparation. Data shows the z-Scores of the mean normalized counts of n=4 technical replicates.
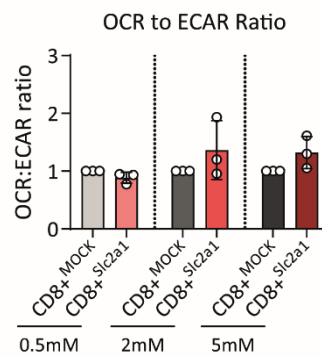
Figure S 2 OCR:ECAR Ratios of CD8+^{Slc2a1} and CD8+^{MOCK} T cells do not show substantial differences

The ratios of mitochondrial and glycolytic baseline values after glucose injection in GLUT1 and MOCK transduced T cells. OCR:ECAR Ratios are calculated for 0.5, 2, and 5mM Glucose.
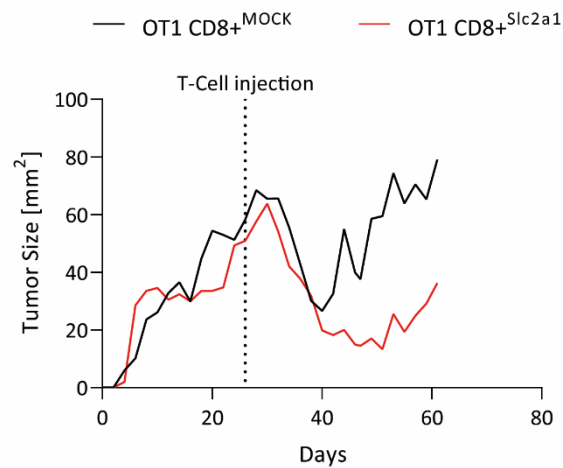
Figure S 3 Preliminary data of delayed T-cell injection shows substantial augmented anti-tumor efficacy of CD8+Slc2a1 in an antigen-specific OT-1-OVA *in vivo* model

$3x10^6$ pancO2-OVA cells were injected s.c. in flanks and treated with 10^7 OT-1 T cells 25 days post-tumor induction. Growth curves represent one biological replicate for both groups, OT-1 CD8+MOCK (black) and OT-1 CD8+Slc2a1 (red)
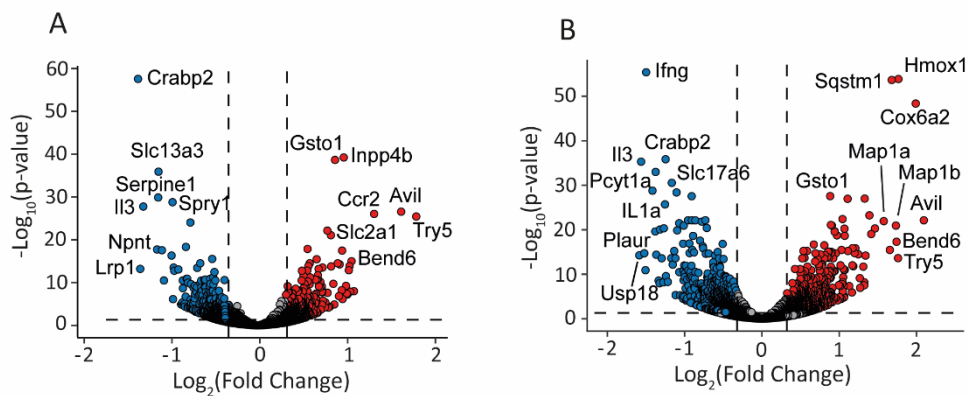
Figure S 4 Volcano plots of differentially expressed genes of CD8Slc2a1 T cells in 5mM and 0.5mM Glucose

Differential Expression Analysis of primary murine CD8+Slc2a1 VS CD8+MOCK T cells in physiologic and hypoglycemic conditions. Genes with $p_{adj} < 0.05$ and $Log_2(FC) < -0.42$ or $Log_2(FC) > 0.32$ were considered as significantly differentially expressed.
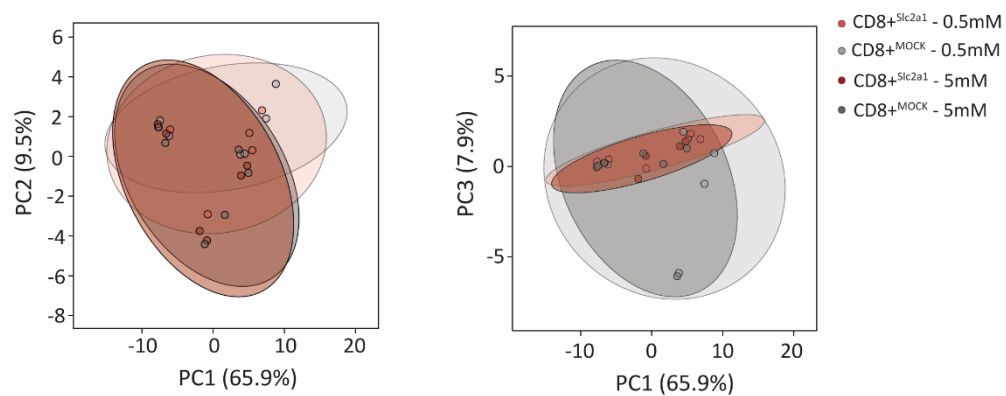
Figure S 5 Two-dimensional depiction of Principal Component Analysis (PCA) of quantified metabolomics analysis

PCA plots are depicted for Components 1 VS 2 and PC1 VS PC3 for CD8+[Slc2a1] and CD8+[MOCK] in 5mM and 0.5mM glucose conditions.
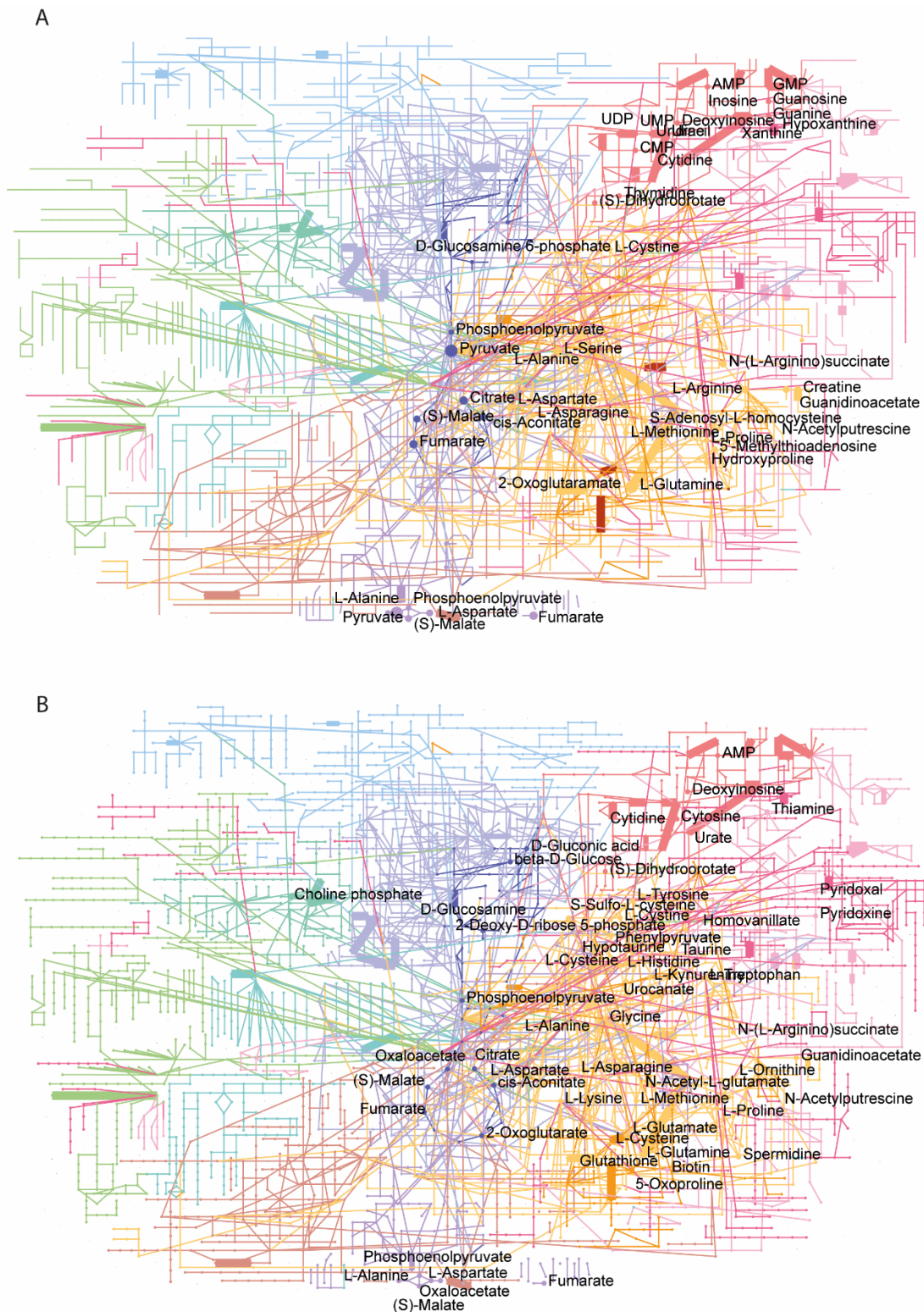
Figure S 6 Metabolic landscape and deregulated metabolites in CD8+^{Slc2a1} T cells in 5mM (A) and 0.5mM (B) glucose

Increased and decreased metabolites in CD8+^{Slc2a1} T cells activated in 5mM (A) and 0.5mM (B) glucose reveal enrichments in the TCA cycle (blue), nucleotide synthesis pathway (red), and amino acid and GSH synthesis pathways (yellow). Enriched enzymes of metabolic pathways are indicated in bold connecting lines and enriched metabolites are displayed as dots. Representatives of pathways significantly enriched in the KEGG pathway are shown. P < 0.05 is considered significantly enriched.

7.2 Supplementary Tables

S Table 1 Betweenness factor and degree of the enrichment from the integrated KEGG pathway analysis in physiologic media

Label	Degree	Betweenness
L-Glutamic acid	10	1214.45
CAT	8	1161.23
CTPS2	5	561.09
Uridine 5'-diphosphate	8	555.66
Acetylcholine	9	535.67
GLS2	8	486.88
L-Arginine	6	460.58
IFNG	5	429.46
L-Malic acid	5	355.29
F2R	7	264.12
Thymidine	5	245.05
P2RY14	5	207.74
Ornithine	5	203.17
Uridine	5	146.67
GNA15	5	112.61
F2RL2	5	112.61

8. List of Figures

9.   List of Tables

10. List of Abbreviations

µM	Micromolar
2-DG	2-Deoxyglucose
AA	Antimycin A
AB	Antibody
ACT	Adoptive T-cell therapy
AKT	Proteinkinase B
ALL	acute lymphoblastic leukemia
AMPK	5' AMP-activated protein kinase
ASS	argininosuccinate synthase
BSA	Bovine Serum Albumin
CAF	Cancer-associated fibroblast
CAR	Chimeric antigen receptor
CD	Cluster of Differentiation
ECM	Extracellular matrix
EpCAM	Epithelial cell adhesion molecule
ETC	Electron transport chain
FA	Fatty acid
FAO	Fatty acid oxidation
FC	Fold Change
FCCP	Carbonyl cyanide-p-trifluoromethoxyphenylhydrazone
GAPDH	Glycerinaldehyd-3-phosphat-Dehydrogenase
GLUT	Human Glucose transporter
GR	Glutathione reductase
GrB	Granzyme B
GSH	Glutathione
GSSG	Glutathione disulfide
GTEx	Genotype Tissue-expression
HBP	Hexosamine biosynthesis pathway
HIF1--α	Hypoxia-inducible factor 1 alpha
HR	Hazard ratio
i.v.	intravenous
IFN-γ	Interferon-gamma

IL	Interleukin
MFI	Median Fluorescent Intensity
mM	Millimolar
mTCM	Murine T-cell medium
NAD+	nicotinamide adenine dinucleotide
NADPH	nicotinamide adenine dinucleotide phosphate
NES	Normalized Enrichment Score
NFAT	Nuclear Factor of Activated T Cells
NFκB	Nuclear factor kappa-light-chain-enhancer of activated B-cells
NRF2	Nuclear Factor Erythroid-derived 2-like 2
OTC	ornithine transcarbamylase
OVA/SIINFEKL	Ovalbumin
PAAD	Pancreatic Adenocarcinoma
PBS	Phosphate Buffered Saline
PDAC	Pancreatic ductal adenocarcinoma
PHD	HIF prolyl hydroxylase
PI3K	Phosphatidylinositol-3-Kinase
PPP	Pentose-Phosphate-Pathway
PRF1	Perforin-1
Rot	Rotenone
s.c.	subcutaneous
scFv	Single-chain variable fragment
SD	Standard deviation
SEM	Standard Error of Mean
SGLT	Sodium-glucose linked transporters
Slc	Murine Solute carrier gene
SLC	Human solute carrier gene
T CM	Central memory
T eff	T effector
T EM	Effector memory
T rm	Tissue-resident memory
TAM	Tumor-associated macrophage
TCA	Tricarboxylic Acid

TCGA	The Cancer Genome Atlas
TCR	T-cell receptor
TIF	Tumor intestinal fluid
TIL	Tumor-infiltrating lymphocyte
TME	Tumor microenvironment
TPM	Transcript per million
WHO	World health organization

11. References

Airley, R. E., and A. Mobasheri. 2007. 'Hypoxic regulation of glucose transport, anaerobic metabolism and angiogenesis in cancer: novel pathways and targets for anticancer therapeutics', *Chemotherapy*, 53: 233-56.

Ancey, P. B., C. Contat, and E. Meylan. 2018. 'Glucose transporters in cancer - from tumor cells to the tumor microenvironment', *FEBS J*, 285: 2926-43.

Andrea, A. E., A. Chiron, S. Bessoles, and S. Hacein-Bey-Abina. 2020. 'Engineering Next-Generation CAR-T Cells for Better Toxicity Management', *Int J Mol Sci*, 21.

Araki, K., A. P. Turner, V. O. Shaffer, S. Gangappa, S. A. Keller, M. F. Bachmann, C. P. Larsen, and R. Ahmed. 2009. 'mTOR regulates memory CD8 T-cell differentiation', *Nature*, 460: 108-12.

Araujo, L., P. Khim, H. Mkhikian, C. L. Mortales, and M. Demetriou. 2017. 'Glycolysis and glutaminolysis cooperatively control T cell function by limiting metabolite supply to N-glycosylation', *Elife*, 6.

'Axicabtagene ciloleucel (Yescarta) for B-cell lymphoma'. 2018. *Med Lett Drugs Ther*, 60: e122-e23.

Bental, M., and C. Deutsch. 1993. 'Metabolic changes in activated T cells: an NMR study of human peripheral blood lymphocytes', *Magn Reson Med*, 29: 317-26.

Binnewies, M., E. W. Roberts, K. Kersten, V. Chan, D. F. Fearon, M. Merad, L. M. Coussens, D. I. Gabrilovich, S. Ostrand-Rosenberg, C. C. Hedrick, R. H. Vonderheide, M. J. Pittet, R. K. Jain, W. Zou, T. K. Howcroft, E. C. Woodhouse, R. A. Weinberg, and M. F. Krummel. 2018. 'Understanding the tumor immune microenvironment (TIME) for effective therapy', *Nat Med*, 24: 541-50.

Bonaventura, P., T. Shekarian, V. Alcazer, J. Valladeau-Guilemond, S. Valsesia-Wittmann, S. Amigorena, C. Caux, and S. Depil. 2019. 'Cold Tumors: A Therapeutic Challenge for Immunotherapy', *Front Immunol*, 10: 168.

Buller, C. L., C. W. Heilig, and F. C. Brosius, 3rd. 2011. 'GLUT1 enhances mTOR activity independently of TSC2 and AMPK', *Am J Physiol Renal Physiol*, 301: F588-96.

Burant, C. F., and G. I. Bell. 1992. 'Mammalian facilitative glucose transporters: evidence for similar substrate recognition sites in functionally monomeric proteins', *Biochemistry*, 31: 10414-20.

Burgess, E. A., and B. Sylven. 1962. 'Glucose, lactate, and lactic dehydrogenase activity in normal interstitial fluid and that of solid mouse tumors', *Cancer Res*, 22: 581-8.

Byersdorfer, C. A. 2014. 'The role of Fatty Acid oxidation in the metabolic reprograming of activated t-cells', *Front Immunol*, 5: 641.

Cai, K., S. Chen, C. Zhu, L. Li, C. Yu, Z. He, and C. Sun. 2022. 'FOXD1 facilitates pancreatic cancer cell proliferation, invasion, and metastasis by regulating GLUT1-mediated aerobic glycolysis', *Cell Death Dis*, 13: 765.

Cao, Y., J. C. Rathmell, and A. N. Macintyre. 2014. 'Metabolic reprogramming towards aerobic glycolysis correlates with greater proliferative ability and resistance to metabolic inhibition in CD8 versus CD4 T cells', *PLoS One*, 9: e104104.

Carey, B. W., L. W. Finley, J. R. Cross, C. D. Allis, and C. B. Thompson. 2015. 'Intracellular alpha-ketoglutarate maintains the pluripotency of embryonic stem cells', *Nature*, 518: 413-6.

Cham, C. M., and T. F. Gajewski. 2005. 'Glucose availability regulates IFN-gamma production and p70S6 kinase activation in CD8+ effector T cells', *J Immunol*, 174: 4670-7.

Chang, C. H., J. D. Curtis, L. B. Maggi, Jr., B. Faubert, A. V. Villarino, D. O'Sullivan, S. C. Huang, G. J. van der Windt, J. Blagih, J. Qiu, J. D. Weber, E. J. Pearce, R. G. Jones, and E. L. Pearce. 2013. 'Posttranscriptional control of T cell effector function by aerobic glycolysis', *Cell*, 153: 1239-51.

Chang, C. H., J. Qiu, D. O'Sullivan, M. D. Buck, T. Noguchi, J. D. Curtis, Q. Chen, M. Gindin, M. M. Gubin, G. J. van der Windt, E. Tonc, R. D. Schreiber, E. J. Pearce, and E. L. Pearce. 2015. 'Metabolic Competition in the Tumor Microenvironment Is a Driver of Cancer Progression', *Cell*, 162: 1229-41.

Chen, X., Y. Qian, and S. Wu. 2015. 'The Warburg effect: evolving interpretations of an established concept', *Free Radic Biol Med*, 79: 253-63.

Chen, X., M. Song, B. Zhang, and Y. Zhang. 2016. 'Reactive Oxygen Species Regulate T Cell Immune Response in the Tumor Microenvironment', *Oxid Med Cell Longev*, 2016: 1580967.

Chen, Y., R. Zander, A. Khatun, D. M. Schauder, and W. Cui. 2018. 'Transcriptional and Epigenetic Regulation of Effector and Memory CD8 T Cell Differentiation', *Front Immunol*, 9: 2826.

Christodoulou, D., A. Kuehne, A. Estermann, T. Fuhrer, P. Lang, and U. Sauer. 2019. 'Reserve Flux Capacity in the Pentose Phosphate Pathway by NADPH Binding Is Conserved across Kingdoms', *iScience*, 19: 1133-44.

Chua, X. Y., and A. Salomon. 2021. 'Ovalbumin Antigen-Specific Activation of Human T Cell Receptor Closely Resembles Soluble Antibody Stimulation as Revealed by BOOST Phosphotyrosine Proteomics', *J Proteome Res*, 20: 3330-44.

Crane, C. A., B. J. Ahn, S. J. Han, and A. T. Parsa. 2012. 'Soluble factors secreted by glioblastoma cell lines facilitate recruitment, survival, and expansion of regulatory T cells: implications for immunotherapy', *Neuro Oncol*, 14: 584-95.

Cretenet, G., I. Clerc, M. Matias, S. Loisel, M. Craveiro, L. Oburoglu, S. Kinet, C. Mongellaz, V. Dardalhon, and N. Taylor. 2016. 'Cell surface Glut1 levels distinguish human CD4 and CD8 T lymphocyte subsets with distinct effector functions', *Sci Rep*, 6: 24129.

Curtsinger, J. M., P. Agarwal, D. C. Lins, and M. F. Mescher. 2012. 'Autocrine IFN-gamma promotes naive CD8 T cell differentiation and synergizes with IFN-alpha to stimulate strong function', *J Immunol*, 189: 659-68.

Dan Dunn, J., L. A. Alvarez, X. Zhang, and T. Soldati. 2015. 'Reactive oxygen species and mitochondria: A nexus of cellular homeostasis', *Redox Biol*, 6: 472-85.

Daneshmandi, S., T. Cassel, P. Lin, R. M. Higashi, G. M. Wulf, V. A. Boussiotis, T. W. Fan, and P. Seth. 2021. 'Blockade of 6-phosphogluconate dehydrogenase generates CD8(+) effector T cells with enhanced anti-tumor function', *Cell Rep*, 34: 108831.

Debela, D. T., S. G. Muzazu, K. D. Heraro, M. T. Ndalama, B. W. Mesele, D. C. Haile, S. K. Kitui, and T. Manyazewal. 2021. 'New approaches and procedures for cancer treatment: Current perspectives', *SAGE Open Med*, 9: 20503121211034366.

DePeaux, K., and G. M. Delgoffe. 2021. 'Metabolic barriers to cancer immunotherapy', *Nat Rev Immunol*, 21: 785-97.

Doedens, A. L., A. T. Phan, M. H. Stradner, J. K. Fujimoto, J. V. Nguyen, E. Yang, R. S. Johnson, and A. W. Goldrath. 2013. 'Hypoxia-inducible factors enhance the effector responses of CD8(+) T cells to persistent antigen', *Nat Immunol*, 14: 1173-82.

Ecker, C., L. Guo, S. Voicu, L. Gil-de-Gomez, A. Medvec, L. Cortina, J. Pajda, M. Andolina, M. Torres-Castillo, J. L. Donato, S. Mansour, E. R. Zynda, P. Y. Lin, A. Varela-Rohena, I. A. Blair, and J. L. Riley. 2018. 'Differential Reliance on Lipid Metabolism as a Salvage Pathway Underlies Functional Differences of T Cell Subsets in Poor Nutrient Environments', *Cell Rep*, 23: 741-55.

Edinger, A. L., and C. B. Thompson. 2002. 'Akt maintains cell size and survival by increasing mTOR-dependent nutrient uptake', *Mol Biol Cell*, 13: 2276-88.

Eggermont, A. M., V. Chiarion-Sileni, J. J. Grob, R. Dummer, J. D. Wolchok, H. Schmidt, O. Hamid, C. Robert, P. A. Ascierto, J. M. Richards, C. Lebbe, V. Ferraresi, M. Smylie, J. S. Weber, M. Maio, L. Bastholt, L. Mortier, L. Thomas, S. Tahir, A. Hauschild, J. C. Hassel, F. S. Hodi, C. Taitt, V. de Pril, G. de Schaetzen, S. Suciu, and A. Testori. 2016. 'Prolonged Survival in Stage III Melanoma with Ipilimumab Adjuvant Therapy', *N Engl J Med*, 375: 1845-55.

Frauwirth, K. A., J. L. Riley, M. H. Harris, R. V. Parry, J. C. Rathmell, D. R. Plas, R. L. Elstrom, C. H. June, and C. B. Thompson. 2002. 'The CD28 signaling pathway regulates glucose metabolism', *Immunity*, 16: 769-77.

Friedman, C. F., C. Spencer, C. R. Cabanski, K. S. Panageas, D. K. Wells, A. Ribas, H. Tawbi, K. Tsai, M. Postow, A. Shoushtari, P. Chapman, J. Karakunnel, S. Bucktrout, P. Gherardini, T. J. Hollmann,

R. O. Chen, M. Callahan, T. LaVallee, R. Ibrahim, and J. Wolchok. 2022. 'Ipilimumab alone or in combination with nivolumab in patients with advanced melanoma who have progressed or relapsed on PD-1 blockade: clinical outcomes and translational biomarker analyses', *J Immunother Cancer*, 10.

Fultang, L., S. Booth, O. Yogev, B. Martins da Costa, V. Tubb, S. Panetti, V. Stavrou, U. Scarpa, A. Jankevics, G. Lloyd, A. Southam, S. P. Lee, W. B. Dunn, L. Chesler, F. Mussai, and C. De Santo. 2020. 'Metabolic engineering against the arginine microenvironment enhances CAR-T cell proliferation and therapeutic activity', *Blood*, 136: 1155-60.

Ganguli, G., U. Mukherjee, and A. Sonawane. 2019. 'Peroxisomes and Oxidative Stress: Their Implications in the Modulation of Cellular Immunity During Mycobacterial Infection', *Front Microbiol*, 10: 1121.

Geiger, R., J. C. Rieckmann, T. Wolf, C. Basso, Y. Feng, T. Fuhrer, M. Kogadeeva, P. Picotti, F. Meissner, M. Mann, N. Zamboni, F. Sallusto, and A. Lanzavecchia. 2016. 'L-Arginine Modulates T Cell Metabolism and Enhances Survival and Anti-tumor Activity', *Cell*, 167: 829-42 e13.

Ghani, K., X. Wang, P. O. de Campos-Lima, M. Olszewska, A. Kamen, I. Rivière, and M. Caruso. 2009. 'Efficient human hematopoietic cell transduction using RD114- and GALV-pseudotyped retroviral vectors produced in suspension and serum-free media', *Hum Gene Ther*, 20: 966-74.

Ghosh, R., and D. L. Mitchell. 1999. 'Effect of oxidative DNA damage in promoter elements on transcription factor binding', *Nucleic Acids Res*, 27: 3213-8.

Ghosh, S., S. Mukherjee, S. Choudhury, P. Gupta, A. Adhikary, R. Baral, and S. Chattopadhyay. 2015. 'Reactive oxygen species in the tumor niche triggers altered activation of macrophages and immunosuppression: Role of fluoxetine', *Cell Signal*, 27: 1398-412.

Giraldo, N. A., R. Sanchez-Salas, J. D. Peske, Y. Vano, E. Becht, F. Petitprez, P. Validire, A. Ingels, X. Cathelineau, W. H. Fridman, and C. Sautes-Fridman. 2019. 'The clinical role of the TME in solid cancer', *Br J Cancer*, 120: 45-53.

Gudmundsdottir, H., A. D. Wells, and L. A. Turka. 1999. 'Dynamics and requirements of T cell clonal expansion in vivo at the single-cell level: effector function is linked to proliferative capacity', *J Immunol*, 162: 5212-23.

Hamilos, D. L., P. Zelarney, and J. J. Mascali. 1989. 'Lymphocyte proliferation in glutathione-depleted lymphocytes: direct relationship between glutathione availability and the proliferative response', *Immunopharmacology*, 18: 223-35.

Hanahan, D., and R. A. Weinberg. 2011. 'Hallmarks of cancer: the next generation', *Cell*, 144: 646-74.

Harvey, C. J., R. K. Thimmulappa, A. Singh, D. J. Blake, G. Ling, N. Wakabayashi, J. Fujii, A. Myers, and S. Biswal. 2009. 'Nrf2-regulated glutathione recycling independent of biosynthesis is critical for cell survival during oxidative stress', *Free Radic Biol Med*, 46: 443-53.

Havens, C. G., A. Ho, N. Yoshioka, and S. F. Dowdy. 2006. 'Regulation of late G1/S phase transition and APC Cdh1 by reactive oxygen species', *Mol Cell Biol*, 26: 4701-11.

Hiemer, S., S. Jatav, J. Jussif, J. Alley, S. Lathwal, M. Piotrowski, J. Janiszewski, R. Kibbey, T. Alves, D. Dumlao, A. Jha, and H. Bandukwala. 2019. 'Integrated Metabolomic and Transcriptomic Profiling Reveals Novel Activation-Induced Metabolic Networks in Human T cells', *bioRxiv*: 635789.

Hildeman, D. A., T. Mitchell, T. K. Teague, P. Henson, B. J. Day, J. Kappler, and P. C. Marrack. 1999. 'Reactive oxygen species regulate activation-induced T cell apoptosis', *Immunity*, 10: 735-44.

Ho, P. C., J. D. Bihuniak, A. N. Macintyre, M. Staron, X. Liu, R. Amezquita, Y. C. Tsui, G. Cui, G. Micevic, J. C. Perales, S. H. Kleinstein, E. D. Abel, K. L. Insogna, S. Feske, J. W. Locasale, M. W. Bosenberg, J. C. Rathmell, and S. M. Kaech. 2015. 'Phosphoenolpyruvate Is a Metabolic Checkpoint of Anti-tumor T Cell Responses', *Cell*, 162: 1217-28.

Hochrein, S. M., H. Wu, M. Eckstein, L. Arrigoni, J. S. Herman, F. Schumacher, C. Gerecke, M. Rosenfeldt, D. Grun, B. Kleuser, G. Gasteiger, W. Kastenmuller, B. Ghesquiere, J. Van den Bossche, E. D.

Abel, and M. Vaeth. 2022. 'The glucose transporter GLUT3 controls T helper 17 cell responses through glycolytic-epigenetic reprogramming', *Cell Metab*, 34: 516-32 e11.

Hombach, A. A., and H. Abken. 2013. 'Of chimeric antigen receptors and antibodies: OX40 and 41BB costimulation sharpen up T cell-based immunotherapy of cancer', *Immunotherapy*, 5: 677-81.

Hou, B., Y. Tang, W. Li, Q. Zeng, and D. Chang. 2019. 'Efficiency of CAR-T Therapy for Treatment of Solid Tumor in Clinical Trials: A Meta-Analysis', *Dis Markers*, 2019: 3425291.

Hu, W., Z. Zi, Y. Jin, G. Li, K. Shao, Q. Cai, X. Ma, and F. Wei. 2019. 'CRISPR/Cas9-mediated PD-1 disruption enhances human mesothelin-targeted CAR T cell effector functions', *Cancer Immunol Immunother*, 68: 365-77.

Jiang, X., J. Wang, X. Deng, F. Xiong, J. Ge, B. Xiang, X. Wu, J. Ma, M. Zhou, X. Li, Y. Li, G. Li, W. Xiong, C. Guo, and Z. Zeng. 2019. 'Role of the tumor microenvironment in PD-L1/PD-1-mediated tumor immune escape', *Mol Cancer*, 18: 10.

Joshi, N. S., W. Cui, A. Chandele, H. K. Lee, D. R. Urso, J. Hagman, L. Gapin, and S. M. Kaech. 2007. 'Inflammation directs memory precursor and short-lived effector CD8(+) T cell fates via the graded expression of T-bet transcription factor', *Immunity*, 27: 281-95.

Joyce, J. A., and J. W. Pollard. 2009. 'Microenvironmental regulation of metastasis', *Nat Rev Cancer*, 9: 239-52.

Kalos, M., and C. H. June. 2013. 'Adoptive T cell transfer for cancer immunotherapy in the era of synthetic biology', *Immunity*, 39: 49-60.

Kamburov, A., R. Cavill, T. M. Ebbels, R. Herwig, and H. C. Keun. 2011. 'Integrated pathway-level analysis of transcriptomics and metabolomics data with IMPaLA', *Bioinformatics*, 27: 2917-8.

Kaminski, M., M. Kiessling, D. Suss, P. H. Krammer, and K. Gulow. 2007. 'Novel role for mitochondria: protein kinase Ctheta-dependent oxidative signaling organelles in activation-induced T-cell death', *Mol Cell Biol*, 27: 3625-39.

Kaminski, M. M., D. Roth, P. H. Krammer, and K. Gulow. 2013. 'Mitochondria as oxidative signaling organelles in T-cell activation: physiological role and pathological implications', *Arch Immunol Ther Exp (Warsz)*, 61: 367-84.

Kaminski, M. M., D. Roth, S. Sass, S. W. Sauer, P. H. Krammer, and K. Gulow. 2012. 'Manganese superoxide dismutase: a regulator of T cell activation-induced oxidative signaling and cell death', *Biochim Biophys Acta*, 1823: 1041-52.

Karches, C. H., M. R. Benmebarek, M. L. Schmidbauer, M. Kurzay, R. Klaus, M. Geiger, F. Rataj, B. L. Cadilha, S. Lesch, C. Heise, R. Murr, J. Vom Berg, M. Jastroch, D. Lamp, J. Ding, P. Duewell, G. Niederfellner, C. Sustmann, S. Endres, C. Klein, and S. Kobold. 2019. 'Bispecific Antibodies Enable Synthetic Agonistic Receptor-Transduced T Cells for Tumor Immunotherapy', *Clin Cancer Res*, 25: 5890-900.

Kawalekar, O. U., R. S. O'Connor, J. A. Fraietta, L. Guo, S. E. McGettigan, A. D. Posey, Jr., P. R. Patel, S. Guedan, J. Scholler, B. Keith, N. W. Snyder, I. A. Blair, M. C. Milone, and C. H. June. 2016. 'Distinct Signaling of Coreceptors Regulates Specific Metabolism Pathways and Impacts Memory Development in CAR T Cells', *Immunity*, 44: 380-90.

Klebanoff, C. A., L. Gattinoni, P. Torabi-Parizi, K. Kerstann, A. R. Cardones, S. E. Finkelstein, D. C. Palmer, P. A. Antony, S. T. Hwang, S. A. Rosenberg, T. A. Waldmann, and N. P. Restifo. 2005. 'Central memory self/tumor-reactive CD8+ T cells confer superior antitumor immunity compared with effector memory T cells', *Proc Natl Acad Sci U S A*, 102: 9571-6.

Kleeff, J., M. Korc, M. Apte, C. La Vecchia, C. D. Johnson, A. V. Biankin, R. E. Neale, M. Tempero, D. A. Tuveson, R. H. Hruban, and J. P. Neoptolemos. 2016. 'Pancreatic cancer', *Nat Rev Dis Primers*, 2: 16022.

Klein Geltink, R. I., J. Edwards-Hicks, P. Apostolova, D. O'Sullivan, D. E. Sanin, A. E. Patterson, D. J. Puleston, N. A. M. Ligthart, J. M. Buescher, K. M. Grzes, A. M. Kabat, M. Stanczak, J. D. Curtis, F. Hassler, F. M. Uhl, M. Fabri, R. Zeiser, E. J. Pearce, and E. L. Pearce. 2020. 'Metabolic conditioning of CD8(+) effector T cells for adoptive cell therapy', *Nat Metab*, 2: 703-16.

Klein Geltink, R. I., D. O'Sullivan, and E. L. Pearce. 2017. 'Caught in the cROSsfire: GSH Controls T Cell Metabolic Reprogramming', *Immunity*, 46: 525-27.

Kohl, A., K. C. Kao, and P. C. Ho. 2021. 'Can tumor cells take it all away?', *Cell Metab*, 33: 1071-72.

Lee, K., P. Gudapati, S. Dragovic, C. Spencer, S. Joyce, N. Killeen, M. A. Magnuson, and M. Boothby. 2010. 'Mammalian target of rapamycin protein complex 2 regulates differentiation of Th1 and Th2 cell subsets via distinct signaling pathways', *Immunity*, 32: 743-53.

Li, Z. Y., Y. L. Shi, G. X. Liang, J. Yang, S. K. Zhuang, J. B. Lin, A. Ghodbane, M. S. Tam, Z. J. Liang, Z. G. Zha, and H. T. Zhang. 2020. 'Visualization of GLUT1 Trafficking in Live Cancer Cells by the Use of a Dual-Fluorescence Reporter', *ACS Omega*, 5: 15911-21.

Lian, G., J. R. Gnanaprakasam, T. Wang, R. Wu, X. Chen, L. Liu, Y. Shen, M. Yang, J. Yang, Y. Chen, V. Vasiliou, T. A. Cassel, D. R. Green, Y. Liu, T. W. Fan, and R. Wang. 2018. 'Glutathione de novo synthesis but not recycling process coordinates with glutamine catabolism to control redox homeostasis and directs murine T cell differentiation', *Elife*, 7.

Ligtenberg, M. A., D. Mougiakakos, M. Mukhopadhyay, K. Witt, A. Lladser, M. Chmielewski, T. Riet, H. Abken, and R. Kiessling. 2016. 'Coexpressed Catalase Protects Chimeric Antigen Receptor-Redirected T Cells as well as Bystander Cells from Oxidative Stress-Induced Loss of Antitumor Activity', *J Immunol*, 196: 759-66.

Liikanen, I., C. Lauhan, S. Quon, K. Omilusik, A. T. Phan, L. B. Bartroli, A. Ferry, J. Goulding, J. Chen, J. P. Scott-Browne, J. T. Yustein, N. E. Scharping, D. A. Witherden, and A. W. Goldrath. 2021. 'Hypoxia-inducible factor activity promotes antitumor effector function and tissue residency by CD8+ T cells', *J Clin Invest*, 131.

Liu, G., Q. Zhang, D. Li, L. Zhang, Z. Gu, J. Liu, G. Liu, M. Yang, J. Gu, X. Cui, Y. Pan, and X. Tian. 2021. 'PD-1 silencing improves anti-tumor activities of human mesothelin-targeted CAR T cells', *Hum Immunol*, 82: 130-38.

Liu, Q., Z. Sun, and L. Chen. 2020. 'Memory T cells: strategies for optimizing tumor immunotherapy', *Protein Cell*, 11: 549-64.

Loschen, G., A. Azzi, and L. Flohe. 1973. 'Mitochondrial H2O2 formation: relationship with energy conservation', *FEBS Lett*, 33: 84-7.

Macintyre, A. N., V. A. Gerriets, A. G. Nichols, R. D. Michalek, M. C. Rudolph, D. Deoliveira, S. M. Anderson, E. D. Abel, B. J. Chen, L. P. Hale, and J. C. Rathmell. 2014. 'The glucose transporter Glut1 is selectively essential for CD4 T cell activation and effector function', *Cell Metab*, 20: 61-72.

Mak, T. W., M. Grusdat, G. S. Duncan, C. Dostert, Y. Nonnenmacher, M. Cox, C. Binsfeld, Z. Hao, A. Brustle, M. Itsumi, C. Jager, Y. Chen, O. Pinkenburg, B. Camara, M. Ollert, C. Bindslev-Jensen, V. Vasiliou, C. Gorrini, P. A. Lang, M. Lohoff, I. S. Harris, K. Hiller, and D. Brenner. 2017. 'Glutathione Primes T Cell Metabolism for Inflammation', *Immunity*, 46: 1089-90.

Manolescu, A. R., K. Witkowska, A. Kinnaird, T. Cessford, and C. Cheeseman. 2007. 'Facilitated hexose transporters: new perspectives on form and function', *Physiology (Bethesda)*, 22: 234-40.

Marelli-Berg, F. M., H. Fu, and C. Mauro. 2012. 'Molecular mechanisms of metabolic reprogramming in proliferating cells: implications for T-cell-mediated immunity', *Immunology*, 136: 363-9.

Melief, C. J. 1992. 'Tumor eradication by adoptive transfer of cytotoxic T lymphocytes', *Adv Cancer Res*, 58: 143-75.

Menk, A. V., N. E. Scharping, R. S. Moreci, X. Zeng, C. Guy, S. Salvatore, H. Bae, J. Xie, H. A. Young, S. G. Wendell, and G. M. Delgoffe. 2018. 'Early TCR Signaling Induces Rapid Aerobic Glycolysis Enabling Distinct Acute T Cell Effector Functions', *Cell Rep*, 22: 1509-21.

Michalek, R. D., V. A. Gerriets, S. R. Jacobs, A. N. Macintyre, N. J. MacIver, E. F. Mason, S. A. Sullivan, A. G. Nichols, and J. C. Rathmell. 2011. 'Cutting edge: distinct glycolytic and lipid oxidative metabolic programs are essential for effector and regulatory CD4+ T cell subsets', *J Immunol*, 186: 3299-303.

Mittal, D., M. M. Gubin, R. D. Schreiber, and M. J. Smyth. 2014. 'New insights into cancer immunoediting and its three component phases--elimination, equilibrium and escape', *Curr Opin Immunol*, 27: 16-25.

Moon, S. J., W. Dong, G. N. Stephanopoulos, and H. D. Sikes. 2020. 'Oxidative pentose phosphate pathway and glucose anaplerosis support maintenance of mitochondrial NADPH pool under mitochondrial oxidative stress', *Bioeng Transl Med*, 5: e10184.

Mueckler, M., and B. Thorens. 2013. 'The SLC2 (GLUT) family of membrane transporters', *Mol Aspects Med*, 34: 121-38.

Nakamura, H., and K. Takada. 2021. 'Reactive oxygen species in cancer: Current findings and future directions', *Cancer Sci*, 112: 3945-52.

Nicholas, D. A., E. A. Proctor, M. Agrawal, A. C. Belkina, S. C. Van Nostrand, L. Panneerseelan-Bharath, A. R. th Jones, F. Raval, B. C. Ip, M. Zhu, J. M. Cacicedo, C. Habib, N. Sainz-Rueda, L. Persky, P. G. Sullivan, B. E. Corkey, C. M. Apovian, P. A. Kern, D. A. Lauffenburger, and B. S. Nikolajczyk. 2019. 'Fatty Acid Metabolites Combine with Reduced beta Oxidation to Activate Th17 Inflammation in Human Type 2 Diabetes', *Cell Metab*, 30: 447-61 e5.

Nishikawa, T., D. Edelstein, and M. Brownlee. 2000. 'The missing link: a single unifying mechanism for diabetic complications', *Kidney Int Suppl*, 77: S26-30.

Nishikawa, T., D. Edelstein, X. L. Du, S. Yamagishi, T. Matsumura, Y. Kaneda, M. A. Yorek, D. Beebe, P. J. Oates, H. P. Hammes, I. Giardino, and M. Brownlee. 2000. 'Normalizing mitochondrial superoxide production blocks three pathways of hyperglycaemic damage', *Nature*, 404: 787-90.

O'Hara, M. H., E. M. O'Reilly, G. Varadhachary, R. A. Wolff, Z. A. Wainberg, A. H. Ko, G. Fisher, O. Rahma, J. P. Lyman, C. R. Cabanski, R. Mick, P. F. Gherardini, L. J. Kitch, J. Xu, T. Samuel, J. Karakunnel, J. Fairchild, S. Bucktrout, T. M. LaVallee, C. Selinsky, J. E. Till, E. L. Carpenter, C. Alanio, K. T. Byrne, R. O. Chen, O. C. Trifan, U. Dugan, C. Horak, V. M. Hubbard-Lucey, E. J. Wherry, R. Ibrahim, and R. H. Vonderheide. 2021. 'CD40 agonistic monoclonal antibody APX005M (sotigalimab) and chemotherapy, with or without nivolumab, for the treatment of metastatic pancreatic adenocarcinoma: an open-label, multicentre, phase 1b study', *Lancet Oncol*, 22: 118-31.

O'Rourke, D. M., M. P. Nasrallah, A. Desai, J. J. Melenhorst, K. Mansfield, J. J. D. Morrissette, M. Martinez-Lage, S. Brem, E. Maloney, A. Shen, R. Isaacs, S. Mohan, G. Plesa, S. F. Lacey, J. M. Navenot, Z. Zheng, B. L. Levine, H. Okada, C. H. June, J. L. Brogdon, and M. V. Maus. 2017. 'A single dose of peripherally infused EGFRvIII-directed CAR T cells mediates antigen loss and induces adaptive resistance in patients with recurrent glioblastoma', *Sci Transl Med*, 9.

O'Sullivan, D. 2019. 'The metabolic spectrum of memory T cells', *Immunol Cell Biol*, 97: 636-46.

Obar, J. J., and L. Lefrancois. 2010. 'Memory CD8+ T cell differentiation', *Ann N Y Acad Sci*, 1183: 251-66.

Pardoll, D. M. 2012. 'The blockade of immune checkpoints in cancer immunotherapy', *Nat Rev Cancer*, 12: 252-64.

Patnaik, A., S. P. Kang, D. Rasco, K. P. Papadopoulos, J. Elassaiss-Schaap, M. Beeram, R. Drengler, C. Chen, L. Smith, G. Espino, K. Gergich, L. Delgado, A. Daud, J. A. Lindia, X. N. Li, R. H. Pierce, J. H. Yearley, D. Wu, O. Laterza, M. Lehnert, R. Iannone, and A. W. Tolcher. 2015. 'Phase I Study of Pembrolizumab (MK-3475; Anti-PD-1 Monoclonal Antibody) in Patients with Advanced Solid Tumors', *Clin Cancer Res*, 21: 4286-93.

Peng, M., N. Yin, S. Chhangawala, K. Xu, C. S. Leslie, and M. O. Li. 2016. 'Aerobic glycolysis promotes T helper 1 cell differentiation through an epigenetic mechanism', *Science*, 354: 481-84.

Phan, A. T., A. L. Doedens, A. Palazon, P. A. Tyrakis, K. P. Cheung, R. S. Johnson, and A. W. Goldrath. 2016. 'Constitutive Glycolytic Metabolism Supports CD8(+) T Cell Effector Memory Differentiation during Viral Infection', *Immunity*, 45: 1024-37.

Pilipow, K., E. Scamardella, S. Puccio, S. Gautam, F. De Paoli, E. M. Mazza, G. De Simone, S. Polletti, M. Buccilli, V. Zanon, P. Di Lucia, M. Iannacone, L. Gattinoni, and E. Lugli. 2018. 'Antioxidant metabolism regulates CD8+ T memory stem cell formation and antitumor immunity', *JCI Insight*, 3.

Ping, Y., F. Li, S. Nan, D. Zhang, X. Shi, J. Shan, and Y. Zhang. 2020. 'Augmenting the Effectiveness of CAR-T Cells by Enhanced Self-Delivery of PD-1-Neutralizing scFv', *Front Cell Dev Biol*, 8: 803.

Powell, J. D., and G. M. Delgoffe. 2010. 'The mammalian target of rapamycin: linking T cell differentiation, function, and metabolism', *Immunity*, 33: 301-11.

Previte, D. M., E. C. O'Connor, E. A. Novak, C. P. Martins, K. P. Mollen, and J. D. Piganelli. 2017. 'Reactive oxygen species are required for driving efficient and sustained aerobic glycolysis during CD4+ T cell activation', *PLoS One*, 12: e0175549.

Rangel Rivera, G. O., H. M. Knochelmann, C. J. Dwyer, A. S. Smith, M. M. Wyatt, A. M. Rivera-Reyes, J. E. Thaxton, and C. M. Paulos. 2021. 'Fundamentals of T Cell Metabolism and Strategies to Enhance Cancer Immunotherapy', *Front Immunol*, 12: 645242.

Rathmell, J. C., M. G. Vander Heiden, M. H. Harris, K. A. Frauwirth, and C. B. Thompson. 2000. 'In the absence of extrinsic signals, nutrient utilization by lymphocytes is insufficient to maintain either cell size or viability', *Mol Cell*, 6: 683-92.

Raz, A., G. Levine, and Y. Khomiak. 2000. 'Acute local inflammation potentiates tumor growth in mice', *Cancer Lett*, 148: 115-20.

Reinfeld, B. I., M. Z. Madden, M. M. Wolf, A. Chytil, J. E. Bader, A. R. Patterson, A. Sugiura, A. S. Cohen, A. Ali, B. T. Do, A. Muir, C. A. Lewis, R. A. Hongo, K. L. Young, R. E. Brown, V. M. Todd, T. Huffstater, A. Abraham, R. T. O'Neil, M. H. Wilson, F. Xin, M. N. Tantawy, W. D. Merryman, R. W. Johnson, C. S. Williams, E. F. Mason, F. M. Mason, K. E. Beckermann, M. G. Vander Heiden, H. C. Manning, J. C. Rathmell, and W. K. Rathmell. 2021. 'Cell-programmed nutrient partitioning in the tumour microenvironment', *Nature*, 593: 282-88.

Rochette, L., M. Zeller, Y. Cottin, and C. Vergely. 2014. 'Diabetes, oxidative stress and therapeutic strategies', *Biochim Biophys Acta*, 1840: 2709-29.

Rosenberg, S. A., B. S. Packard, P. M. Aebersold, D. Solomon, S. L. Topalian, S. T. Toy, P. Simon, M. T. Lotze, J. C. Yang, C. A. Seipp, and et al. 1988. 'Use of tumor-infiltrating lymphocytes and interleukin-2 in the immunotherapy of patients with metastatic melanoma. A preliminary report', *N Engl J Med*, 319: 1676-80.

Royal, R. E., C. Levy, K. Turner, A. Mathur, M. Hughes, U. S. Kammula, R. M. Sherry, S. L. Topalian, J. C. Yang, I. Lowy, and S. A. Rosenberg. 2010. 'Phase 2 trial of single agent Ipilimumab (anti-CTLA-4) for locally advanced or metastatic pancreatic adenocarcinoma', *J Immunother*, 33: 828-33.

Sahin, I. H., G. Askan, Z. I. Hu, and E. M. O'Reilly. 2017. 'Immunotherapy in pancreatic ductal adenocarcinoma: an emerging entity?', *Ann Oncol*, 28: 2950-61.

Scheepers, A., H. G. Joost, and A. Schurmann. 2004. 'The glucose transporter families SGLT and GLUT: molecular basis of normal and aberrant function', *JPEN J Parenter Enteral Nutr*, 28: 364-71.

Sena, L. A., S. Li, A. Jairaman, M. Prakriya, T. Ezponda, D. A. Hildeman, C. R. Wang, P. T. Schumacker, J. D. Licht, H. Perlman, P. J. Bryce, and N. S. Chandel. 2013. 'Mitochondria are required for antigen-specific T cell activation through reactive oxygen species signaling', *Immunity*, 38: 225-36.

Shyer, J. A., R. A. Flavell, and W. Bailis. 2020. 'Metabolic signaling in T cells', *Cell Res*, 30: 649-59.

Sukumar, M., J. Liu, Y. Ji, M. Subramanian, J. G. Crompton, Z. Yu, R. Roychoudhuri, D. C. Palmer, P. Muranski, E. D. Karoly, R. P. Mohney, C. A. Klebanoff, A. Lal, T. Finkel, N. P. Restifo, and L. Gattinoni. 2013. 'Inhibiting glycolytic metabolism enhances CD8+ T cell memory and antitumor function', *J Clin Invest*, 123: 4479-88.

Sullivan, M. R., L. V. Danai, C. A. Lewis, S. H. Chan, D. Y. Gui, T. Kunchok, E. A. Dennstedt, M. G. Vander Heiden, and A. Muir. 2019. 'Quantification of microenvironmental metabolites in murine cancers reveals determinants of tumor nutrient availability', *Elife*, 8.

Tang, Z., C. Li, B. Kang, G. Gao, C. Li, and Z. Zhang. 2017. 'GEPIA: a web server for cancer and normal gene expression profiling and interactive analyses', *Nucleic Acids Res*, 45: W98-W102.

Terres, G., and R. L. Coffman. 1998. 'The role of IL-4 and IL-10 cytokines in controlling an anti-tumor response in vivo', *Int Immunol*, 10: 823-32.

Thangasamy, T., P. Jeyakumar, S. Sittadjody, A. G. Joyee, and P. Chinnakannu. 2009. 'L-carnitine mediates protection against DNA damage in lymphocytes of aged rats', *Biogerontology*, 10: 163-72.

Tian, Y., Y. Li, Y. Shao, and Y. Zhang. 2020. 'Gene modification strategies for next-generation CAR T cells against solid cancers', *J Hematol Oncol*, 13: 54.

Tirichen, H., H. Yaigoub, W. Xu, C. Wu, R. Li, and Y. Li. 2021. 'Mitochondrial Reactive Oxygen Species and Their Contribution in Chronic Kidney Disease Progression Through Oxidative Stress', *Front Physiol*, 12: 627837.

'Tisagenlecleucel (Kymriah) for ALL'. 2017. *Med Lett Drugs Ther*, 59: 177-78.

Tokarew, N., J. Ogonek, S. Endres, M. von Bergwelt-Baildon, and S. Kobold. 2019. 'Teaching an old dog new tricks: next-generation CAR T cells', *Br J Cancer*, 120: 26-37.

Turrens, J. F., B. A. Freeman, J. G. Levitt, and J. D. Crapo. 1982. 'The effect of hyperoxia on superoxide production by lung submitochondrial particles', *Arch Biochem Biophys*, 217: 401-10.

Ullman, N. A., P. R. Burchard, R. F. Dunne, and D. C. Linehan. 2022. 'Immunologic Strategies in Pancreatic Cancer: Making Cold Tumors Hot', *J Clin Oncol*, 40: 2789-805.

van der Windt, G. J., D. O'Sullivan, B. Everts, S. C. Huang, M. D. Buck, J. D. Curtis, C. H. Chang, A. M. Smith, T. Ai, B. Faubert, R. G. Jones, E. J. Pearce, and E. L. Pearce. 2013. 'CD8 memory T cells have a bioenergetic advantage that underlies their rapid recall ability', *Proc Natl Acad Sci U S A*, 110: 14336-41.

Verfaillie, T., E. Cox, L. T. To, D. Vanrompay, H. Bouchaut, N. Buys, and B. M. Goddeeris. 2001. 'Comparative analysis of porcine cytokine production by mRNA and protein detection', *Vet Immunol Immunopathol*, 81: 97-112.

Wang, J., M. Jensen, Y. Lin, X. Sui, E. Chen, C. G. Lindgren, B. Till, A. Raubitschek, S. J. Forman, X. Qian, S. James, P. Greenberg, S. Riddell, and O. W. Press. 2007. 'Optimizing adoptive polyclonal T cell immunotherapy of lymphomas, using a chimeric T cell receptor possessing CD28 and CD137 costimulatory domains', *Hum Gene Ther*, 18: 712-25.

Wang, L., Y. J. Ahn, and R. Asmis. 2020. 'Sexual dimorphism in glutathione metabolism and glutathione-dependent responses', *Redox Biol*, 31: 101410.

Wang, M., J. Zhao, L. Zhang, F. Wei, Y. Lian, Y. Wu, Z. Gong, S. Zhang, J. Zhou, K. Cao, X. Li, W. Xiong, G. Li, Z. Zeng, and C. Guo. 2017. 'Role of tumor microenvironment in tumorigenesis', *J Cancer*, 8: 761-73.

Wang, R., C. P. Dillon, L. Z. Shi, S. Milasta, R. Carter, D. Finkelstein, L. L. McCormick, P. Fitzgerald, H. Chi, J. Munger, and D. R. Green. 2011. 'The transcription factor Myc controls metabolic reprogramming upon T lymphocyte activation', *Immunity*, 35: 871-82.

Warburg, O., F. Wind, and E. Negelein. 1927. 'The Metabolism of Tumors in the Body', *J Gen Physiol*, 8: 519-30.

Wieman, H. L., J. A. Wofford, and J. C. Rathmell. 2007. 'Cytokine stimulation promotes glucose uptake via phosphatidylinositol-3 kinase/Akt regulation of Glut1 activity and trafficking', *Mol Biol Cell*, 18: 1437-46.

Wienke, J., M. P. Dierselhuis, G. A. M. Tytgat, A. Kunkele, S. Nierkens, and J. J. Molenaar. 2021. 'The immune landscape of neuroblastoma: Challenges and opportunities for novel therapeutic strategies in pediatric oncology', *Eur J Cancer*, 144: 123-50.

Wu, J., G. Li, L. Li, D. Li, Z. Dong, and P. Jiang. 2021. 'Asparagine enhances LCK signalling to potentiate CD8(+) T-cell activation and anti-tumour responses', *Nat Cell Biol*, 23: 75-86.

Xia, J., and D. S. Wishart. 2011. 'Web-based inference of biological patterns, functions and pathways from metabolomic data using MetaboAnalyst', *Nat Protoc*, 6: 743-60.

Yang, J., Q. Zhang, J. Wang, Y. Lou, Z. Hong, S. Wei, K. Sun, J. Wang, Y. Chen, J. Sheng, W. Su, X. Bai, and T. Liang. 2022. 'Dynamic profiling of immune microenvironment during pancreatic cancer development suggests early intervention and combination strategy of immunotherapy', *EBioMedicine*, 78: 103958.

Yarosz, E. L., and C. H. Chang. 2018. 'The Role of Reactive Oxygen Species in Regulating T Cell-mediated Immunity and Disease', *Immune Netw*, 18: e14.

Yeo, D., C. Giardina, P. Saxena, and J. E. J. Rasko. 2022. 'The next wave of cellular immunotherapies in pancreatic cancer', *Mol Ther Oncolytics*, 24: 561-76.

Yu, M., H. Yongzhi, S. Chen, X. Luo, Y. Lin, Y. Zhou, H. Jin, B. Hou, Y. Deng, L. Tu, and Z. Jian. 2017. 'The prognostic value of GLUT1 in cancers: a systematic review and meta-analysis', *Oncotarget*, 8: 43356-67.

Yu, T., J. L. Robotham, and Y. Yoon. 2006. 'Increased production of reactive oxygen species in hyperglycemic conditions requires dynamic change of mitochondrial morphology', *Proc Natl Acad Sci U S A*, 103: 2653-8.

Zhang, L., and P. Romero. 2018. 'Metabolic Control of CD8(+) T Cell Fate Decisions and Antitumor Immunity', *Trends Mol Med*, 24: 30-48.

Zhao, R. Z., S. Jiang, L. Zhang, and Z. B. Yu. 2019. 'Mitochondrial electron transport chain, ROS generation and uncoupling (Review)', *Int J Mol Med*, 44: 3-15.

Zhao, Y., X. Hu, Y. Liu, S. Dong, Z. Wen, W. He, S. Zhang, Q. Huang, and M. Shi. 2017. 'ROS signaling under metabolic stress: cross-talk between AMPK and AKT pathway', *Mol Cancer*, 16: 79.

Zhou, J., M. T. Bethune, N. Malkova, A. M. Sutherland, B. Comin-Anduix, Y. Su, D. Baltimore, A. Ribas, and J. R. Heath. 2018. 'A kinetic investigation of interacting, stimulated T cells identifies conditions for rapid functional enhancement, minimal phenotype differentiation, and improved adoptive cell transfer tumor eradication', *PLoS One*, 13: e0191634.

Zou, X., Z. Feng, Y. Li, Y. Wang, K. Wertz, P. Weber, Y. Fu, and J. Liu. 2012. 'Stimulation of GSH synthesis to prevent oxidative stress-induced apoptosis by hydroxytyrosol in human retinal pigment epithelial cells: activation of Nrf2 and JNK-p62/SQSTM1 pathways', *J Nutr Biochem*, 23: 994-1006.

12. Acknowledgments

The last four and a half years, the doctoral program i-Target was a strong constant that not only helped me to grow as a critically thinking scientist but also brought many joyful memories and new friends to my life. Thank you to Prof. Dr. Stefan Endres, Dr. Katharina Dennemarck, and Prof. em. Dr. Wolfgang Zimmermann for creating such a great, motivating and family-like environment for young scientist.

To Ann-Sophie Schuecke, Amar Hadzic and Ludovica Vona for teaching me how to supervise students. I very much appreciate your patience with me – My thinking and explanations could be very confusing sometimes. I hope you could learn from me as much as I did from you!

Thanks to Prof. Dr. Marion Subklewe and her entire group for being very good colleagues, outstanding friends, and simply the best lab neighbours possible. Your help and support make work life easy.

Danke an meine Freunde in München und Dahoam. Ihr habt mich immer wieder auf den Boden geholt und vor allem für die nötige Ablenkung und Abwechslung gesorgt. Ihr seid der Grund, dass meine work-life balance immer perfekt im Ausklang war. Ihr seid unersetzbar und die Besten!

An meine gesamte Familie, insbesondere Papa, Mama und Michi. Auf euren Rückhalt konnte ich mich immer verlassen. Es ist wirklich das Schönste, zu wissen, dass man jederzeit zu euch heimkommen kann! Auch danke für das „Funding" - die finanzielle Unterstützung während des Studiums hat es mir ermöglicht mich völlig auf die wesentlichen Dinge zu fokussieren. Ihr seid immer für mich da und dafür bin ich unendlich Dankbar!

To Dr. Lisa Rohrbacher. You are my constant, my steady companion. Many things would have gone differently, if we did not meet. You are the reason I write my dissertation on this project and the reason I met all these wonderful people. Since we are together you have always had an open ear for personal or scientific advice. You were always empathetic in case I was frustrated and helped me get back on track. Your support is tremendous. It would have not been possible without you! I can`t find words to thank you enough!

13. Affidavit
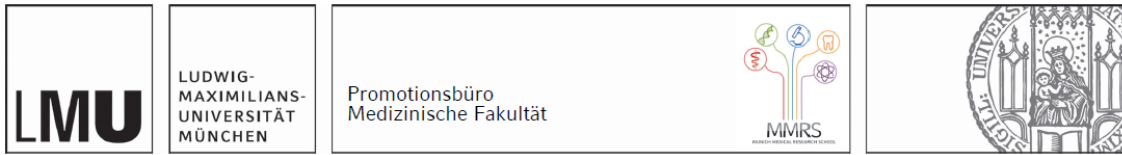
Affidavit

Kirmaier, Martin Edwin
_____
Surname, first name

Feodor-Lynen Straße 25 (Gene Center Munich)
_____
Street

81377, München, Deutschland
_____
Zip code, town, country

I hereby declare, that the submitted thesis entitled:

Metabolic engineering of murine cytotoxic T cells by solute carrier _Slc2a1_/GLUT1 overexpression to enhance anti-tumor activity

is my own work. I have only used the sources indicated and have not made unauthorised use of services of a third party. Where the work of others has been quoted or reproduced, the source is always given.

I further declare that the dissertation presented here has not been submitted in the same or similar form to any other institution for the purpose of obtaining an academic degree.
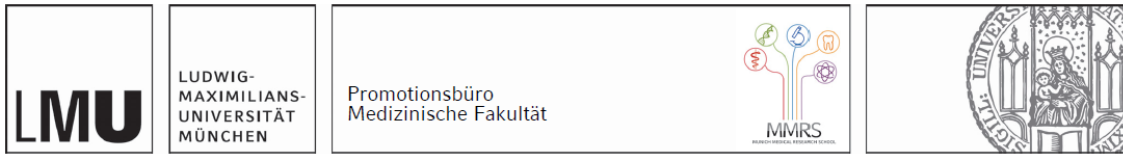
15.11.23, Munich   Martin Edwin Kirmaier
place, date   Signature doctoral candidate

14. Confirmation of congruency

Confirmation of congruency between printed and electronic version of

the doctoral thesis

Kirmaier, Martin Edwin

_____
Surname, first name

Feodor-Lynen Straße 25 (Gene Center Munich)

_____
Street

81377, München, Deutschland

_____
Zip code, town, country

I hereby declare, that the submitted thesis entitled:

Metabolic engineering of murine cytotoxic T cells by solute carrier _Slc2a1_/GLUT1 overexpression to enhance anti-tumor activity

is congruent with the printed version both in content and format.

15.11.23, Munich   Martin Edwin Kirmaier

place, date   Signature doctoral candidate